UNIVERSITÀ DI PARMA

UNIVERSITÀ DEGLI STUDI DI PARMA

Dottorato di Ricerca in Tecnologie dell'Informazione

XXXVI Ciclo

Performance Analysis of 5G Networks: a Joint Experimental and Simulative Approach

Coordinatore:

Chiar.mo Prof. Marco Locatelli

Tutor:

Chiar.mo Prof. Gianluigi Ferrari

Co-Tutor:

Chiar.mo Prof. Luca Davoli

Dottorando: *Sunil Mathew*

Anni Accademici 2020/2021 - 2022/2023

To who always believed in me,
to my family.

Contents

Acronyms **v**

List of Figures **xii**

List of Tables **xix**

Introduction **1**

1 State of the Art **5**

1.1 Fifth Generation Cellular Technology (5G) Frequencies 6

1.2 5G Protocol Stack 7

1.2.1 5G User Plane Protocol Stack 7

1.2.2 5G Control Plane Protocol Stack 8

1.3 Communication Channels in 5G 9

1.3.1 DL Physical Channels 10

1.3.2 UL Physical Channels 11

1.3.3 Signals in 5G Physical Channels 12

1.3.4 DL and UL Transport Channels 13

1.4 Frame Structure 13

1.5 Comparison between 4G and 5G Technologies 14

1.6 Critical Values for Vehicular Communications 15

2 Matlab-handled 5G Modem **19**
2.1 Simulation of a 5G Connection 19
2.2 5G System Model 20
2.3 Numerical Findings 22
2.4 Hardware/Software *Co-design* 24
2.5 Experimental Devices 25
2.5.1 Zynq UltraScale+ MPSoC ZCU102 Evaluation Kit 26
2.5.2 Analog Devices AD-FMCOMMS3-EBZ 27
2.6 Experimental Architecture 27
2.6.1 Loopback Model 28
2.6.2 Point-to-Point (P2P) model 30
2.6.3 Testbed Calibration 31
2.7 Device Setup 34
2.8 Hardware-Software Implementative Approach 34
2.9 Preliminary Results with 4G Networks 36
2.10 5G Experimental Trials 39
2.10.1 DownLink (DL) Transmission and Reception 39
2.10.2 UpLink (UL) Waveform Transmission and Reception 47
2.10.3 UL and DL P2P Communication 49
2.11 Limitations of the system abstraction 50
2.11.1 Hybrid Automatic Repeat reQuest (HARQ) 51

3 Experimental Performance Analysis **53**
3.1 Performance Metrics 53
3.2 Commercial Off-The-Shelf (COTS) 5G Modem 55
3.2.1 Quectel 5G Modem 55
3.2.2 Telit 5G Module 60
3.2.3 Sierra Wireless Modem 62
3.3 Antennas 64
3.3.1 ASK 5G Antenna 64
3.3.2 LTE/5G NR Terminal Mount Monopole Antenna 64

3.4 Stemedu Vk-162 GNSS Module 66
3.5 Graphical User Interface (GUI) 67
3.5.1 Main Page 67
3.5.2 Configuration Overview 69
3.5.3 Post Processing 70
3.6 Matlab-based Post Processing 71
3.7 Road Tests 72
3.8 Experimental Results: Impact of Distance 75
3.8.1 Reference Signal Received Power (RSRP) as a function of the Distance 77
3.8.2 Reference Signal Strength Indicator (RSSI) as a function of the Distance 78
3.8.3 Reference Signal Received Quality (RSRQ) as a function of the Distance 78
3.8.4 Joint RSRP and DL Throughput Analysis 78
3.9 Experimental Results: Impact of Velocity 80
3.9.1 RSRP as a function of Velocity 80
3.9.2 RSSI as a function of Velocity 81
3.9.3 RSRQ as a function of Velocity 81
3.9.4 DL Throughput Analysis 82
3.10 Experimental Results: Impact of Environment 84
3.10.1 RSRP as a function of Distance 84
3.10.2 RSSI as a function of Distance 85
3.10.3 RSRQ as a function of Distance 85
3.10.4 DL Throughput Analysis 86

4 Handover Analysis **89**
4.1 Experimental Analysis of 5G Network during HOs 90
4.1.1 Reference Experimental Path 90
4.1.2 Experimental Evaluation 91
4.2 Classic HO procedure 94

4.3 HandOver (HO) Reduction Strategy 99
4.3.1 Small Cells 100
4.3.2 Small Cell-based UHO Reduction Strategy 102
4.3.3 Unnecessary HO Mitigation through Linear Regression . . . 107

Conclusion **111**

List of Publications **115**

Bibliography **117**

Thanks **129**

Acronyms

3G Third Generation

3GPP Third Generation Partnership Project

4G Fourth Generation Cellular Technology

5G Fifth Generation Cellular Technology

5GLAN 5G Local Area Network

ACK Acknowledgement

AMF Access and Mobility Management Function

APK Android Application PacKage

APN Access Point Name

ARM Advanced RISC Machine

BCH Broadcast CHannel

BS Base Station

BW BandWidth

CC Critical Communications

CDL Clustered Delay Line

CLI Command Line Interface

COTS Commercial Off-The-Shelf

CP Cyclic Prefix

CPE Common Phase Error

CRC Cyclic Redundancy Check

CSI Channel State Information

CSI-RS Channel State Information Reference Signal

CSI-RSRP Channel State Information - Reference Signal Received Power

CW Code Word

DL DownLink

DLSCH DownLink Shared CHannel

DMRS DeModulation Reference Signal

DNS Domain Name System

E-UTRA-ARFCN Evolved Universal Terrestrial Radio Access-Absolute Radio Frequency Channel Number

eMBB Enhanced Mobile Broadband

ETSI European Telecommunications Standards Institute

EVB Evaluation Board

FDD Frequency Division Duplex

FE Front End

FFT Fast Fourier Transform

FMC FPGA Mezzanine Card

FPGA Field Programmable Gate Array

Gbps Gigabits per second

GHz Giga Hertz

GLOSA Green Light Optimal Speed Advisory

gNB Next Generation NodeB

GNSS Global Navigation Satellite Systems

GSM Global System for Mobile Communications

GUI Graphical User Interface

HARQ Hybrid Automatic Repeat reQuest

HDL Hardware Description Language

HO HandOver

IoT Internet of Things

IoT Internet of Things

IP Internet Protocol

km/h kilometers per hour

LAC Location Area Code

LDPC Low-Density Parity-Check

LOS Line of sight

LTE Long Term Evolution

MAC Medium Access Control

Mbps Megabits per second

MCC Mobile Country Code

MIB Master Information Block

MIMO Multiple Input Multiple Output

mIoT Massive Internet of Things

mmWave millimiter Wave

MNC Mobile Network Code

MU-MIMO Multi User MIMO

N-LOS Non-Line of sight

NR New Radio

NSA Non-Standalone Mode

OFDM Orthogonal Frequency Division Multiplexing

OSI Open Systems Interconnection

P2P Point-to-Point

PBCH Physical Broadcast CHannel

PDCCH Physical Downlink Control CHannel

PDCP Packet Data Convergence Protocol

PDSCH Physical Downlink Shared CHannel

PHY Physical layer

ppm parts per million

PRACH Physical Random Access CHannel

PSC Primary Scrambling Code

PSS Primary Synchronization Signal

PTRS Phase-Tracking Reference Signal

PUCCH Physical Uplink Control CHannel

PUSCH Physical Uplink Shared CHannel

QAM Quadrature Amplitude Modulation

QoS Quality of Service

RAC Routing Area Code

RB Resource Block

RE Resource Element

RLC Radio Link Control

RNTI Radio Network Temporary Identifier

RRC Radio Resource Control

RSCP Received Signal Code Power

RSRP Reference Signal Received Power

RSRQ Reference Signal Received Quality

RSSI Reference Signal Strength Indicator

SA Standalone Mode

SDAP Service Data Adaptation Protocol

SIM Subscriber Identification Module

SINR Signal-to-Noise and Interference Ratio

SNR Signal-to-Noise Ratio

SoC System-on-Chip

SRS Sounding Reference Signal

SSB Synchonization Signal Block

SSS Secondary Synchronization Signal

TAC Tracking Area Code

TDD Time Division Duplexing

TDL Tapped Delay Line

TDL-B Tapped Delay Line-B

TDL-D Tapped Delay Line-D

TTT Time-to-Trigger

UART Universal Asynchronous Receiver-Transmitter

UE User Equipment

UHO Unnecessary HandOver

UL UpLink

ULSCH UpLink Shared CHannel

UMTS Universal Mobile Telecommunications System

URLLC Ultra-Reliable and Low-Latency Communications

USB Universal Serial Bus

UTRA-ARFCN Universal Terrestrial Radio Access-Absolute Radio Frequency Channel Number

V2X Vehicle-to-Everything

WCDMA Wideband Code Division Multiple Access

List of Figures

1.1 Frequencies used in 5G networks. 7
1.2 User plane protocol stack. 8
1.3 Control plane protocol stack. 8
1.4 Diagram of 5G channels. 10
1.5 5G Frame Structure. 14
1.6 Examples of applications of 5G technology in the vehicular field. . . 16

2.1 Block diagram of the 5G connection simulation: (a) Physical Downlink Shared CHannel (PDSCH) channel transmission and (b) Physical Uplink Shared CHannel (PUSCH) channel transmission. 21
2.2 Throughput, represented as a percentage, plotted against Signal-to-Noise Ratio (SNR) for the PDSCH channel transmission. 23
2.3 Throughput, illustrated as a percentage, in relation to SNR for the PUSCH channel transmission. 24
2.4 Illustration of the comprehensive system layout. 25
2.5 Blueprint of the system during the nascent phase of prototype formulation. 25
2.6 Zynq UltraScale+ MPSoC ZCU102 Evaluation Kit. 26
2.7 Analog Devices AD-FMCOMMS3-EBZ Front End: (a) top view; (b) bottom view. 27
2.8 Block diagram of the used configuration. 29
2.9 Experimental setup with wired *loopback*. 29

2.10 Antenna used in the tests. 30
2.11 Experimental setup with Wireless Loopback model. 30
2.12 Block diagram (with photos) of exclusive UL/DL model. 32
2.13 Block diagram of the contemporary UL/DL model. 32
2.14 Real deployment of the contemporary UL/DL model. 33
2.15 Calibration of the Front End (FE)s. 33
2.16 5G Toolbox in Matlab and 5G channels: (a) DL channel mapping; (b) UL channels 35
2.17 5G Wireless Waveform Generator App within the 5G Toolbox. . . . 36
2.18 Block diagram of the LTE network search. 37
2.19 Result of the experiment for the retrieval of the Cell ID and MIB. . . 38
2.20 Block diagram of the conducted experiment for encoding and transmitting an image. 40
2.21 Spectrum of the transmitted signal. 42
2.22 Power spectrum of the received signal. 43
2.23 Example of PSS correlation for different frequency offset values. . . 44
2.24 Correlation of the received signal with possible SSS sequences. . . . 45
2.25 Transmitted (a) and received (b) image. 46
2.26 Schematic diagram of the UL communication. 47
2.27 UL P2P image transmission. 49
2.28 UL only in P2P image transmission. 50
2.29 HARQ implementation. 51

3.1 Quectel Modem. 56
3.2 Experimental setup for Quectel Modem tests. 57
3.3 Telit 5G Module - FN980. 60
3.4 Setup using the Telit modem for experimental purposes. 61
3.5 Block diagram of the experimental setup with the Telit FN980. . . . 62
3.6 Sierra Wireless EM9191 5G module. 63
3.7 Block diagram of the experimental testbed. 63
3.8 LTE/5G NR ASK Antenna. 64

3.9 LTE/5G NR ASK Antenna side and top views. 65
3.10 Average gain comparison between the ASK antenna (yellow line) and the reference antenna (blue and red lines). 65
3.11 LTE/5G NR Terminal Mount Monopole Antenna. 66
3.12 Experimental setup: ASK antenna (left) and reference antenna (right). 66
3.13 Stemedu Vk-162 GNSS Module. 67
3.14 Initial view of the GUI developed for running the experimental evaluations. 68
3.15 Configuration tab view of the GUI developed for running the experimental evaluations. 70
3.16 Post processing tool. 71
3.17 Geographical globe plot. 72
3.18 Geoplot3 depicting a single data set (RSRP) collected along a single path, with red and blue lines representing trials using different antennas. 73
3.19 Geoplot3 representing two data sets: RSRP (color) and DL throughput (height). 73
3.20 Graphical representation of RSRP model. 75
3.21 Path loss as a function of distance for three different vehicle speeds: (A) 60 kilometers per hour (km/h), (B) 90 km/h, and (C) 120 km/h. . 76
3.22 Projected RSRP for Tapped Delay Line-B (TDL-B) and Tapped Delay Line-D (TDL-D) channel models, corresponding to Non-Line of sight (N-LOS) and Line of sight (LOS) conditions respectively. . . . 77
3.23 RSRP as a Function of the Distance, charted across a test path. The reference antenna serves as a benchmark for the ASK antenna. . . . 78
3.24 RSSI plotted against distance, based on data from a test path with the reference antenna providing a benchmark for the ASK antenna. . . . 79
3.25 RSRQ in relation to distance, presented with data from a test path, using the reference antenna as a benchmark for the ASK antenna. . . 79
3.26 A combined presentation of RSRP (color) and DL throughput (line height) across a test path, utilizing the ASK antenna. 80

3.27 A combined presentation of RSRP (color) and DL throughput (line height) using the reference antenna, based on tests conducted across a test path. 81
3.28 Comparison of RSRP as a function of velocity, with results shown for vehicle speeds of (A) 60 Kmph and (B) 90 Kmph. The ASK and reference antennas are represented by green/black and blue/red lines, respectively. 82
3.29 Comparison of RSSI as a function of velocity, with results shown for vehicle speeds of (A) 60 Kmph and (B) 90 Kmph. The ASK and reference antennas are represented by green/black and blue/red lines, respectively. 83
3.30 Comparison of RSRQ as a function of velocity, with results shown for vehicle speeds of (A) 60 Kmph and (B) 90 Kmph. The ASK and reference antennas are represented by green/black and blue/red lines, respectively. 84
3.31 RSRP comparison between ASK and reference antennas in (A) urban (green and black lines) and (B) rural (blue and red lines) environments. 85
3.32 RSSI comparison between ASK and reference antennas in (A) urban (green and black lines) and (B) rural (blue and red lines) environments. 86
3.33 RSRQ comparison between ASK and reference antennas in (A) urban (green and black lines) and (B) rural (blue and red lines) environments. 87

4.1 A visual depiction of a vehicle experiencing multiple HOs (during its journey) due to fluctuating signal strengths and coverage areas from various Next Generation NodeB (gNB)s. 90
4.2 Illustration of the selected path for evaluation, highlighted with blue dots. 91
4.3 Experimental throughput achieved at various data rates by the User Equipment (UE) moving along the reference path shown in Fig 4.2. Cell IDs are indicated at the bottom of the plots. 92

4.4 Experimental latency achieved at various data rates by the UE moving along the reference path shown in Fig 4.2. Cell IDs are indicated at the bottom of the plots. 93
4.5 Experimental cell IDs recorded during different experimental trials along the reference path shown in Fig 4.2. 94
4.6 Experimental RSRP values recorded during different experimental trials along the reference path shown in Fig 4.2. 95
4.7 Experimental RSRQ values recorded during different experimental trials along the reference path shown in Fig 4.2. 95
4.8 Classic HO Procedure. 98
4.9 5G small cell (provided by Ericsson [1]) installed on a street light. . 100
4.10 Illustration of the selected area, featuring the reference path (as presented in Fig4.2) in a blue hue, a simulated small cell marked by a green indicator, and a 200 m radius coverage area delineated by a red circle. 102
4.11 RSRP as a function of the distance between UE and gNB: average simulated (blue line with 95% confidence interval bars) and experimental (orange line with asterisks) values are directly compared. . . 105
4.12 RSRP values obtained by means of different simulation trials with a 5G small cell along the reference path shown in Fig 4.10. 106
4.13 Comparison between experimental (in red color) and simulated (in green color) RSRP values retrieved and obtained (after the installation of a 5G small cell) along the reference path (shown in Fig 4.10) at various points during multiple trials. 106
4.14 Simulated cell IDs obtained by means of different trials in the presence of a 5G small cell along the reference path shown in Fig 4.10. . 107
4.15 RSRP values linear regression-based identification of cell ID $\hat{N}_{\text{cell}}^{\text{ID}}$ along the considered path. 108

List of Tables

1.1 Comparison between 4G, sub-6GHz 5G, and mmWave 5G specifications. 15
1.2 Requirements for warning messages for 5G vehicular networks. . . 17

2.1 Parameters for PDSCH simulation. 22
2.2 Parameters for PUSCH simulation. 23
2.3 Parameters selected for the PDSCH. 41

3.1 Comparison of DL throughput as a function of vehicle speed, showcasing results for (A) 60 Kmph and (B) 90 Kmph. The ASK and reference antennas are evaluated across maximum, minimum, and average throughput values. 83
3.2 DL throughput comparison between ASK and reference antennas in (A) urban and (B) rural environments. 87

4.1 Simulation parameters for 5G NR DL. 104

Introduction

Fifth-generation (5G) technology is poised to bring about a revolutionary era in wireless communications, offering substantial improvements in terms of data speeds, latency, and connectivity. In detail, 5G is set to revolutionize different sectors, facilitating real-time interactions, expanding the Internet of Things (IoT) ecosystem, and enabling breakthroughs in autonomous vehicles and smart urban development. Through the implementation of sophisticated technologies (such as beamforming, the use of millimeter-wave bands, and the deployment of small cell networks), 5G is well-equipped to cater to the escalating demands for data and connectivity, ensuring a network infrastructure that is both faster and more efficient. This positions 5G as a crucial technology in the next wave of industrial innovation, opening the door to novel technological advancements and a plethora of innovative applications.

5G's introduction marks a monumental shift in wireless communications, especially beneficial for vehicular communications where the need for instantaneous data exchange is crucial for maintaining road safety, improving traffic flow, and enabling autonomous driving capabilities. Utilizing COTS modems for 5G is a practical and efficient approach in this context, offering a standardized solution that accelerates integration, simplifies development challenges, and is invaluable for real-world testing to assess 5G performance in various vehicular communication scenarios.

However, the high-speed mobility of vehicles in 5G networks necessitates a critical examination of handover processes to ensure continuous and reliable connectivity. The complexity of handover in 5G is intricate but vital, demanding thorough optimization to address potential issues such as latency, packet loss, and service in-

terruptions that could hinder real-time communication in vehicular systems.

This doctoral thesis embarks on an extensive (experimental and simulative) exploration of 5G technology, its significant advancements over its predecessor (4G), and its application in the realm of vehicular communications. In detail, this doctoral thesis meticulously dissects the 5G protocol stack, delves into signals and channels, and conduct experimentations in a Matlab environment. Furthermore, it delves deep into the functionalities and performance of COTS 5G modems, different antennas, and road test setups, culminating in an empirical analysis of handover performance within 5G networks. Through extensive experimental campaigns, this doctoral thesis examines handover procedures, highlighting the benefits of small cells in minimizing unnecessary handovers. This investigation enhances vehicular communication systems using 5G for a safer and more efficient future.

Thesis Structure

Chapter 1 presents the state of the art of 5G architecture, offering a comparative analysis of 4G and 5G, detailing the 5G protocol stack, the different channels and signals in 5G protocol stack, alongside exploring crucial aspects of vehicular communication.

Chapter 2 disseminates the activities performed in order to simulate a 5G gNB and UE using Matlab, also describing the development of a 5G communication system using a hardware-software co-design approach (through Matlab 5G Toolbox and Field Programmable Gate Array (FPGA)s), and presents the results obtained using this Matlab-handled 5G modem.

Chapter 3 focus on a performance analysis at both physical and application layers. It provides an overview of COTS 5G modems and antennas that have been used for road testing, experimental setup for road tests, the development of a GUI for real-time data collection, post-processing tools developed using Matlab, and the performance analysis derived from the road tests conducted using different antennas and impact of distance, velocity and environment.

Chapter 4 embarks on an experimental journey to analyze throughput and latency during handover by conducting experimental road tests. Then it discusses about unnec-

essary handovers and how to reduce them by the use of 5G small cells which, in turn, increase the coverage area and signal strength, and by the use of linear regression-based techniques to reduce the number of these particular events, which can ensure a robust and seamless communication experience during mobility.

Chapter 1

State of the Art

5G refers to a set of technologies whose standards ensure performance superior to the previous generation (Fourth Generation Cellular Technology, 4G). In detail 5G aims at delivering data transmission speeds that are 10 to 100 times faster than the current Fourth Generation Cellular Technology (4G) networks, with download speeds in the order of Gigabits per second (Gbps), far overcoming the tens of Megabits per second (Mbps) offered by 4G [2, 3].

Moreover, 5G enhances the capabilities of 4G services in multiple dimensions as follows [4].

- **Enhanced Mobile Broadband (eMBB)**: 5G is characterized by its increased data rates: in outdoor settings, a DL speed up to 50 Mbps, while in indoor environments, specifically in 5G Local Area Network (5GLAN), data rates up to 1 Gbps. UL data rates are approximately half of the DL values. Various case studies have explored these enhancements, including applications in aviation, where eMBB has been instrumental in delivering a bitrate of 1.2 Gbps to airborne flights.

- **Critical Communications (CC)** and **Ultra-Reliable and Low-Latency Communications (URLLC)**: These features are essential in scenarios demanding unparalleled reliability. For example, remote process automation control requires a staggering 99.9999% reliability, coupled with user-experienced data

rates reaching 100 Mbps and end-to-end latency not exceeding 50 ms. Such performance metrics are achievable, in part, due to the integration of Edge Computing capabilities.

- **Massive Internet of Things (mIoT)**: Numerous applications need 5G networks to accommodate an exceptionally high density of device traffic. The mIoT requirements encompass operational elements tailored to the diverse array of Internet of Things (IoT) devices and services expected to proliferate during the era of 5G.

- **Flexible Network Operations**: 5G provides a suite of distinct features, encompassing facets like network slicing, the revelation of network capabilities, scalability, varied mobility, enhanced security, efficient content dissemination, as well as migration and interworking.

1.1 5G Frequencies

As shown in Figure 1.1, in 5G technology the utilized frequencies are divided into two bands: Sub-6 Giga Hertz (GHz), where the frequency used is below 6 GHz, and millimiter Wave (mmWave) where the frequency used is above 24 GHz. Millimeter waves are so named because the wavelength at these frequencies is of the order of a few millimeters.

The higher speeds that truly distinguish 5G from 4G/Long Term Evolution (LTE) are achieved through the use of high-frequency mmWave bands. These high frequencies have very BandWidth (BW)s, making them ideal for handling a large number of active connections in crowded environments, such as stadiums. However, at these frequencies, the path attenuation suffered by electromagnetic waves is rather high, thus making transmission possible over fairly limited distances (of the order of a few tens of meters) [5]. In 5G, these two frequency bands have been defined as:

- Frequency Range-1 (FR1), for the Sub-6 GHz bands;

- Frequency Range-2 (FR2), for the mmWave, i.e., above 24 GHz [6].

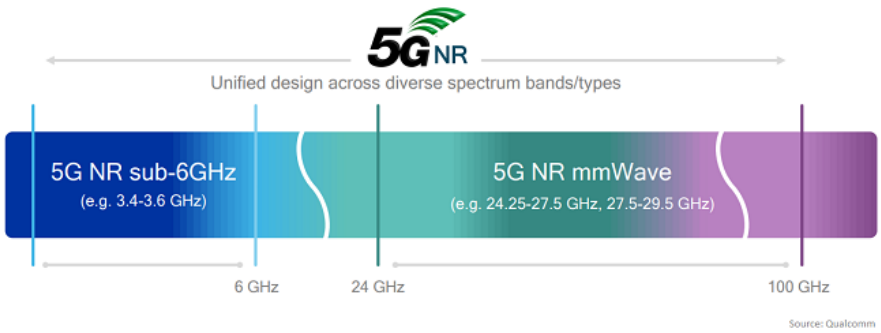

Figure 1.1: Frequencies used in 5G networks.

1.2 5G Protocol Stack

The 5G protocol stack is divided into two levels: (i) user plane protocol stack, related to the functionalities provided to the network users, and (ii) control plane protocol stack, related to the control and management of the network itself.

1.2.1 5G User Plane Protocol Stack

The *user plane protocol stack* is present in both end users (User Equipment, UE) and base radio stations, gNB in 5G terminology) and is composed of the following levels, starting from the highest, as shown in Figure 1.2:

- Service Data Adaptation Protocol (SDAP), responsible for the management of Quality of Service (QoS) flows;
- Packet Data Convergence Protocol (PDCP), responsible for header compression, data encryption, and integrity;
- Radio Link Control (RLC) and Medium Access Control (MAC), handling radio link management, multiplexing/demultiplexing, and channel access;
- Physical layer (PHY), where operations like encoding and decoding, modulation and demodulation, and beam mapping of antennas are performed.

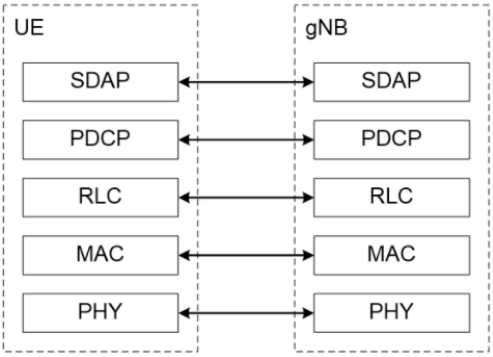

Figure 1.2: User plane protocol stack.

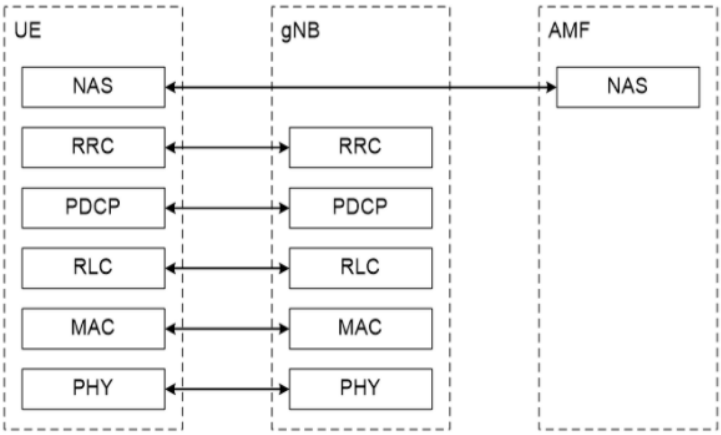

Figure 1.3: Control plane protocol stack.

1.2.2 5G Control Plane Protocol Stack

The *control plane protocol stack* is present in UE, gNB, and in the core entity responsible for managing access and mobility of nodes, known as Access and Mobility Management Function (AMF).

The four lower levels are identical to those detailed in Section 1.2.1, while the two upper levels are the following:

- *Non-access stratum*, present on UE and AMF, and responsible for authentica-

tion procedures, mobility management, and security aspects;

- Radio Resource Control (RRC), which operates (at the IP level) between UE and gNB, with its main functions being establishment/release of connection, distribution of system information, and creation of communication channels (*radio bearer*).

1.3 Communication Channels in 5G

To transport data across the 5G access network, information is organized into a series of channels. In this way, a 5G communication system is able to handle various data streams and process them appropriately. Indeed, the data to be transferred are diverse; therefore, the network must be capable of transferring both user data and the control and management information of the network itself.

Various data channels have been defined for radio communications. In order to group the data to be sent on the 5G radio access network, data is organized logically. The higher-level channels are "mapped" or contained within others down to the physical level, where the channel contains all data from the higher-level channels. In this way, there is a logical data flow manageable from the higher levels of the protocol stack down to the physical level.

There are three types of data channels used in 5G networks, schematically depicted in Figure 1.4:

- logical channels, divided into two groups:
  - control channels, used for transferring data from the control plane;
  - traffic channels, used for transferring user plane data;
- transport channels, which multiplex the logical data that needs to be transported by the physical layer and its channels on the radio interface;
- physical channels, which are closest to the actual transmission of data on the radio interface.

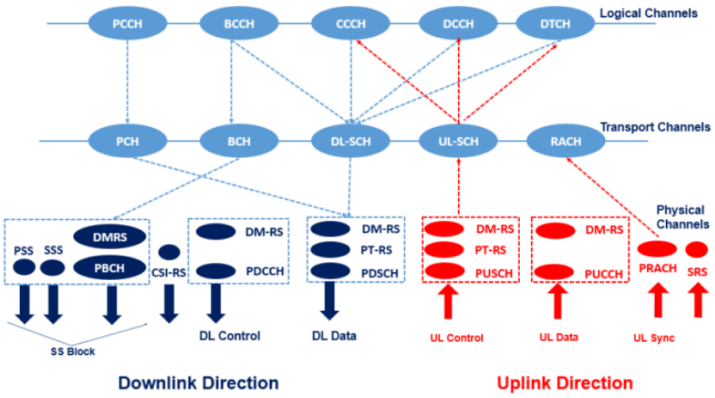

Figure 1.4: Diagram of 5G channels.

Physical and transport channels are the channels of interest, as the objective is to create a functioning point-to-point link in 5G technology. Therefore, in the following a precise description, distinguishing between communication from gNB to UE (DL) and vice versa (UL), is provided.

1.3.1 DL Physical Channels

The physical channels of interest in DL are the following.

- PDSCH, which is the channel that carries informational content, carries various types of data: user data, higher-level control messages, messages to signal the arrival of data to the UE (according to the mechanism known as *paging*), and System Information Blocks, SIB. The latter contain system information such as parameters for cell selection, timing synchronization parameters, etc.

- Physical Downlink Control CHannel (PDCCH), which is the channel that carries DL control data and whose main function is to schedule DL transmissions on the PDSCH and also UL data transmissions on the PUSCH. The PDCCH uses a modulation and encoding scheme based on *Quadrature Phase Shift Keying* (QPSK) and polar encoding.

- Physical Broadcast CHannel (PBCH), a channel included in the Synchonization Signal Block (SSB), whose function is to provide the UE with the Master Information Block (MIB), necessary for decoding the SIBs. Specifically, the SSB is an information block that encloses what is necessary for the UE to decode the various synchronization messages. Another function of the PBCH in combination with the PDCCH is to support synchronization in time and frequency. The PBCH uses QPSK modulation and transmits a specific cell demodulation reference signal known as DeModulation Reference Signal (DMRS). This signal can be used as an aid for forming the *beam* transmitted by the antenna.

1.3.2 UL Physical Channels

The physical channels of interest in UL are the following.

- Physical Random Access CHannel (PRACH), which is the channel dedicated to random access to the physical medium. In PRACH, an initial random access preamble consisting of Zadoff-Chu sequences [7] is transmitted, which can be of two different lengths: (i) a sequence of 839 symbols, used with sub-carrier spacing of 1.25 kHz and 5 kHz; (ii) a sequence of 139 symbols, used with sub-carrier spacing of 15 kHz and 30 kHz (FR1 bands) and 60 kHz and 120 kHz (FR2 bands).

- PUSCH, which represents the UL counterpart of the PDSCH in DL. It is used to transport data from its associated transport channel and higher channels, using frequency and time multiplexing. The allocation of frequency resources is performed using Resource Block (RB)s together with a flexible modulation and encoding scheme, which takes into account the signal-to-noise ratio of the link. To support the estimation and demodulation of the channel link, the PUSCH contains DMRS reference signals.

- Physical Uplink Control CHannel (PUCCH), which carries UL control data. It is also possible that, depending on the resource allocation, the information or

control data of the UL link can also be sent on the PUSCH (in DL, instead, control information is always sent on the PDCCH).

1.3.3 Signals in 5G Physical Channels

In the following, the signals used in physical channels are described [8, 9].

- DL/UL DMRS: It is the reference signal used by the receiver to estimate the quality of the radio channel and for decoding the physical channel associated with the DMRS transmission itself. The DMRS is specific for each UE and the various DMRS signals are specific for each physical channel described in the previous section. Usually, more DMRS, orthogonal to each other, can be transmitted in the case of Multiple Input Multiple Output (MIMO) configurations. In scenarios where the channel does not vary much, the DMRS is only sent during the initial phases of communication. Contrariwise, in high mobility scenarios, to be able to follow the variations of the channel, DMRS signals are sent periodically.

- DL/UL Phase-Tracking Reference Signal (PTRS): It is used to minimize the effect of oscillator phase noise on system performance. As the phase noise of a transmitter increases with the operating frequency, the PTRS plays a crucial role especially at mmWave frequencies. One of the negative effects that phase noise introduces in an OFDM signal appears as a common phase rotation to all subcarriers, known as Common Phase Error (CPE).

- DL Channel State Information Reference Signal (CSI-RS): It is received by the UE and is used to estimate the channel and report the information on its quality to the gNB. During MIMO operations, different approaches are followed for managing the antennas, based on the carrier frequency. At lower frequencies, the system uses a modest number of active antennas for Multi User MIMO (MU-MIMO) and adds Frequency Division Duplex (FDD) operations. In this case, the UE needs the CSI-RS to calculate the Channel State Information (CSI) and report it in the opposite direction.

- DL Primary Synchronization Signal (PSS) and DL Secondary Synchronization Signal (SSS): These are the signals used for synchronization (for example, during the search for a cell to attach to).

- UL Sounding Reference Signal (SRS): It is a UL-only signal, specific for each UE. The SRS is transmitted by the UE to assist the gNB in obtaining the Channel State Information (CSI) for each user. The CSI provides an estimate of the channel between the UE and gNB and represents the combined effect of scattering, fading, and power decrease with distance. The system uses SRS for resource planning, radio link adaptation, for *massive* MIMO, and beam management.

1.3.4 DL and UL Transport Channels

The transport channels of interest for this doctoral thesis are the Broadcast CHannel (BCH) and the DownLink Shared CHannel (DLSCH).

The BCH encodes information that is required by the UE to access the network and for sending the MIB, which in turn contains the parameters used at the radio level (e.g., frame number, subcarrier spacing, etc.). The information contained in the BCH is then mapped into the physical channel PBCH.

The DLSCH transport channel encodes user data and control information. The data are mapped into the physical channel PDSCH. Its counterpart in UL is the UpLink Shared CHannel (ULSCH), which is the only transport channel in UL that contains transport blocks. Also, regarding the ULSCH channel, it is mapped into the physical channel PUSCH.

1.4 Frame Structure

In the 5G standard, the frame represents a fundamental unit with which information is encoded in the transmitted waveform. The frame structure, both in the time domain and the frequency domain, is shown in Figure 1.5, where it can be seen how a series of 12 consecutive subcarriers forms a so-called RB. The single unit of a subcarrier

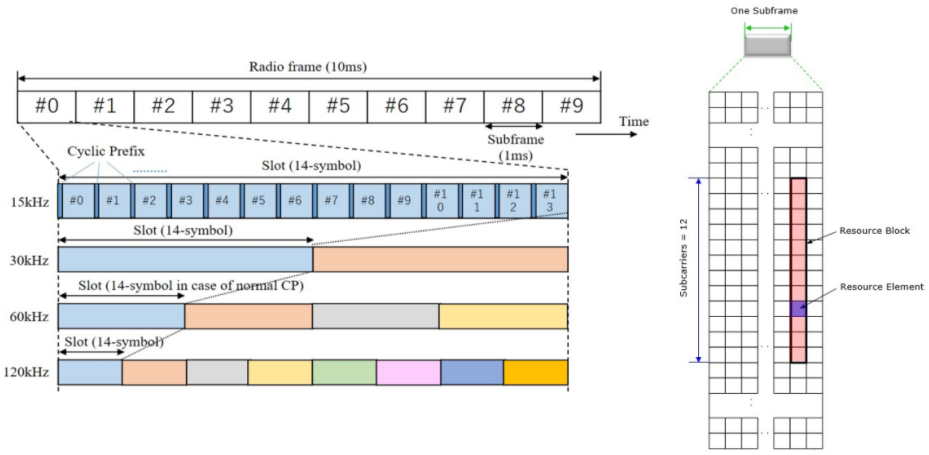

Figure 1.5: 5G Frame Structure.

(in the frequency domain) and its corresponding OFDM symbol (in the time domain) form a so-called Resource Element (RE). The 5G technology uses a non-fixed frame structure, with different SubCarrier Spacing (SCS) equal to (in kHz): 15, 30, 60, 120, 240. The duration of the OFDM symbol and the length of its Cyclic Prefix (CP), are inversely proportional to the SCS. As an example, with a SCS of 15 kHz, the duration of the OFDM symbol is about 66.6 μs, and the CP length is about 4.7 μs. Each doubling of SCS corresponds to a halving of the durations of the OFDM symbol and the CP. Data transmission is performed on a slot or possibly on fractions of a slot. In this way, short transmissions manage to meet the requirements for low latency services.

1.5 Comparison between 4G and 5G Technologies

In the following section, we provide a comparison between the main characteristics of 4G and 5G technologies is provided, in order to highlight the major changes that 5G will introduce compared to 4G. Table 1.1 highlights the main differences between the two physical layer standards, considering transmission parameters such as: frequency bands; modulation and encoding format, number of antennas used. In par-

Table 1.1: Comparison between 4G, sub-6GHz 5G, and mmWave 5G specifications.

Parameter	**4G**	**5G (sub 6GHz)**	**5G (mmWave)**
Frequency Range	700 MHz - 2700 MHz	410 MHz – 7125 MHz	24250 MHz – 52600 MHz
Supported Channel BW (MHz)	1.4 - 20	5, 10, 15, 20, 25, 30, 40, 50, 60, 80, 90, 100	50, 100, 200, 400
Subcarrier Spacing (KHz)	15	15, 30, 60	60, 120, 240
OFDM	DL	DL and UL	
Coding	Turbo and Convolutional	Polar and LDPC	
HARQ	UL-Synchronous DL-Asynchronous	UL and DL - Asynchronous HARQ	
Number of Antennas	4	96	128-256

ticular, the use of higher frequency bands, combined with advanced modulation and coding formats and arrays with a large number of antennas, allows reaching much higher transmission speeds, with an increase of an order of magnitude compared to the speed supported by 4G.

1.6 Critical Values for Vehicular Communications

5G networks will have a significant impact, especially on vehicular communications. Connectivity between vehicles (Vehicle-to-Vehicle, V2V) and, more generally, between a vehicle and any other entity (pedestrian, infrastructure, electronic device), known as Vehicle-to-Everything (V2X), is crucial to ensure various services in *automotive* scenarios, especially for [10]:

- safety, to handle emergency situations (emergency braking), intersection management, collision warning, and lane changing;
- vehicle management, operated by manufacturers, to improve efficiency, and to ensure the maintenance and monitoring of the vehicle itself;

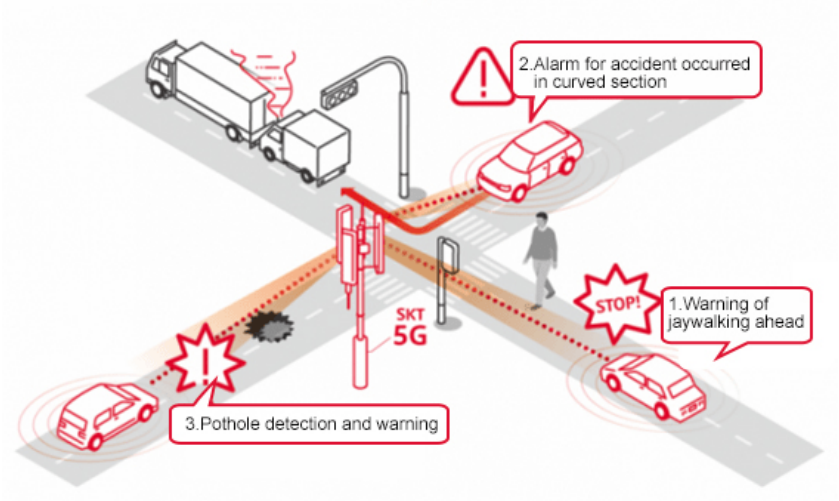

Figure 1.6: Examples of applications of 5G technology in the vehicular field.

- *infotainment*, to provide assisted/cooperative navigation services and intelligent parking services;
- autonomous driving, with integration with augmented reality services for remote driving support, map management, and cooperation between vehicles;
- *platooning*, to determine the position of vehicles during a "cooperative" driving, of particular interest for public transport and freight traffic;
- traffic management and reduction of harmful emissions in the environment, through the use of tools such as Green Light Optimal Speed Advisory (GLOSA), optimization of the routes to be followed (*smart routing*), and traffic information;
- interaction with "vulnerable" users, (Vulnerable Road User,VRU), to provide priority services (for example, green light) to emergency units such as ambulances, police, firefighters, or also to notify an accident and, consequently, optimally divert traffic.

Table 1.2: Requirements for warning messages for 5G vehicular networks.

Scenario	**Latency [ms]**	**Reliability [%]**	**Data Rate [Mbps]**
Cooperative collision avoidance between UEs supporting V2X applications	10	99.99	10
Emergency trajectory alignment between UEs supporting V2X applications	3	99.999	30
Intersection safety information between an RSU and UEs supporting V2X applications	n/a	n/a	50 (DL)
Video sharing between UEs and a V2X application	n/a	n/a	10 (UL)

Examples of applications of 5G technology in the vehicular field are shown in Figure 1.6.

Some numerical requirements about warning messages in vehicular scenarios, defined by the European Telecommunications Standards Institute (ETSI) [11], are provided in Table 1.2.

Chapter 2

Matlab-handled 5G Modem

The objective was to develop a 5G modem for vehicular communication and to conduct performance analysis of various antennas. This might be seen as an interesting and useful research activity especially in the case, public networks are not available in the immediate and surrounding neighbourhood geographic areas of interest. Consequently, it could be possible to exploit Matlab and its well-known toolboxes in order to define a 5G modem, in detail designing both gNB and UE. This chapter outlines the various phases involved in developing such a system, beginning with simulations, followed by detailing the experimental setup, trials conducted, and preliminary experimental results.

2.1 Simulation of a 5G Connection

As a first step, an overall evaluation of the potential of the Matlab 5G Toolbox, selected for building the envisioned 5G prototype is needed. In detail, this toolbox offers functionalities compliant with standards and provides representative benchmarks to model, simulate, and authenticate 5G communication systems.[1] It aids in the configuration, emulation, and comprehensive assessment of a 5G connection. The toolbox

[1] As of September 2020, the toolbox is undergoing continuous enhancements, with each software update bringing new capabilities.

encompasses a multitude of sample benchmarks, which are modifiable for the conception and execution of various 5G technologies and apparatus.

Then, in order to evaluate the software tool's efficacy, different simulations of a 5G link have been executed, and performance metrics were analyzed with a focus on *throughput*. This metric was gauged utilizing the default examples present in the *toolbox*, particularly on the PDSCH [12] and PUSCH [13] channels. In fact, these channels are pivotal as they serve as the primary conduits for transmitting informational data.

Latency was not a focal point in this initial evaluation due to a couple of reasons:

- given that both the receiving and transmitting functions operate on a singular machine, any latency evaluation becomes rather inconsequential;
- assessing performance based on latency is complex as it intricately relates to the processing duration of the devices in use, making it a challenging metric to pinpoint accurately.

2.2 5G System Model

The block diagram of the simulated system is shown in Figure 2.1, considering both the PDSCH channel (case (a)) and the PUSCH channel (case (b)).

In both scenarios, the transmitted signal is crafted utilizing the *Matlab 5G Toolbox*, which carries out all standard processes, encompassing coding and OFDM modulation with an accompanying cyclic prefix. Post generation, the signal navigates the channel, incurring distortions from fading and Additive White Gaussian Noise (AWGN). The fading emerges via the renowned Clustered Delay Line (CDL) model for the PDSCH, and the acclaimed Tapped Delay Line (TDL) model for the PUSCH. Both transmissions utilized a 2x2 MIMO configuration. At the receiver's end, following waveform demodulation and noise estimation, the payload undergoes decoding, enabling throughput computation as the SNR shifts.

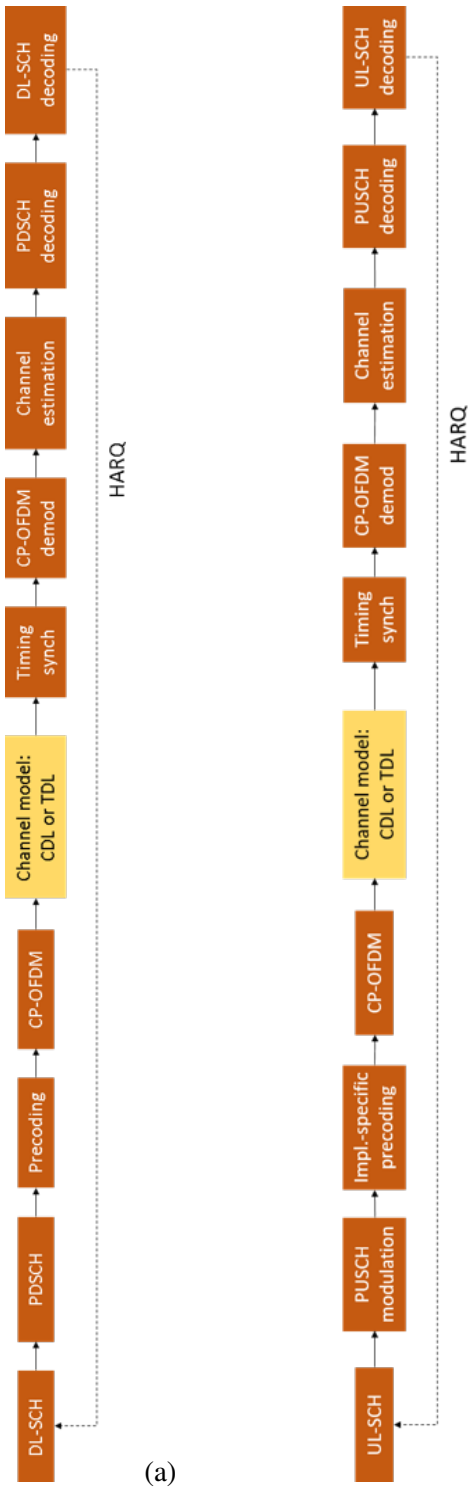

Figure 2.1: Block diagram of the 5G connection simulation: (a) PDSCH channel transmission and (b) PUSCH channel transmission.

Table 2.1: Parameters for PDSCH simulation.

Antenna Configuration	2×2
Subcarrier Spacing	15 kHz
Bandwidth	10 MHz
Cyclic Prefix	Normal
Number of RB	52
Coding Rate	0.5
Modulation Format	16-Quadrature Amplitude Modulation (QAM)
Channel Delay Spread	300 ns
Channel Doppler Shift	10 Hz
PDSCH Levels	2

2.3 Numerical Findings

Table 2.1 and Table 2.2 encapsulate the parameters employed during the PDSCH and PUSCH channel transmission simulations. Figure 2.2 portrays the throughput (denoted as a percentage) versus the SNR within the PDSCH channel transmission context.

The graph accentuates outcomes at representative SNRs: -5 dB, 0 dB, and 5 dB. Anticipatingly, throughput surges as SNR elevates; superior SNR denotes enhanced communication channel quality, thereby augmenting the throughput. Particularly, with an SNR at 5 dB, a throughput nearing 95% is achieved, translating to approximately 60.33 Mbps.

Subsequently, Figure 2.3 unveils the throughput (expressed in percentages) against SNR within the PUSCH channel transmission framework.

Analogous deductions can be inferred as those articulated for the PDSCH channel depiction. Notably, with an SNR set at 5 dB, a throughput approximating 100% is discerned, equivalent to nearly 7.42 Mbps.

Table 2.2: Parameters for PUSCH simulation.

Antenna Configuration	2×2
Subcarrier Spacing	15 kHz
Bandwidth	10 MHz
Cyclic Prefix	Normal
Number of RB	52
Coding Rate	0.5
Modulation Format	QPSK
Channel Delay Spread	30 ns
Channel Doppler Shift	10 Hz

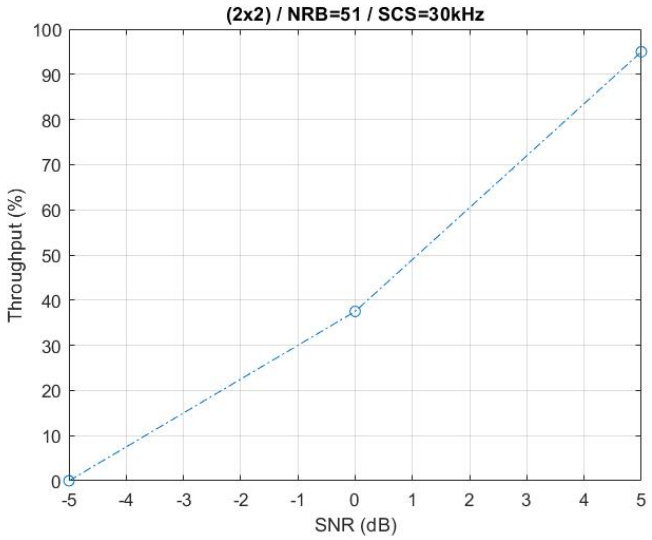

Figure 2.2: Throughput, represented as a percentage, plotted against SNR for the PDSCH channel transmission.

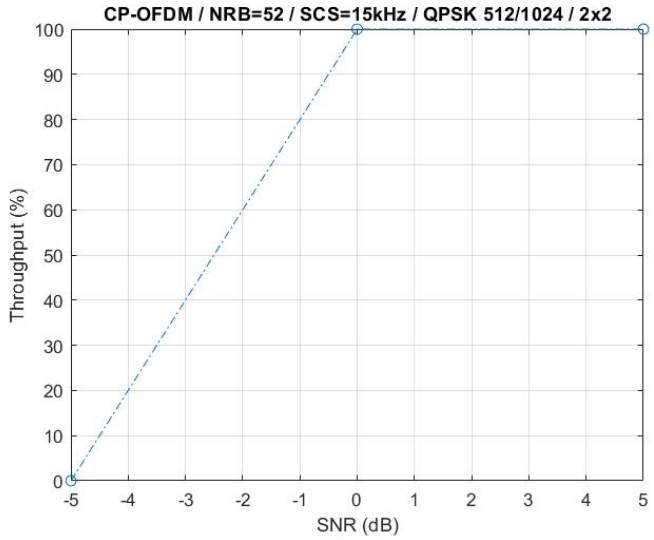

Figure 2.3: Throughput, illustrated as a percentage, in relation to SNR for the PUSCH channel transmission.

2.4 Hardware/Software *Co-design*

Latency plays a crucial role in 5G V2X communications, underscoring the necessity of its accurate measurement. As discussed earlier, it's impractical to simulate latency, and the results vary greatly based on the device employed. A more pragmatic approach is to leverage standalone devices, adhering to the 5G protocol stack, which transmit waveform compliant with the said standard.

For this undertaking, the FPGA emerges as the go-to standalone device, as it accepts a payload, sourced from the vehicle's onboard sensors, which is then relayed using an radio front-end (FE). Another FPGA on the receiving end is tasked with decoding this transmitted waveform. This communication blueprint is depicted in Figure 2.4.

In the formative experimental phase, a transitional system was conceived as a precursor to the final structure illustrated in Figure 2.4. Here, the waveform genesis is spearheaded by a laptop, whereas the FPGA serves a "transparent" role, facilitat-

Figure 2.4: Illustration of the comprehensive system layout.

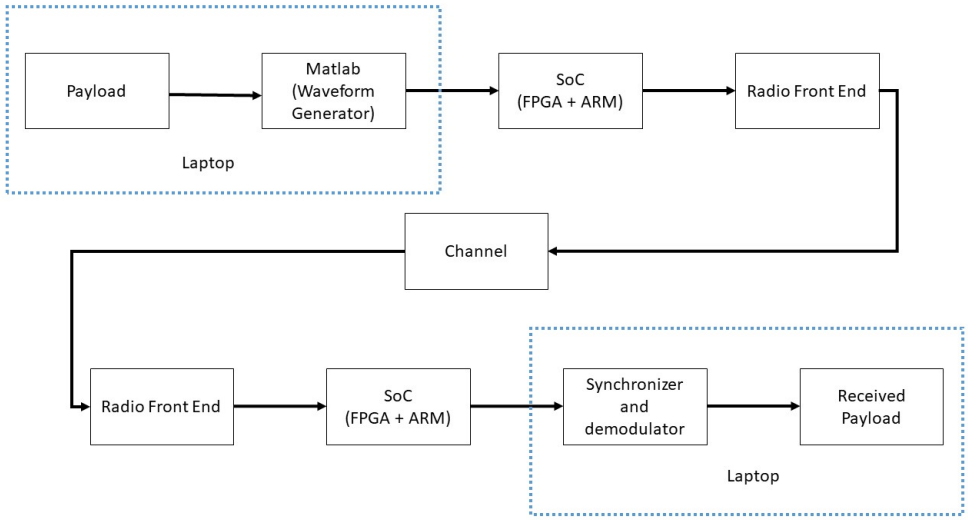

Figure 2.5: Blueprint of the system during the nascent phase of prototype formulation.

ing the waveform passage to the radio FE. The schematic of this interim system is elucidated in Figure 2.5.

Elaborating further, in this setup, the FPGA isn't actually programmed. Instead, the development board—which amalgamates the FPGA and a microprocessor—functions as a bridge to the radio FE.

2.5 Experimental Devices

The main devices used in the experimental phase are the following:

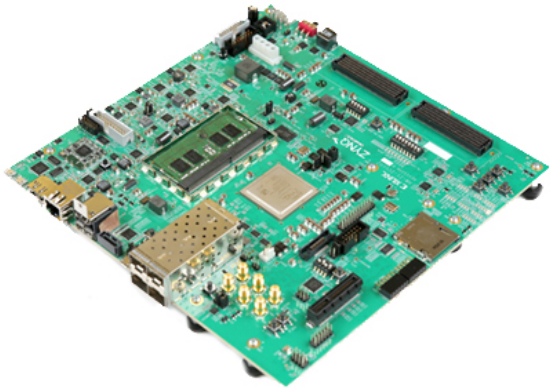

Figure 2.6: Zynq UltraScale+ MPSoC ZCU102 Evaluation Kit.

- a System-on-Chip (SoC), which represents the "intelligent" part of the system to be developed, consisting of an FPGA and an Advanced RISC Machine (ARM) processor;
- a FE, which serves as the radio interface used by the SoC to communicate with (possible) other devices, to which both SMA/SMA cables and antennas can be connected.

The specific devices used as SoC and FE are briefly illustrated in the following subsections.

2.5.1 Zynq UltraScale+ MPSoC ZCU102 Evaluation Kit

The SoC used is a Zynq UltraScale+ XCZU9EG-2FFVB1156E MPSoC (Multiprocessor SoC) board, based on the Xilinx UltraScale MPSoC architecture [14]. This board was chosen based on its compatibility with Matlab and its support for the required features for generating HDL code from Matlab. In the rest of the doctoral thesis, it will be referred as Xilinx, for notation simplicity.

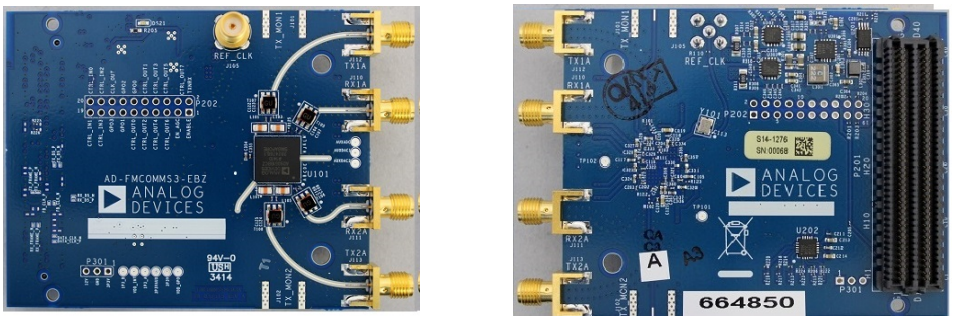

(a) (b)

Figure 2.7: Analog Devices AD-FMCOMMS3-EBZ Front End: (a) top view; (b) bottom view.

2.5.2 Analog Devices AD-FMCOMMS3-EBZ

The device used as FE is an Analog Devices AD-FMComms3-EBZ board (hereafter referred to as FE, for simplicity of notation). In detail, this device allows operation in the frequency range of 70 MHz ÷ 6 GHz, with a BW that can vary within the range of 200 kHz ÷ 56 MHz and supports a multi-antenna configuration (MIMO). Moreover, it is powered through the FPGA Mezzanine Card (FMC) port used for connecting to the Xilinx and supports phase and frequency synchronization.

2.6 Experimental Architecture

Since the ultimate goal is the development of a 5G modem (which a vehicle can be equipped with) applicable to different testbeds and antennas, various testbeds have been considered. More in detail, the starting phase was to conduct simulations, then followed by trials with signal transmission over the air.

The following test models have been considered: loopback model and P2P model.

2.6.1 Loopback Model

The initial model under consideration is the loopback model, whose block diagram is shown in Figure 2.8. This model primarily comprises a laptop equipped with a Matlab 2020a [15] instance operating at the software level. Then, the laptop is interfaced with a Xilinx Zynq [14] board, which a FE is connected to, serving both transmission and reception purposes. On the basis of this setup, the waveform, crafted by a Matlab script, is broadcasted continuously with the combined efforts of the Xilinx Zynq board and the FE. The same FE subsequently receives the signal, with its receiver ports (attached to antennas) capturing the airborne signal. Post-capture, another Matlab script processes this signal, estimating the traversed channel. Following this estimation, the data contained in the PDSCH (on the UE) or the PUSCH (on the gNB) is decoded. The final step involves decoding the output bits and contrasting them with the original transmitted bits, facilitating the evaluation of the bit error rate. It's pivotal to note that since all operations deploy singular FEs, the generated carrier frequencies remain consistent. Consequently, there's no pressing need to calibrate the FE.

Wired loopback

Figure 2.9 shows the experimental setup of a wired loopback arrangement. A cable is used to connect the antenna ports TX1A and RX1A of the FE.

Wireless loopback

In the wireless configuration, on the other hand, the cable was replaced by two omni directional antennas, depicted in Figure 2.10, connected to the TX1A and RX1A ports. The main features of the used antennas are:

- a maximum gain equal to 10dbi;
- support for 2.4 GHz and 5.8 GHz frequencies;
- an input impedance equal to 50 Ohm;

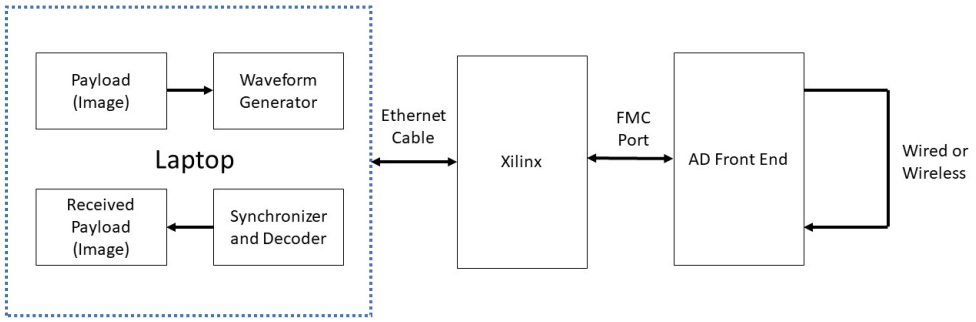

Figure 2.8: Block diagram of the used configuration.

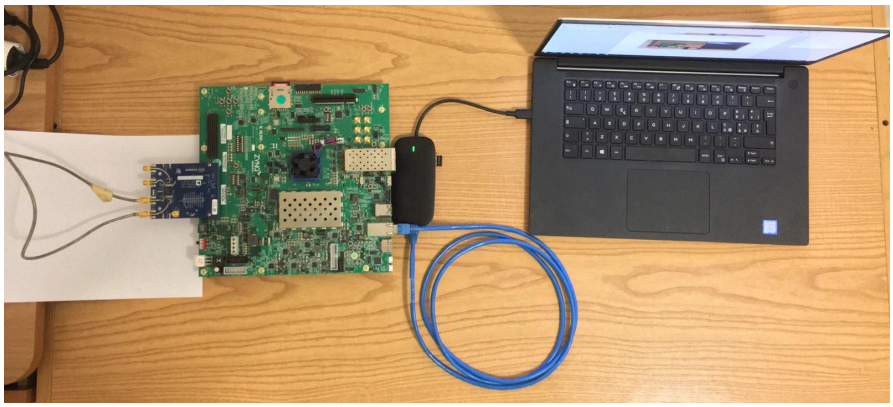

Figure 2.9: Experimental setup with wired *loopback*.

- a Voltage Standing Wave Ratio (VSWR) equal to 1.5.

An image of the used antennas is shown in Figure 2.10, while the wireless *loopback* setup is depicted in Figure 2.11.

Figure 2.10: Antenna used in the tests.

Figure 2.11: Experimental setup with Wireless Loopback model.

2.6.2 P2P model

The loopback model, as outlined in Section 2.6.1, served as the basis for initial evaluations and to conduct some rudimentary tests. Subsequent efforts aimed to emulate real-world operational conditions by designating one pair of FPGAs and FEs to function as a gNB, and another pair to emulate the behavior of a UE. This distinction is paramount to realize a genuine P2P setup. As such, the creation of a P2P connection involved multiple configurations, contingent upon the waveform intended for transmission. The distinct P2P models employed in the development of a Matlab-centric 5G modem include: (i) exclusive UL/DL, and (ii) simultaneous UL/DL.

Exclusive UL/DL Model

As shown in Figure 2.12, two laptops, each running an instance of Matlab, are used in this "exclusive" configuration. Specifically, one laptop, paired with its associated Xilinx Zynq board, functions as the (UL/DL) transmitter. In contrast, the second laptop operates as the (UL/DL) receiver. The chosen center carrier frequencies, in line with the Third Generation Partnership Project (3GPP) R15 standards, have been set to 2.1 GHz for the DL and to 1.92 GHz for the UL. Further experimental trials using varied carrier frequencies have been conducted, still adhering to the 3GPP R15 guidelines. It's noteworthy to mention that this exclusive configuration is suitable for either UL or DL communications.

Simultaneous UL/DL Model

In the model discussed in Section 2.6.2 either the UL and the DL are operated at a time. In the current scenario, instead, the model adopted is a combination of UL and DL, as shown in Figure 2.13. In detail, in this case the P2P communication system is composed, as shown in Figure 2.14, by a laptop running simultaneously two Matlab instances: one acts as a gNB and the other one acts as a UE. The laptop is connected to an Ethernet switch which is connected to the gNB and UE nodes (FPGA+FE) using CAT5 cables. The gNB transmits DL waveforms and decodes the UL waveforms received from the UE. On the opposite, the other Matlab instance receives the DL waveform, decodes it, creates the UL waveform, and transmits it.

2.6.3 Testbed Calibration

As discussed in Section 2.6.1, a loopback model-based system does not require a calibration phase. This is no longer true in the case of a P2P-based communication system, where two FEs have to be used. In detail, this requirement has been highlighted after some initial evaluations, which clearly showed the presence of errors in the decoded data—the same codes, used in loopback configuration for waveform decoding, did not show any error after the decoding phase. The reason behind the error was due to the fact that the oscillators used in the FE are not accurate in the

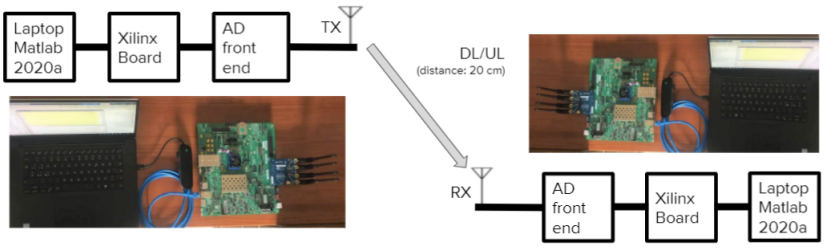

Figure 2.12: Block diagram (with photos) of exclusive UL/DL model.

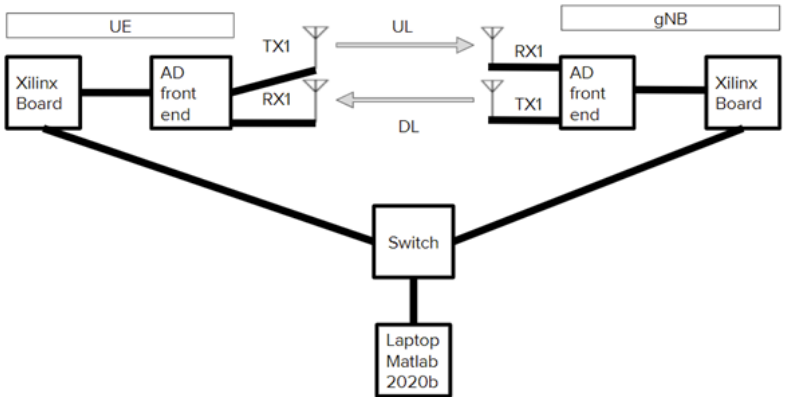

Figure 2.13: Block diagram of the contemporary UL/DL model.

parts per million (ppm) range, thus resulting in carrier frequencies being different at transmitter and receiver sides. This issue can be overcome by calibrating the FE: both devices have to be calibrated and have to transmit with the same central frequency to be able to perform a proper decoding of the received data. In detail, as a first solution, the simplest way was to calibrate both the FEs by transmitting a sine wave from a FE and receiving the same signal with the other FE. Then, the receiver FE detects the signal and compares it with the preset sine wave at 10 kHz, highlighting the difference in the carrier frequencies. Accordingly to this result, the carrier frequency of the receiver is updated, in detail adjusting the central frequency by 2.8610 kHz. This offset leads to a useful realignment, with both the devices transmitting and receiving

Figure 2.14: Real deployment of the contemporary UL/DL model.

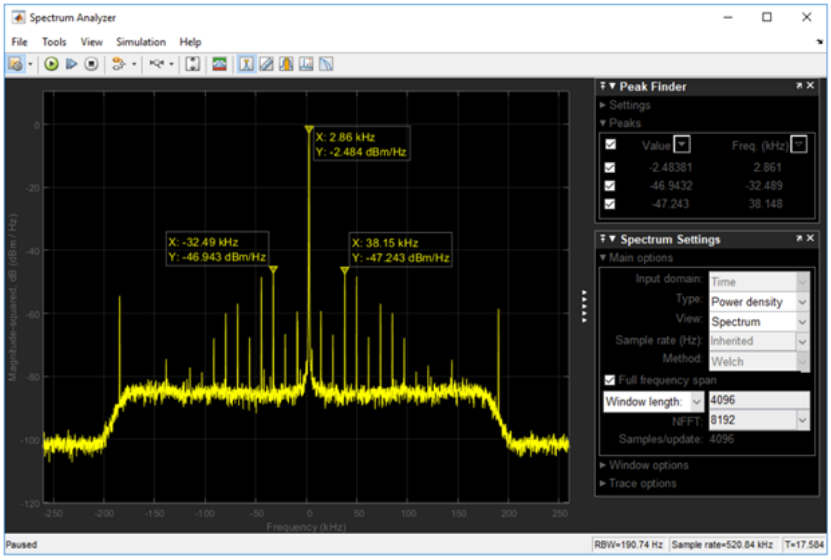

Figure 2.15: Calibration of the FEs.

at same central frequency.

In Figure 2.15, the difference in the carrier frequencies is shown. In detail, the frequency offset used for the calibration is determined by using two Matlab scripts, one for the transmitter entity and another one for the receiver entity. The transmitter then sends a 10 kHz tone and the receiver detects the transmitted tone using a Fast

Fourier Transform (FFT)-based detection method. Then, the offset between the transmitted 10 kHz tone and the received one can be estimated and used to compensate for the offset at the receiver side [16].

2.7 Device Setup

The ultimate goal of the experimental phase is the transmission of an image, appropriately encoded in 5G physical channels and transmitted through different experimental architectures previously discussed.

The various operations performed are detailed below. Specifically, the *wireless* scenario, of greater interest in the direction of antenna development, has been targeted. Additionally, the wired *loopback* configuration is the same and results in error-free transmission.

More in details, the FE connected to the Xilinx has been configured using the *Communications Toolbox Support Package*, selecting, the following parameters:

- *baseband sample rate* equal to 61.44 Msample/s on a 40 MHz BW [17];
- transmitting antenna gain equal to -10 dBi (given the short distance between the two antennas);
- receiving antenna gain equal to 0 dBi;
- transmission frequency equal to 4.1 GHz.

2.8 Hardware-Software Implementative Approach

During the prototyping phase, directly developing code in Hardware Description Language (HDL) for FPGA resulted in being not deemed efficient: it would be time-consuming and lack the flexibility of alternative approaches. Instead, there has been opted for the hardware/software co-design model. This development strategy enables the delineation of tasks between the programmable logic of the FPGA and the processor on the development board. Once the design is finalized, the requisite code (HDL

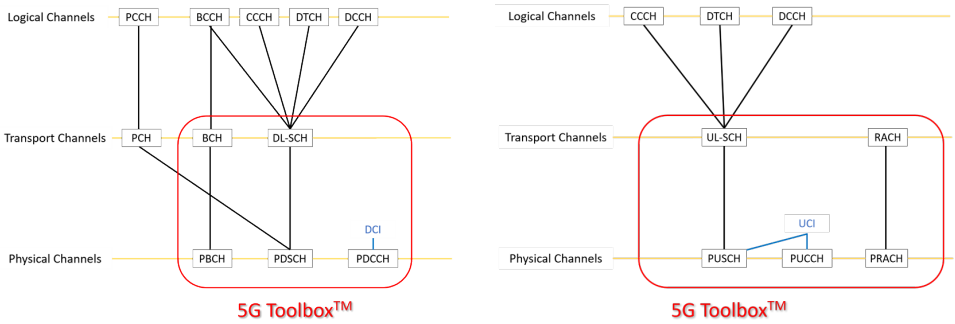

(a) (b)

Figure 2.16: 5G Toolbox in Matlab and 5G channels: (a) DL channel mapping; (b) UL channels

.

for FPGA and C for the processor) can be auto-generated using specific Matlab functionalities.

As alluded to in Section 2.7, we utilized Matlab 2020a, throughout the development phase, has been selected and used in this phase. Notably, the 5G Toolbox has been of particular relevance, providing standard-compliant 5G functions and reference examples that are instrumental for modeling, simulation, and verification of 5G New Radio (NR) communication systems.

This is moreover true since the 5G Toolbox facilitates the generation of UL and DL waveforms by allowing the customization of desired parameters such as subcarrier spacing, coding rate, and encoding scheme. The range of channels that can be accessed through this toolbox is depicted in Figure 2.16. An integral component of the toolbox is the Wireless Waveform Generation App, with its primary interface illustrated in Figure 2.17. This application not only assists in generating transmittable waveforms but also integrates seamlessly with a spectrum analyzer within the Matlab ecosystem. It provides a comprehensive platform to configure all the parameters associated with the physical layer of 5G technology, along with the parameters pertinent to channel modeling.

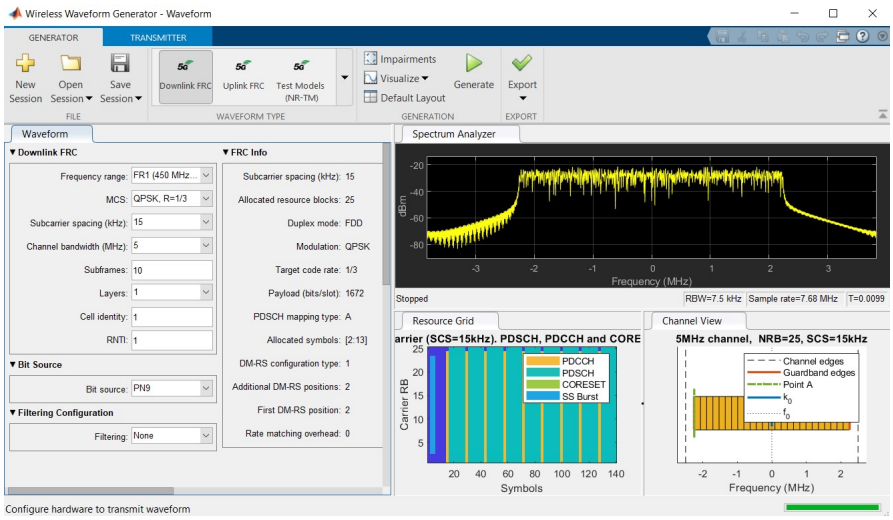

Figure 2.17: 5G Wireless Waveform Generator App within the 5G Toolbox.

2.9 Preliminary Results with 4G Networks

The preliminary tests focused on validating the hardware considered in this phase of the doctoral activities using the 4G/LTE network. This choice was compelled by the absence, at the time of development, of a 5G network to use for the experimental phase. Moreover, through these tests, it is possible to verify the proper functioning of the hardware itself on a commercial network like 4G.

The test carried out involved scanning the LTE network [18], and looking for available cells in the 1820 MHz band. In the test, the laptop was connected via an Ethernet cable to the Xilinx, which in turn is connected to the FE via the FMC port. The block diagram of the cell search procedure is shown in Figure 2.18. Specifically, the decoding procedure allows the extraction of the MIB from the signal, which contains information about the number of DL RBs (NDLRB), including the used BW, the frame number (System Frame Number, SFN), and the error correction configuration (LTE networks use the HARQ scheme).

In detail, the signal is detected by the FE, and the signal synchronization is performed; then the OFDM signal is demodulated, and the resource grid is created,

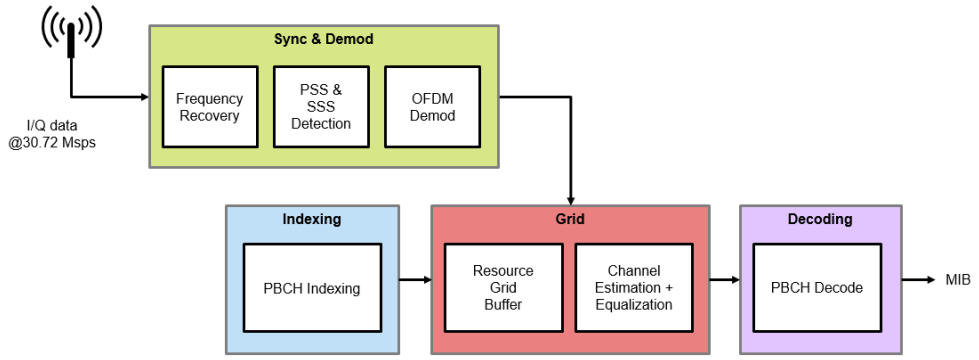

Figure 2.18: Block diagram of the LTE network search.

containing information on the number of subframes and the cell ID. The subframe indexed at 0 contains the MIB; the cell ID is used to identify the reference signal associated with a cell (Cell-specific Reference Signal , CRS) and to initialize the descrambling sequence for PBCH decoding.

After estimating the CRS, the CRS value is compared with the expected values, and the phase offset is calculated. The channel estimates for each CRS are then averaged over time, and the channels of the subcarriers that do not contain CRS are estimated using linear interpolation.

The next step is the decoding of the PBCH. The PBCH is always allocated in the 6 central RBs of sub-frame 0, in the first 4 OFDM symbols of the second slot. The PBCH occupies all elements of this block, except for the elements allocated to the CRS. The elements related to the CRS are first identified, and then the elements related to the PBCH (240 symbols) are obtained. The data contained in the PBCH are first equalized using the channel estimate obtained through the CRS, and then the 240 symbols are decoded. At the end of this operation, the information shown in Figure 2.19 is obtained: in the upper part of the chart, the frequencies where a signal (thus a cell) was detected are shown in blue, and the currently scanned frequency is in red; in the lower part, among various pieces of information, the main one of interest

Figure 2.19: Result of the experiment for the retrieval of the Cell ID and MIB.

is the cell ID.

The above process can be carried out in two ways:

- entirely on the SoC, partly on the FPGA and partly on the ARM processor (both on board the Xilinx);
- partly on the FPGA and partly in Simulink on a laptop.

The task of the ARM/Simulink is to control the FPGA: the values to be used in the estimation and decoding processes are checked, and the final results are sent to the laptop to be displayed.

2.10 5G Experimental Trials

The experimental phase specifically involved the transmission of an image. Two configurations were considered, a wired and a wireless one. In both configurations, the Xilinx, connected to the laptop via an Ethernet cable, is used in a "transparent" manner and serves as an intermediate interface between the laptop and the FE. All processing operations are thus carried out on the laptop, via Matlab scripts. In both the wired and wireless configurations, a single laptop acts both as a transmitter and receiver, and one port of the FE is used for transmission and another for reception. MIMO transmissions are not considered in this preliminary phase. This configuration is, for this reason, referred to as *loopback*. A schematic of the configuration is shown in Figure 2.8.

In the wired configuration, the two ports of the front-end used for transmission and reception, namely TX1A and RX1A, are connected via an SMA cable. An image of the wired *loopback* setup is shown in Figure 2.9.

Furthermore, this scheme serves as a verification of the overall functioning of the system. In fact, in this configuration, a nearly ideal channel is emulated, with almost zero latency and minimal losses and distortions introduced by the cable itself. The elimination of errors on the communication channel thus allows any implementation issues to be isolated.

2.10.1 DL Transmission and Reception

During the experimental phase, Matlab scripts were developed for both the transmitter and receiver. Development began with the *NR PDSCH Throughput* [19] and *NR Synchronization Procedures* [20] examples, available among Matlab's resources. Figure 2.20 shows the DL arrangement. The first step was configuring the SSB parameters, specifically choosing the following values:

- 40 MHz BW;
- SCS equal to 30 kHz;
- 106 RBs according to standards[21];

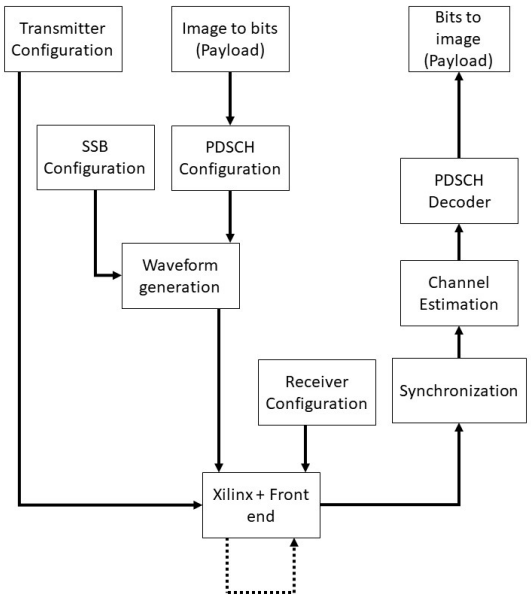

Figure 2.20: Block diagram of the conducted experiment for encoding and transmitting an image.

- OFDM prefix chosen as cyclic;
- Cell ID fixed at 136;
- *block pattern* fixed as "Case B" according to the standard.

In the current architecture, the transmitter does not estimate the channel, as there is no feedback system to provide information on the channel's status. This choice is due to the specific configuration, with the transmitter and receiver on a single laptop, making such adaptation impossible. To manage the wireless channel and minimize the error rate as much as possible, a transmission scheme with a low coding rate (1/3)

Table 2.3: Parameters selected for the PDSCH.

Parameter	Prefered Value	Selected Value
DM-RS port	n/a	0
PDSCH mapping	A (slot-wise) B (non slot-wise)	A
Front-loaded DM-RS symbols	1, 2	1
Additional DM-RS symbol positions	0...3	0
DM-RS configuration type	1, 2	2
CDM groups without data	n/a	1
Scrambling identity	0...65535	1
Scrambling initialization	0, 1	0
Disable interleaved resource mapping	n/a	0

and reduced constellation modulation (16-QAM) is used.

Using these parameters, the transport block size (the length of a slot) is 22032 bits (obtained using the Matlab function “PDSCHTBS”). Since the original image has a size equal to 86528 bits, it must be resized to fit within a single slot. This condition is dictated by the Matlab version available at the time of system development: frame numbering is not available, so only one frame can be transmitted at a time. The image is therefore resized by a factor of 0.05, and the color format set to 8 bits, resulting in a final size of 6936 bits. This size allows the image to be transferred in a single sub-frame. Although this does not make it directly distinguishable in its details, it allows the experiment to proceed.

PDSCH Parameters and Encoding

The first step regarded the configuration of the PDSCH parameters, listed in Table 2.3.

The PDSCH channel is added, along with the SSB, to the resource grid, which initially contains zero values. It is necessary to specify the subcarrier’s position to

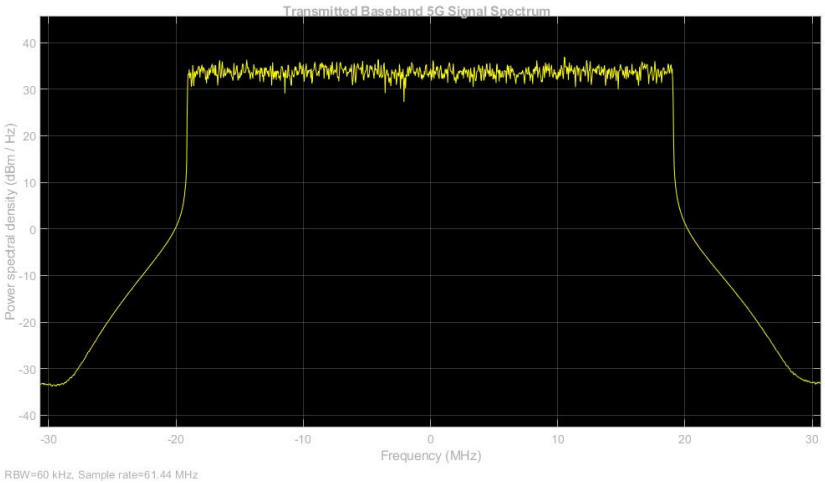

Figure 2.21: Spectrum of the transmitted signal.

avoid overlaps. For the packet encoding, a DLSCH encoder is created, and finally, the transport block size is calculated to be 22032 bits (again calculated using the Matlab function “PDSCHTBS”).

Since the transport block size calculation is carried out at the PDSCH level, the image in the developed code is scaled only after selecting the various PDSCH-related parameters and completing the transport block size calculation. After configuring the PDSCH-related parameters, the image is scaled and then converted into 8-bit unsigned binary symbols; using the PDSCH parameters, the DLSCH encoder and the transport block are generated. The latter is then modulated with a 16-QAM format.

From this operation, the PDSCH symbols are obtained, which are then mapped onto the resource grid in the blocks reserved for them. The SSB grid is then modulated with the OFDM format, and the waveform, whose spectrum is shown in Figure 2.21, is repeatedly transmitted. Since the same device is used both as a transmitter and receiver, sending and receiving packets cannot be executed simultaneously. Therefore, once the image is transmitted, it is buffered in the ARM processor, and the receiver’s FE captures it and sends it to the laptop.

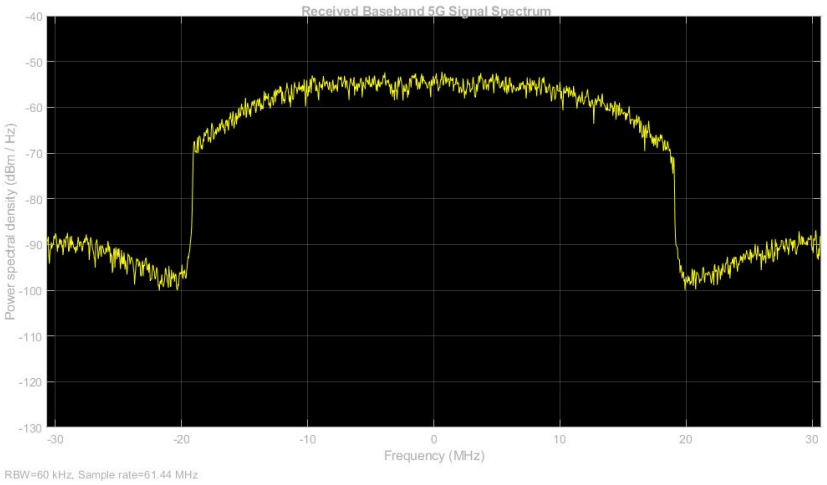

Figure 2.22: Power spectrum of the received signal.

Waveform Reception

At the receiver, the radio signal is captured for a time equal to the sum of the duration of the *frames* (which last 10 ms) that need to be received, and the duration of a "guard" *frame*. The latter is used to avoid the loss of a *frame*. For example: sending 10 *frames*, the duration is 10·10 ms =100 ms; in case of a synchronization error, one of the *frames* would only arrive partially. For this reason, the receiving radio interface remains on for an additional time equal to a *frame*, in order to correctly receive all the informational content.

In the case of the experiments described in this report, we refer to the reception of a single *frame* at a time, whose waveform is shown in Figure 2.22. The receiving radio thus remains on for a time equal to 2 *frames*.

Time and Frequency Synchronization

A fundamental aspect to have a correct data reception is the synchronization in the time and frequency domain. Therefore, the first operation performed by the receiver is to execute the search for the primary synchronization signal (PSS). This procedure

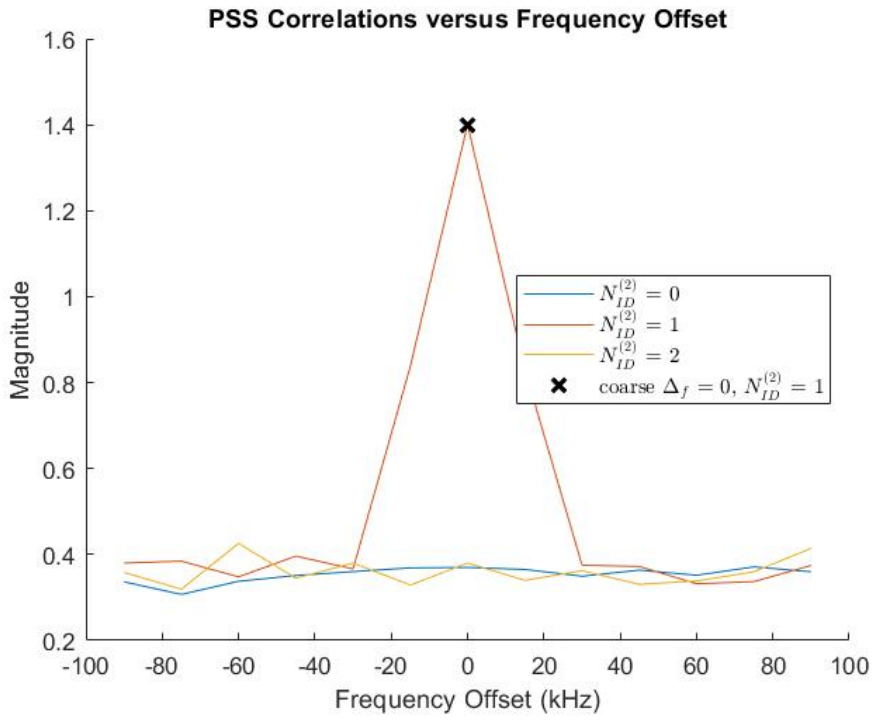

Figure 2.23: Example of PSS correlation for different frequency offset values.

consists of correlating the received waveform (considering all the SS/PBCH blocks) with each of the three possible PSS sequences and extracting the strongest correlation peak. The SS / PBCH block with the strongest correlation peak indicates which *beam* is most effective in directing the signal towards the receiver. In particular, the index relative to the beam is contained in the MIB; once the PSS signal is received and decoded, the MIB obtains information about the beam with the greatest correlation and the transmission will take place in the direction of that particular beam. The frequency offset of the received waveform is also determined, evaluating several possible values, trying to correct for each of them, and finding the one that provides the strongest correlation. Figure 2.23 shows an example of PSS sequence correlation at different frequency offset values.

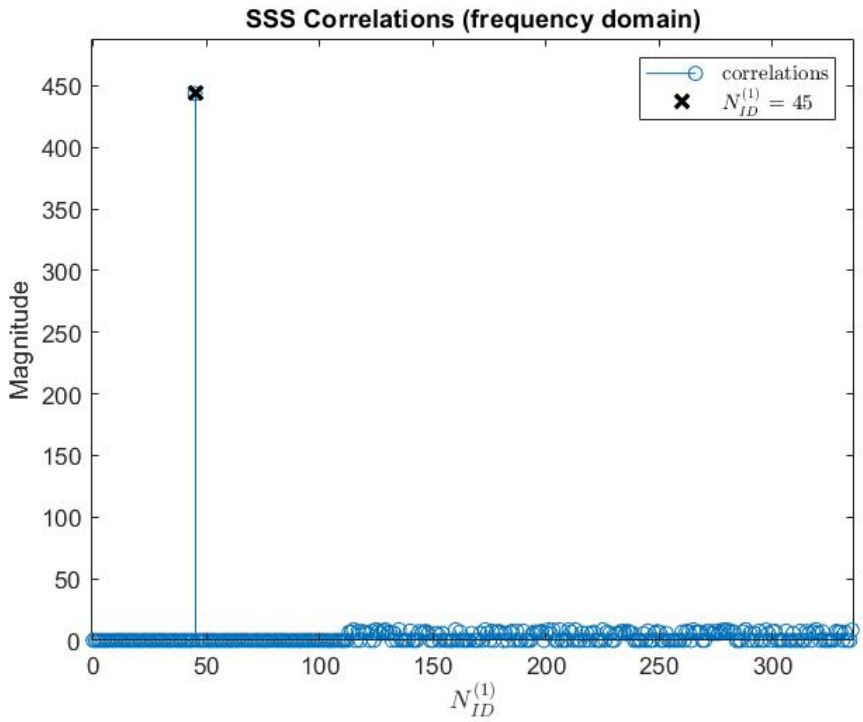

Figure 2.24: Correlation of the received signal with possible SSS sequences.

The time offset for the strongest PSS sequence correlation is used to synchronize the waveform in time. It is then possible to calculate a fine estimate of the frequency offset by performing the correlation between the cyclic prefix of each OFDM symbol in SSB and the corresponding useful parts of the OFDM symbols. The phase of this correlation is proportional to the frequency offset in the waveform.

The PSS correlation peak value is used to synchronize the waveform, and OFDM demodulation is performed. The subcarriers associated with the secondary synchronization signal (SSS) are extracted and correlated with each of the 336 possible SSS sequences. Figure 2.24 shows the correlation between the SSS sequences. The indices of the strongest PSS and SSS sequences are combined to provide the physical layer cell identity, necessary for PBCH DM-RS and PBCH processing.

(a) (b)

Figure 2.25: Transmitted (a) and received (b) image.

OFDM demodulation is performed on the received data to recreate the resource grid, including padding in case the synchronization leads to an incomplete sub-frame. The PDSCH channel symbols are extracted from the resource grid, and then the symbols are equalized (using the Matlab function *nrEqualizeMMSE*). The physical PDSCH channel and subsequently the DLSCH transport channel are then decoded. Finally, the informational content is extracted and the image is reconstructed: the bits are scaled to the correct length, converted into a new format (*int16*), and finally, the image is recreated.

In the general case of sending multiple *frames* (foreseen as future development), after decoding operations, before reconstructing the image, the MIB takes care of the reordering of the *frames*, which are received unordered. However, since in the experiment described only one *frame* is received at a time, the MIB performs no operation. All operations described in this section are performed cyclically for each received *frame*.

The transmitted image is recreated and shown in Figure 2.25. The bit error rate (BER) of the received image is equal to 0, meaning that there were no errors of any kind. In fact, the experiments were carried out in ideal conditions with a perfect channel and a modulation format with low spectral efficiency but high energy efficiency. An important observation also concerns latency, a fundamental parameter of 5G networks. Regarding latency, finally, in this preliminary experimental phase, latency cannot be measured: the system is in a *loopback* configuration and works under

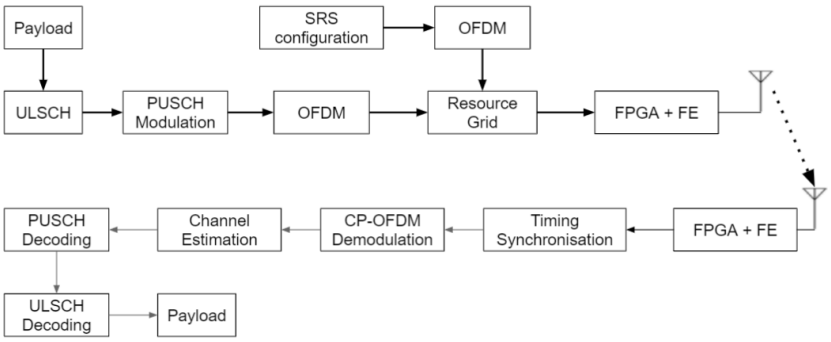

Figure 2.26: Schematic diagram of the UL communication.

ideal conditions where latency is intrinsically almost nil (and in any case not significant). The only source of latency is represented by the execution of the Matlab scripts on the laptop, which do not reflect a real situation of system use in the development phase.

2.10.2 UL Waveform Transmission and Reception

As shown in Figure 2.26, in the UL communication, the data is attached to the PUSCH. As will be highlighted in the following, the workflow of transmission and reception after the generation of PUSCH is composed by the following tasks: (i) generation of the resource grid, (ii) waveform transmission, and (iii) waveform reception and data decoding [22].

- **UpLink Shared CHannel (ULSCH) Encoding:** The ULSCH encoding process consists of different operations, such as (i) Cyclic Redundancy Check (CRC), (ii) code block segmentation, (iii) Low-Density Parity-Check (LDPC) encoding, (iv) rate matching and (v) code block concatenation. Then, the payload is attached to the ULSCH in the form of bits and later encoded into the PUSCH [23].
- **PUSCH Encoding:** The PUSCH encoding consists of scrambling with scram-

bling identity, performing symbol modulation with modulation scheme, and a layer mapping. To this end, the Code Word (CW) specifies an ULSCH code word [24].

- **SRS:** The SRS input carrier specifies the carrier configuration parameters for a specific Orthogonal Frequency Division Multiplexing (OFDM) numerology [25].
- **Transmission and Reception:** The generated waveform is then changed to the format that can be used with the testbed and transmitted repeatedly. Then, at the receiver side, the signal is captured over the air using another testbed, and the signals capturing duration is computed according to the time needed to capture the required number of frames. At the current stage of development, in the UL communication data is scaled so as to fit in one frame.
- **Timing Synchronization:** The received waveform is correlated with the PUSCH DMRS, while the synchronized signal is OFDM-demodulated.
- **PUSCH Decoding:** The PUSCH decoding consists of different tasks, such as (i) layer de-mapping, (ii) symbols demodulation with a proper modulation scheme, and (iii) de-scrambling with scrambling identity. The input Radio Network Temporary Identifier (RNTI) is of the UE [26].
- **ULSCH Decoding:** The ULSCH decoding consists of the following steps: (i) rate recovery, (ii) LDPC decoding, (iii) de-segmentation, and (iv) CRC decoding. More in detail, this process is the inverse operation of the ULSCH encoding process [27].
- **Image Recreation:** Finally, ULSCH-decoded data is in the form of bits. At this point, data from different slots are combined together, since the processes are at physical layer of the Open Systems Interconnection (OSI) stack. Then, since the format and the dimensions of the image has been already recorded in the receiver, the combined bits are used to recreate the transmitted image.

Figure 2.27: UL P2P image transmission.

UL reception

In the UL waveform, the image file is converted into bits and attached with PUSCH, OFDM modulated and is attached to the resource grid and are converted to the FPGA + FE format and transmitted over the air. At the receiver side, the signal is received using FPGA + FE and, upon reception, the timing is synchronized. Then, the signal is OFDM demodulated and, using the demodulated waveform channel, it is estimated and PUSCH is decoded and data transmitted is retrieved. Finally, the image is re-created using the received data. The result of this process is shown in Figure 2.27, where both transmitted and received images are depicted. As a side note, the tests have been carried out using a carrier frequency equal to 1.92 GHz.

2.10.3 UL and DL P2P Communication

A parallel execution of UL and DL in a P2P communication system corresponds to the next development step. In particular, the testbeds were arranged according to the model discussed in Section 2.6.2, with 2.1 GHz DL and 1.9 GHz UL carrier frequencies, respectively. In detail, in Figure 2.5 the block diagram of the communication system for image transmission is shown, in which both gNB and UE are simultaneously active, so that communications in both directions are possible. The transmitted images are used for illustrative purposes. Hence, the processes carried out in this

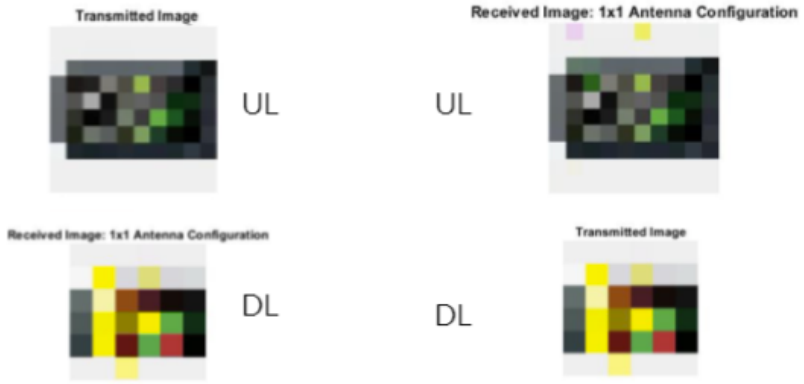

Figure 2.28: UL only in P2P image transmission.

model are the combination of UL and DL detailed earlier.

In this case, four Matlab instances have been used: two running in the laptop representing the gNB; and two running in the opposite laptop and representing the UE. Hence, in the laptop representing the gNB, there are two Matlab instances acting as the transmitter DL and the receiver UL, while in the laptop representing the UE one Matlab instance acts as a receiver DL and the other one acts as a transmitter UL. The carrier frequencies used in DL and UL are equal to 2.1 GHz and 1.92 GHz, respectively, with the images re-created from the received waveform. In Figure 2.28 the transmitted and received images, on both DL and UL sides, are shown.

2.11 Limitations of the system abstraction

After the initial development phase, various tests were conducted using different configurations. The complete 5G protocol stack was not available. Although experiments were possible, the absence of control plane functions proved to be a drawback. The limitation to outdoor experiments hindered testing in certain scenarios. The constraints were primarily due to transmission power limitations and a restricted range. Additionally, the processing time was extended due to the hardware/software

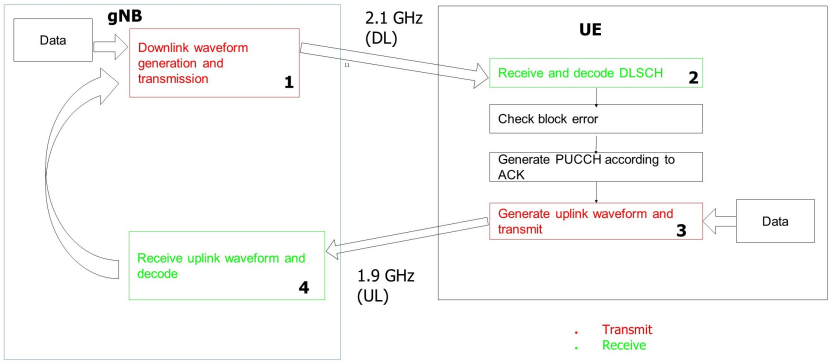

Figure 2.29: HARQ implementation.

co-design employed in the system.

2.11.1 HARQ

A drawback identified in the previous section was the lack of utilization of the HARQ. Thus, efforts were made to implement the HARQ. However, a challenge encountered during this implementation was the extended duration required by the Laptop to create both the UL and DL frames. Figure 2.29 illustrates the standard cycle for the entire P2P communication process. If only one Matlab instance had been responsible for all procedures, it might have been feasible. However, due to the experimental design chosen, which necessitated four parallel-running Matlab instances, both the gNB and the UE were unable to receive the correct Acknowledgement (ACK) bits. This was attributed to the system's prolonged processing time. Consequently, further development in this direction was halted.

Chapter 3

Experimental Performance Analysis

In this chapter, in in-depth analysis into the design of experimental test beds, together with associated parameters, is done, as well as the creation of a Graphical User Interface (GUI) is presented. Finally, some performance results from road tests to showcase the system's performance.

3.1 Performance Metrics

It is well and widely known that 5G communication systems aim to surpass their 4G predecessors in terms of performance, primarily in data transmission rates and latency. With regard to the need to estimate in such a way how 5G can outperforms 4G-based communications, some performance metrics are needed. In this doctoral thesis, the following are considered.

- **Reference Signal Received Power (RSRP, dimension: [dBm]):**: This parameter is crucial for evaluating the signal strength and coverage quality of a 5G network. It provides a measure of the received power level of a reference signal, helping to gauge network performance and identify potential areas of signal

degradation [28]. It is defined as:

$$\mathrm{RSRP} = 10 \cdot \log_{10}\left(\frac{1}{N_{\mathrm{RE}}}\sum_{i=1}^{N_{\mathrm{RE}}} P_{r,i}\right) \tag{3.1}$$

where: N_{RE} represents the number of usable Resource Elements (REs) within the measurement frequency BW; $P_{r,i}$ [dimension: mW] denotes the power contribution of the i-th RE.

- **Received Signal Strength Indicator (RSSI, dimension: [dBm])**: This metric indicates the overall received signal strength, encompassing the connected cell signal, signals from neighboring cells, and thermal noise. It is a fundamental parameter for assessing network connectivity and the robustness of the signal [28].

- **Reference Signal Received Quality (RSRQ, dimension:[dB])**: This metric provides insight into the quality of the received reference signals and is crucial for evaluating interference levels and potential signal degradation. High RSRQ values correlate with a better user experience and are vital for maintaining signal quality during handovers [28]. It is defined as:

$$\mathrm{RSRQ} = \frac{N_{\mathrm{PRB}} \cdot \mathrm{RSRP}}{\mathrm{RSSI}} \tag{3.2}$$

where: N_{PRB} is the number of Physical Resource Blocks (PRBs), and RSRP and RSSI are as previously defined.

- **Latency**: This is the time required for data packets to travel from the source to the destination. Low latency is crucial for real-time communication applications such as augmented reality, autonomous vehicles, and telemedicine. 5G aims to achieve a maximum latency of 4 ms, compared to the 20 ms reference latency in 4G communications [29].

- **Throughput**: This represents the rate at which data is transferred through a network or communication channel. High throughput is essential in 5G networks to accommodate BW-intensive applications and ensure a seamless user

experience. The expected support is up to 20 Gbps for downlink and 10 Gbps for uplink [30].

Additionally, the 5G NR cell ID value is a critical parameter, as it uniquely identifies each cell within a cellular network, playing a vital role in network management and ensuring seamless handovers for an uninterrupted service [31].

3.2 COTS 5G Modem

As anticipated in Chapter 2, the Matlab-handled 5G modem has a main limitation: it cannot be connected to a commercial gNB—a gNB deployed by a cellular network operator and installed in a real environment and providing real cellular connectivity. Therefore, in order to overcome this limitation, various commercial modems has been used (during various experimental activities) for the purpose of connecting to real gNBs. In detail, on a general plance, a 5G modem consists of a 5G NR module mounted over an Evaluation Board (EVB) which has slots for inserting the 5G-enabled Subscriber Identification Module (SIM) card. With regard to the target cellular operator, for short-term trial purposes a 5G WindTre [32] SIM has been used, since commercial WindTre gNBs are declared to be available in both the cities of Parma and Reggio Emilia, Italy which have been the proposed test sites where the experimental activities detailed in this doctoral thesis took place.

3.2.1 Quectel 5G Modem

A first example of a real 5G modem exploited for experimental characterizations is the AG550Q-EU 5G NR module, which is an automotive-grade 5G NR sub-6GHz module that adheres to the 3GPP Release 15 (R15) specifications. In detail, it supports both standalone (Standalone Mode (SA)) and non-standalone (Non-Standalone Mode (NSA)) modes. Specifically, the AG550Q-EU offers a maximum downlink rate of 2.12 Gbps and a maximum uplink rate of 900 Mbps. Furthermore, this module is backward compatible with existing Global System for Mobile Communica-

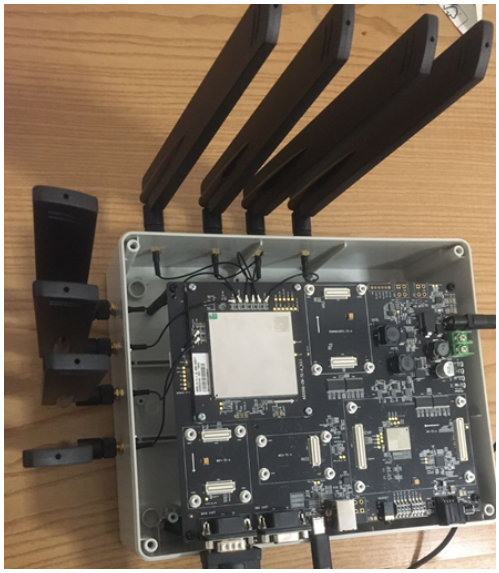

Figure 3.1: Quectel Modem.

tions (GSM), Universal Mobile Telecommunications System (UMTS), and LTE networks [33].

Figure 3.1 depicts the Quectel modem mounted on an EVB, with antennas connected to it. It is noticeable how the EVB uses both serial and Universal Serial Bus (USB) Type-C communications and can be powered via an external power supply adapter.

To this end, the overall testbed is showcased in Figure 3.2, featuring the 5G modem connected to a laptop running Ubuntu OS, with connections facilitated by USB-to-Universal Asynchronous Receiver-Transmitter (UART) cables. Additionally, the UART port on the EVB board is linked to the laptop's USB port via the cable.

Quectel Modem Configuration

Referring to Figure 3.2, the physical setup and configuration of the Quectel modem are summarized as follows. Configuration and status checks of the board can be performed using a serial communication-enabled tool, such as `GtkTerm` [34], a GUI-

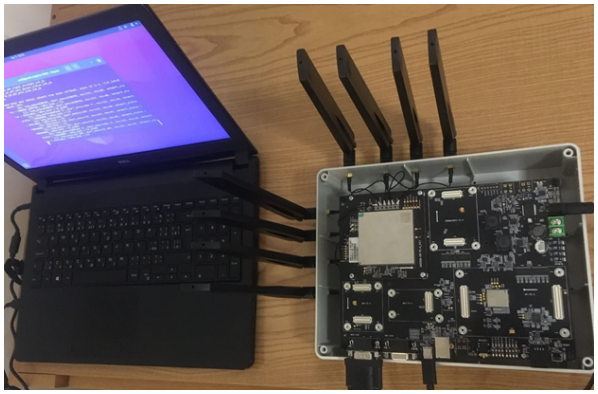

Figure 3.2: Experimental setup for Quectel Modem tests.

based serial port terminal emulator compatible with POSIX-compliant OSs, including Linux. Then, these have been the operating steps to be performed in order to let the Quectel 5G NR modem running and connecting to the reference 5G network.

1. Attach eight antennas to the 5G module, connecting the module ports to the antennas using cables.
2. Power the EVB using a power adapter, connected to both the electrical power source and the device.
3. Acquire WindTre SIMs and insert one into the corresponding slot on the 5G module, given the deployment of commercially-available gNBs by WindTre inthe identified test sites.
4. Connect the board to a Linux PC using a UART-to-USB cable.
5. Press the `PWRKEY` button to power on the board.
6. Open the `GtkTerm` utility.
7. Select the appropriate communication port.
8. Set the baud rate as required.

9. Toggle the reset button in the `GtkTerm` utility.
10. Enter `AT` commands to verify the device's functionality. If the responses are correct, turn off the board.
11. Connect the 5G modem to the PC using a USB Type C-to-USB Type B cable.
12. Open a terminal and install the Android Debug Bridge (ADB) tool.
13. Set the Access Point Name (APN) and retrieve the Domain Name System (DNS) server details.
14. Configure the DNS server on the Linux laptop.
15. Disconnect and then reconnect the USB Type C cable.

At this point, a 5G Internet connectivity should be established, with network parameters being possibly measured using the `AT` commands discussed in Section 3.2.1, and verified either using the `GtkTerm` utility or Command Line Interface (CLI) commands provided by the 5G NR modem's manufacturer (Quectel)..

`AT` Commands

The `AT` commands facilitate communication with the Quectel board, and should be entered through a CLI. For instance, the command `AT+QENG=servingcell` fetches the network information of the serving cell. More generally, the `AT+QENG` command can be paired with the following arguments to request various types of information:

- `celltype`: Returns information about different cells, such as the serving cell or neighbouring cells.
- `state`: Returns the UE state, e.g., "SEARCH," "NOCONN," "CONNECT."
- `is_tdd`: Returns the LTE Time Division Duplexing (TDD) or FDD mode.
- `mcc`: Returns the Mobile Country Code (MCC).

- `mnc`: Returns the Mobile Network Code (MNC).
- `lac`: Returns the Location Area Code (LAC).
- `cellid`: Returns the cell identifier.
- `pcid`: Returns the physical cell identifier.
- `uarfcn`: Returns the Universal Terrestrial Radio Access-Absolute Radio Frequency Channel Number (UTRA-ARFCN) of the scanned cell.
- `earfcn`: Returns the Evolved Universal Terrestrial Radio Access-Absolute Radio Frequency Channel Number (E-UTRA-ARFCN) of the scanned cell.
- `freq band ind`: Returns the E-UTRA frequency band.
- `ul bandwidth`: Returns the uplink BW.
- `dl bandwidth`: Returns the downlink BW.
- `tac`: Returns the Tracking Area Code (TAC).
- `psc`: Returns the Primary Scrambling Code (PSC) of the scanned cell.
- `rac`: Returns the Routing Area Code (RAC).
- `rscp`: Returns the Received Signal Code Power (RSCP) level of the scanned cell.
- `ecio`: Returns the Carrier to Noise ratio.
- `rsrp`: Returns the RSRP.
- `rsrq`: Returns the RSRQ.
- `rssi`: Returns the RSSI.
- `sinr`: Returns the logarithmic value of the Signal-to-Noise and Interference Ratio (SINR), with values in 1/5-th of a dB, and a range of $0 \div 250$ translating to $-20 \div +30$dB.

Figure 3.3: Telit 5G Module - FN980.

Finally, experimental tests were conducted on the available LTE network (as 5G networks were not available) to evaluate relevant performance metrics and gain familiarity with the modem's functionalities.

3.2.2 Telit 5G Module

A *second* 5G modem evaluated in this doctoral thesis is the Telit FN980, shown in Figure 3.3. In detail, it is a 5G data card suitable for sub-6 GHz 5G communications connecting to an EVB featuring an M.2 data card port, and supporting the connection of up to four antennas for LTE/5G connectivity. The Telit FN980 module provides compatibility with a variety of 5G FR1 bands: n1, n2, n3, n5, n7, n12, n14, n20, n28, n30, n41, n66, n71, n77, n78, and n79 [35]. Additionally, it supports numerous LTE (4G) and Wideband Code Division Multiple Access (WCDMA) (3G) bands, alongside the Global Navigation Satellite Systems (GNSS) L1 band for satellite-based location tracking. Theoretically, the Telit FN980 5G modem can achieve DL and UL throughputs of 5.5 Gbps and 2.7 Gbps, respectively, and is compatible with both SA and NSA modes.

Experimental Setup for the Telit Modem

The setup for experimentation involves the connection of the Telit FN980 module onto the EVB, and the attachment of four antennas to the board's antenna ports. Then,

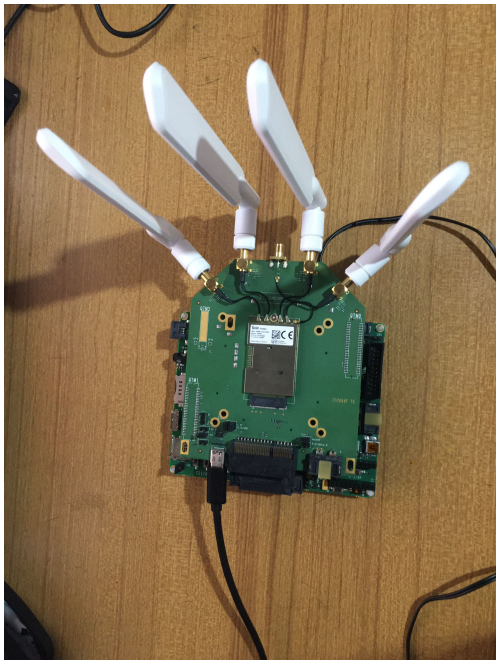

Figure 3.4: Setup using the Telit modem for experimental purposes.

a WindTre network operator SIM card is inserted into the EVB, and a Type-C USB cable establishes a connection between the board and a laptop running the GUI. This setup facilitates the capture of signal strength, corresponding physical layer performance metrics, and GNSS values through serial port communication. Although Telit offers software for modem parameter monitoring, this experimental test solely relied on serial communications managed by Python scripts. Upon setup completion and board power-up, the system connected to the board gains Internet access. Figure 3.4 illustrates the experimental setup, while Figure 3.5 provides a block diagram of the setup.

In subsequent sections, the GUI developed to offer a user-friendly interface for assessing the modem's performance will be showcased.

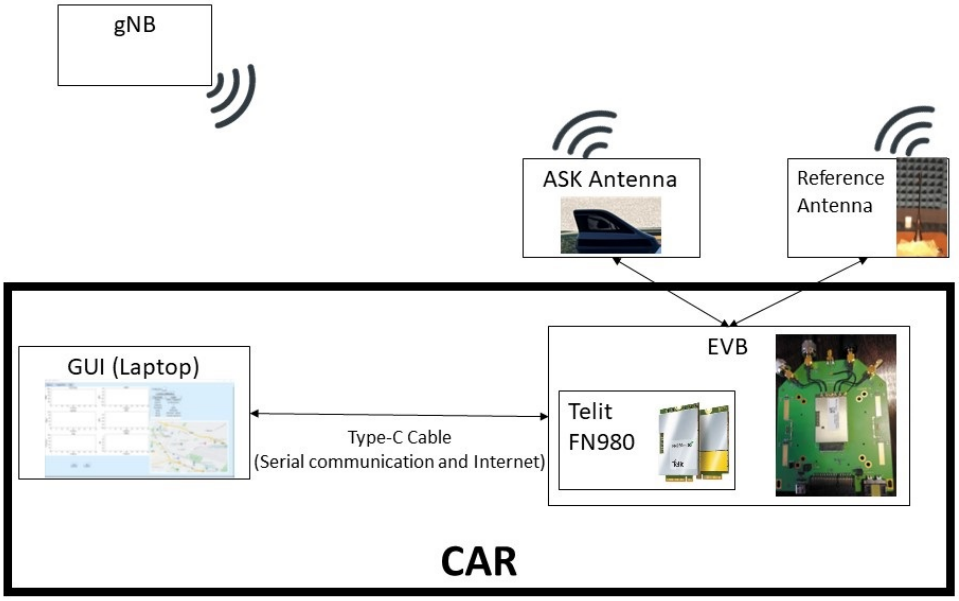

Figure 3.5: Block diagram of the experimental setup with the Telit FN980.

3.2.3 Sierra Wireless Modem

A *third* 5G modem evaluated and exploited for experimental activities in this doctoral thesis is the Sierra Wireless EM9191 module, shown in Figure 3.6, is a 5G data card suitable for sub-6 GHz 5G communications, that can be connected to an EVB equipped with an M-2 data card port, in the end supporting LTE and Third Generation (3G) technologies. Moreover the EM9191 boasts data transfer speeds, offering up to 4.5 Gbps for download and 660 Mbps for upload [36].

Experimental Setup for Sierra Wireless EM9191

With regard to the Sierra Wireless EM9191 5G modem, the experimental testbed comprises an EM9191 5G Evaluation Board (EVB) integrated with a wireless modem. Then, a SIM card from the 5G provider of the selected gNB is installed in the EVB. Consequently, in order to establish a connection to the gNB, an antenna is

Figure 3.6: Sierra Wireless EM9191 5G module.

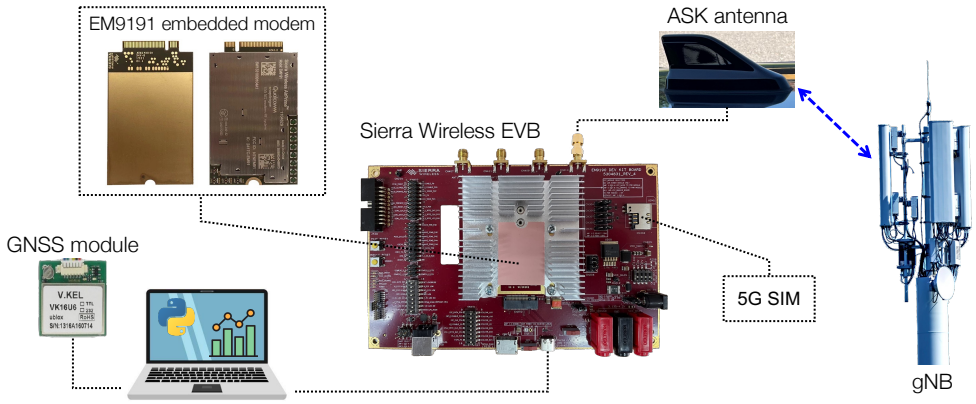

Figure 3.7: Block diagram of the experimental testbed.

mounted on the top of a car and connected to the EVB. This connection is facilitated using a SubMiniature version A (SMA) cable. Further more, a Type-C cable with serial communication capabilities is used to link the EVB to a laptop. Throughout the experiment, different readings were meticulously monitored and collected utilizing AT commands specific to the Sierra Wireless modem.

Figure 3.8: LTE/5G NR ASK Antenna.

3.3 Antennas

As previously mentioned, one of the components of all the experimental activities has been related to the presence of one or more external antennas to be connected to the envisioned 5G modems. To this end, with regard to the Sierra Wireless EM9191 5G modem, the antenna designed to be connected to this equipment has been evaluated in terms of performance using the developed testbed and a carefully devised experimental setup.

3.3.1 ASK 5G Antenna

Figure 3.8 shows the antenna developed by an Italian company named ASK Industries S.p.A. [37], which supports sub-6 GHz 5G NR and LTE bands. More in detail, the top and side views of the antenna, revealed after removing its cover, are shown in Figure 3.9. In Figure 3.10, the average gain of the ASK-developed antenna (indicated by the yellow line at 0 m elevation) is compared with that of the reference antenna (represented by the red line at 0 m elevation and the blue line at 0-30 m elevation).

3.3.2 LTE/5G NR Terminal Mount Monopole Antenna

In a similar manner, a generic antenna (shown in Figure 3.11) will replace the ASK antenna, connected to the antenna port and serving as a reference antenna for the tests. For the road tests, the ASK antenna will be mounted on top of a vehicle, as shown on the left side in Figure 3.12, while the reference antenna will also be mounted on the vehicle's roof, as shown on the right side in Figure 3.12.

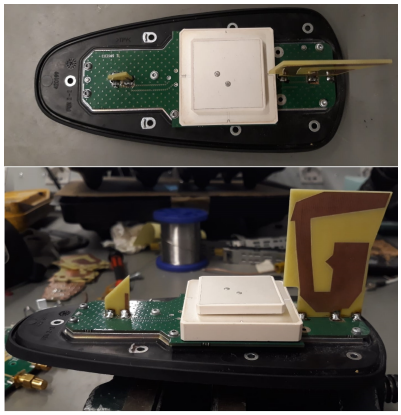

Figure 3.9: LTE/5G NR ASK Antenna side and top views.

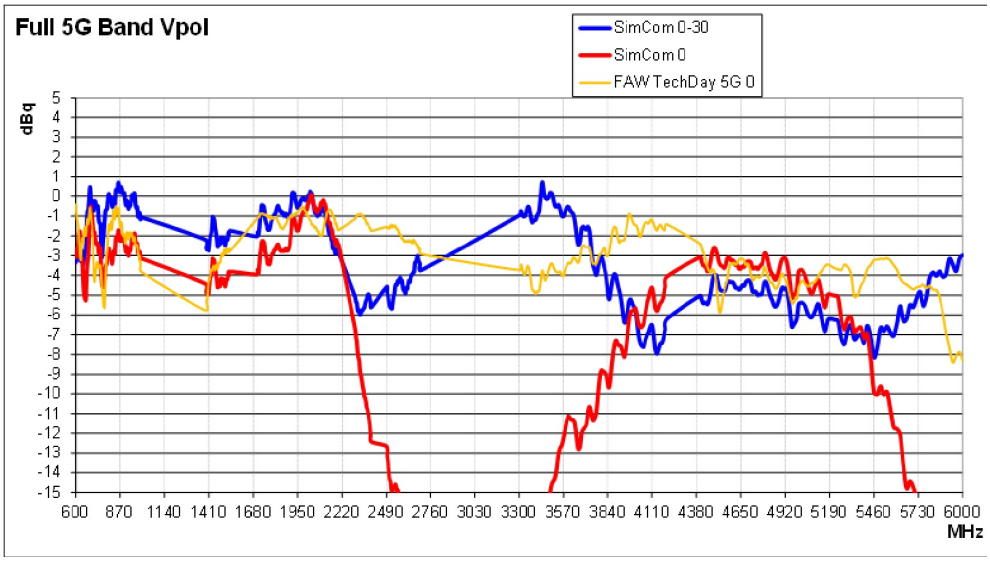

Figure 3.10: Average gain comparison between the ASK antenna (yellow line) and the reference antenna (blue and red lines).

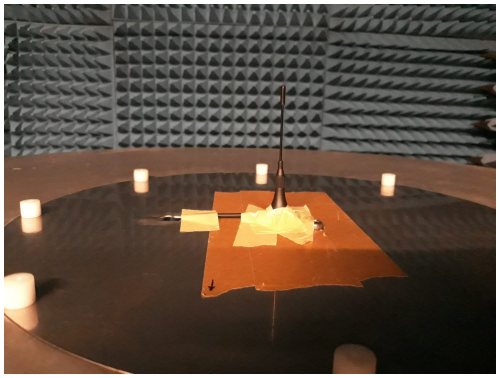

Figure 3.11: LTE/5G NR Terminal Mount Monopole Antenna.

Figure 3.12: Experimental setup: ASK antenna (left) and reference antenna (right).

3.4 Stemedu Vk-162 GNSS Module

The Stemedu Vk-162 GNSS module, shown in Figure 3.13, plays a crucial role in the experimental setup detailed in Section 3.2.3, providing accurate geolocation information through the GNSS. This compact, highly efficient module ensures precise tracking and navigation by connecting to multiple satellite systems, including GPS,

Figure 3.13: Stemedu Vk-162 GNSS Module.

GLONASS, and BeiDou [38].

3.5 GUI

Focusing on the software layer, in order to facilitate a flexible performance evaluation and data recording for post-processing, a GUI has been developed using the Python language alongside various frameworks. This Section outlines the different frames within the GUI.

3.5.1 Main Page

Upon the software launch, the Start Page, shown in Figure 3.14, unveils under the *Realtime* tab, showcasing real-time evaluated parameters. More in detail, this view hosts various features including multiple graphs, tabs, and configuration buttons. Moreover, the page introduces a real-time map, reflecting the current location and tracking car movement post-test initiation, exploiting Google Maps Android Application PacKage (APK) and GNSS module data. Moreover, the current configuration tab provides insight into the modem, antenna setup, throughput evaluation methods (via iperf3 [39] or speedtest servers), server Internet Protocol (IP) address (if using iperf3), throughput tests (DL, UL, or both), and the connected commercial network.

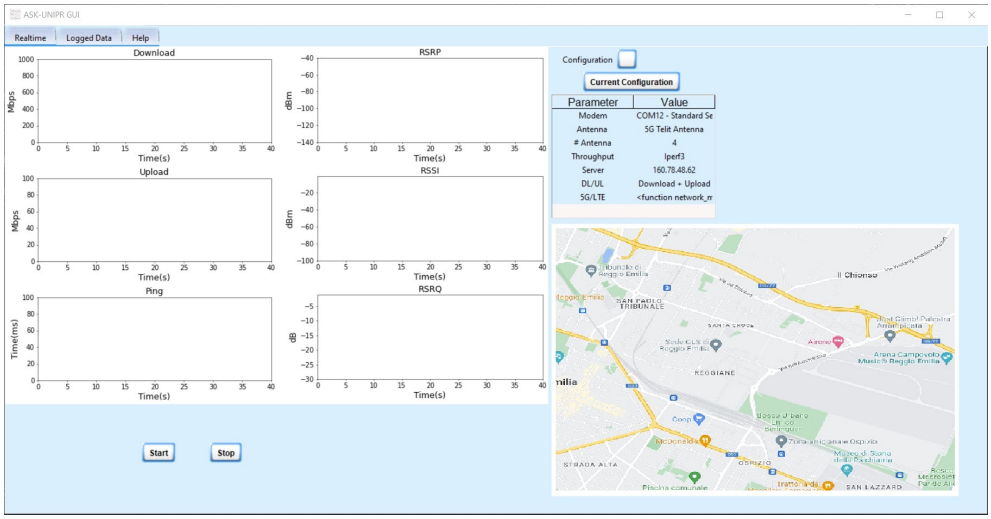

Figure 3.14: Initial view of the GUI developed for running the experimental evaluations.

Download and Upload

Even with reference to Figure 3.14, the two top graphs are dedicated to showing download and upload throughput (dimension: [Mbps]) over the time. Throughput is calculated using two application-level tools:

- Iperf3 - A tool for measuring maximum achievable BW on IP networks [39], useful for analyzing performance with various configurations related to timing, buffers, and protocols.
- Speedtest CLI - A tool for measuring performance metrics like download, upload, and latency [40], commonly used for throughput and latency measurements.

Latency

Latency [41], shown in the graph in the start page, can be measured in two ways depending on the application-level throughput measurement tool used:

- With iperf3, latency is measured by sending a `ping` request toward a remote server.
- With Speedtest, the connected server itself provides latency measurements.

Signal Strength Indicators

The remaining three graphs on the start page depict the RSRP, RSRQ, RSSI, evaluated using the "AT" commands supported by the modem as described in the previous sections.

3.5.2 Configuration Overview

As shown in Figure 3.15, the GUI facilitates various configuration settings allowing customization according to testing needs. These configurations are accessible via the Start Page, and are categorized under "General", "Throughput and Latency", "Module Selection", "Log Folder and File Name", and "GNSS" Configuration.

- **General Configuration:** Features options to enable real-time graph plotting, throughput testing, reference signal strength measurement, GNSS location recovery, and data logging in `CSV` format.
- **Throughput and Latency Settings:** Provides settings for throughput measurement tools like speedtest and iperf3 with various configurable parameters like server selection, port selection, measurement intervals, BW limitation, and transmission time.
- **Module Selection:** Allows selection of commercial modems for testing purposes, ensuring versatility in testing various modems and/or antenna systems. Also, provides options to select the COM port and baud rate for the module, ensuring correct communication setup.
- **Log Folder and File Name:** Configuration for specifying the folder and file name prefix for saving recorded data.

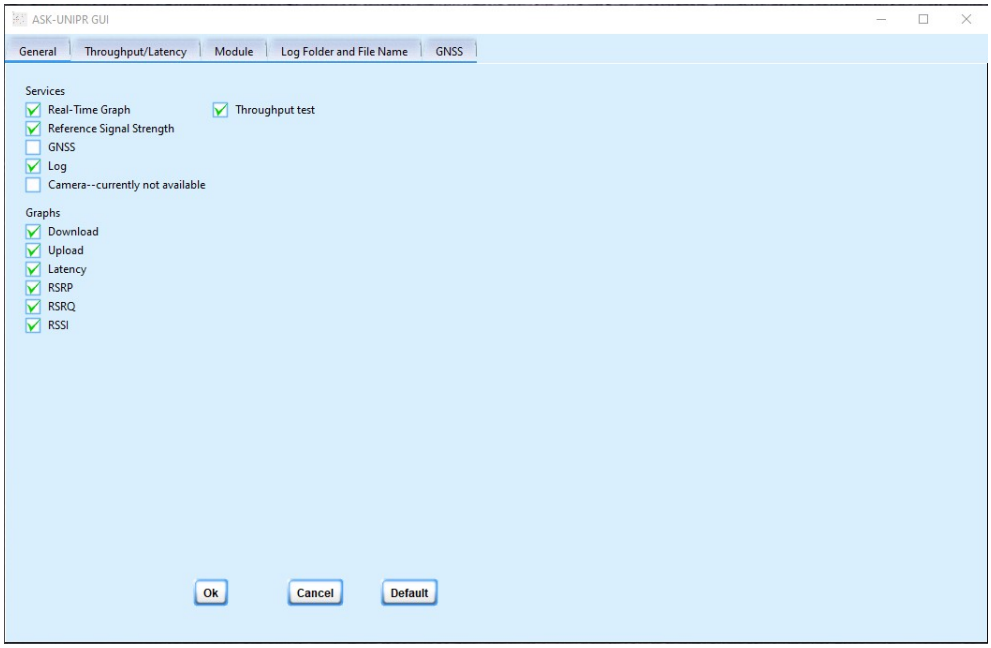

Figure 3.15: Configuration tab view of the GUI developed for running the experimental evaluations.

- **GNSS Configuration:** Enables selection of GNSS device for testing, allowing either an integrated GNSS module in the 5G modem or a distinct module.

Once the configurations have been set and the devices are connected, the experimental tests can be initiated.

3.5.3 Post Processing

Once the tests conclude, the data is logged to specific files in `CSV` file format, enabling post-processing. Specifically, the recorded data can be visualized using the tab denoted as "Post-processing" by selecting the desired graphs and the CSV file of the interested test. Figure 3.16 illustrates the plotting of recorded data from one of the previous tests.

Figure 3.16: Post processing tool.

The GUI serves as a tool for test configuration, real-time data plotting, and recorded data visualization.

3.6 Matlab-based Post Processing

In Section 3.5 it has been anticipated how the data collected through different experimental campaigns conducted with 5G modems, controlled through a GUI, might receive a post-processing using the GUI. In order to enhance the interactivity of post processing, a Matlab-based tool has been defined and implemented.

Geographic Globe Plot - Geoplot3

Geoplot3 is a mapping toolbox designed for plotting data on a global scale using GNSS data, alongside other relevant datasets. It generates a 3D globe, overlaying the data for visual analysis. Figure 3.17 illustrates a world-wide view generated by Geoplot3 [42].

The post processing tool, utilized within the GUI, provided only a 2D map displaying the tracked path. Another separate graph was employed for depicting col-

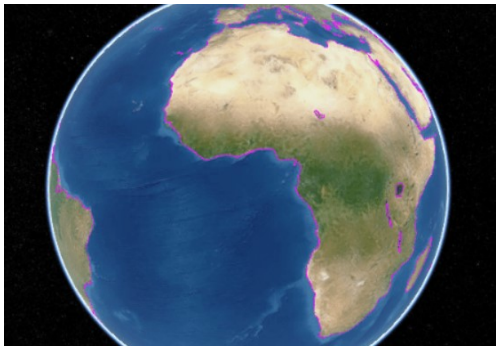

Figure 3.17: Geographical globe plot.

lected RSRP and additional data. Figure 3.16 revisits the output from this previous iteration of the proposed tool.

Moreover, the discussed experimental tests encompass a variety of data sets. Geoplot3, for instance, can plot RSRP values as heights, enhancing the effectiveness of post processing and aiding in the comprehension of system performance. Figure 3.18 displays a tracked path, where the line's height correlates with the RSRP value at respective coordinates. The red and blue lines represent trials conducted using reference and ASK antennas, respectively.

Geoplot3 also facilitates the simultaneous representation of two parameters, such as RSRP and DL throughput. Here, RSRP is depicted through line color, while DL throughput influences the line's height. Figure 3.19 provides an example of this dual-parameter representation.

A Matlab script-based tool has been developed to read data from the CSV file and to generate plots using Geoplot3. Figure 3.19 serves as an illustrative example of the capabilities of this tool.

3.7 Road Tests

Three distinct types of tests have been defined, each focusing on specific characteristics as detailed in the following.

Figure 3.18: Geoplot3 depicting a single data set (RSRP) collected along a single path, with red and blue lines representing trials using different antennas.

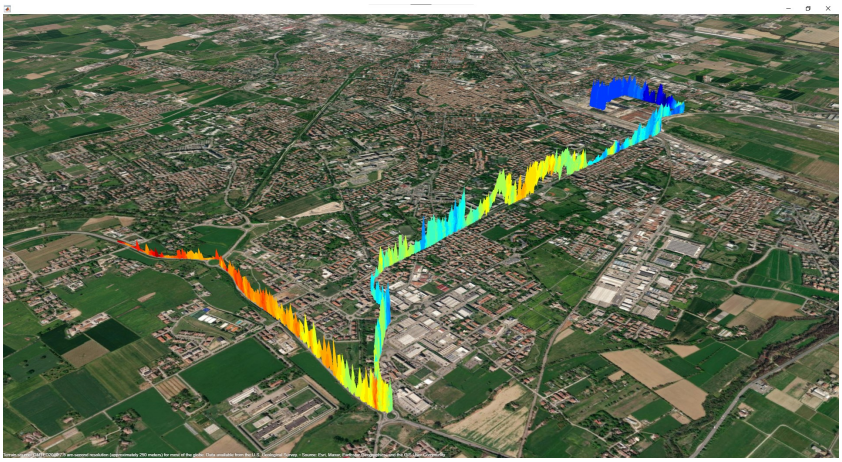

Figure 3.19: Geoplot3 representing two data sets: RSRP (color) and DL throughput (height).

Impact of Distance

The distance between the gNB and the UE significantly influences the RSRP of the received signal [43]. In fact, RSRP depends on various parameters [44], which in the

context of 5G can be summarized and specified as follows:

- Frequency BW : 20 MHz
- Transmit power per sub-carrier : 12.2 dBm
- Antenna gain : 16 dBi
- Feeder loss : 3 dB
- Power from antenna = Transmit power per sub-carrier + Antenna gain - Feeder loss : 25.2 dBm

Consequently, RSRP can be computed as:

- RSRP = Power from antenna - Path loss

Additionally, RSSI [45] and RSRQ [46] can be calculated as follows:

- RSSI = Serving Cell Power + Neighbour Co-Channel Cells Power + Thermal Noise
- $$RSRQ = \frac{N \cdot RSRP}{RSSI} \tag{3.3}$$

where N denotes the number of RBs.

Figure 3.20 illustrates the RSRP as a function of the distance between the UE and the gNB, showcasing a decrease in RSRP as the UE moves farther away. The RSRQ, being proportional to the ratio of RSRP to RSSI, also exhibits a dependence on the UE's distance from the gNB.

Impact of Velocity

The velocity of the UE affects the path loss, as demonstrated in [47]. Figure 3.21 displays the path loss for three different velocities: (A) 60 km/h, (B) 90 km/h, and (C) 120 km/h. The results indicate a minor increase in path loss, quantified in a few dBm, for higher velocities.

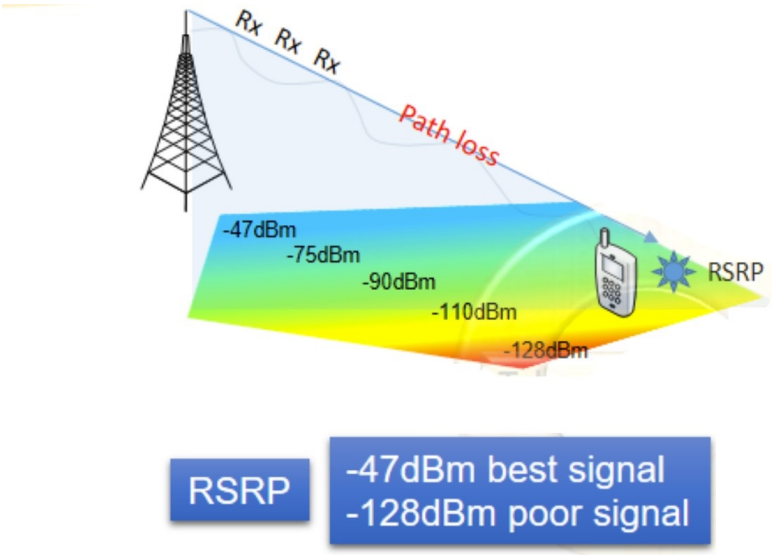

Figure 3.20: Graphical representation of RSRP model.

Impact of Environment

The surrounding environment of the communication link between the UE and the gNB plays a vital role in affecting throughput performance. It is particularly interesting to contrast the performance of the UE in urban and rural settings. The lower building density in rural areas results in a higher proportion of Line-of-Sight (LOS) links, as opposed to urban areas where higher building density leads to more Non-Line-of-Sight (N-LOS) links. Figure 3.22 presents the expected RSRP values across different distances under both LOS (represented by TDL-D) and N-LOS (represented by TDL-B [48]) conditions.

3.8 Experimental Results: Impact of Distance

In the following, a summary of the results derived from various road tests, conducted with the modem placed inside a moving vehicle to ensure a realistic analysis of its performance, is presented.

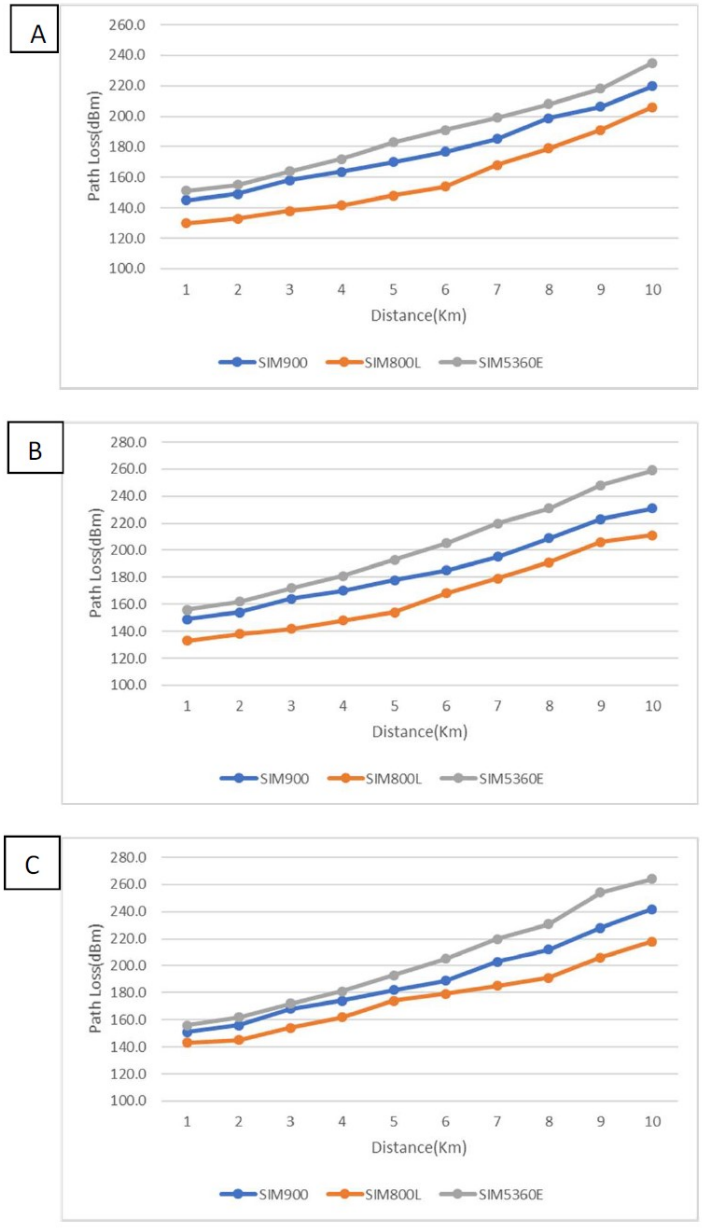

Figure 3.21: Path loss as a function of distance for three different vehicle speeds: (A) 60 km/h, (B) 90 km/h, and (C) 120 km/h.

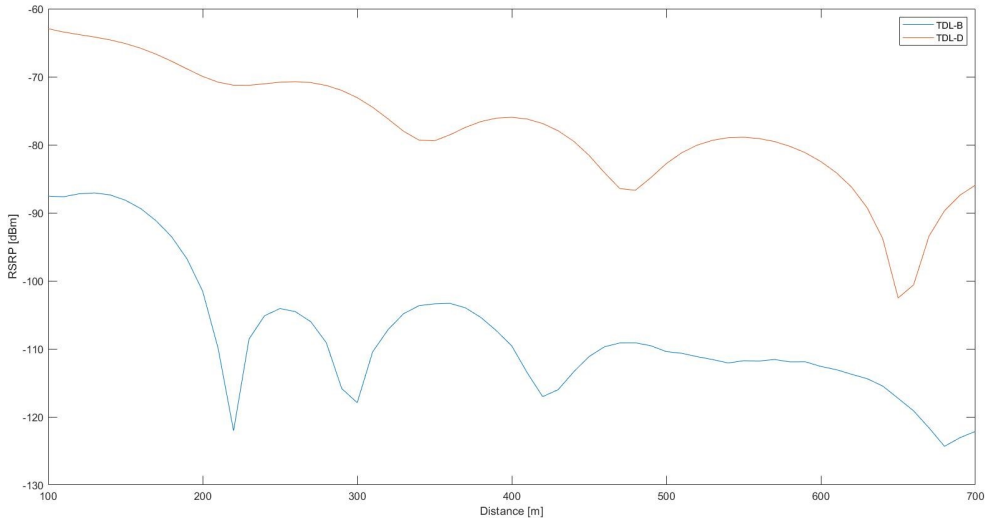

Figure 3.22: Projected RSRP for TDL-B and TDL-D channel models, corresponding to N-LOS and LOS conditions respectively.

3.8.1 RSRP as a function of the Distance

As delineated earlier, the RSRP is subject to changes induced by path loss. Figure 3.23 illustrates a comparison of RSRP values when using reference and ASK antennas. With the ASK antenna, the RSRP dips to a minimum of -109 dBm before disconnection, while the reference antenna maintains connection until -96 dBm. On the upper end, the ASK antenna achieves a maximum RSRP of -61 dBm, surpassing the -71 dBm maximum of the reference antenna. These results highlight a peculiar trend: at greater distances, the RSRP can actually be higher compared to shorter distances, potentially due to the transition from N-LOS to LOS conditions. During testing, certain areas experienced low coverage, leading to instances where the modem did not connect to the gNB. This resulted in missing data points on the graphs, and the plotted data intervals were affected by this occurrence.

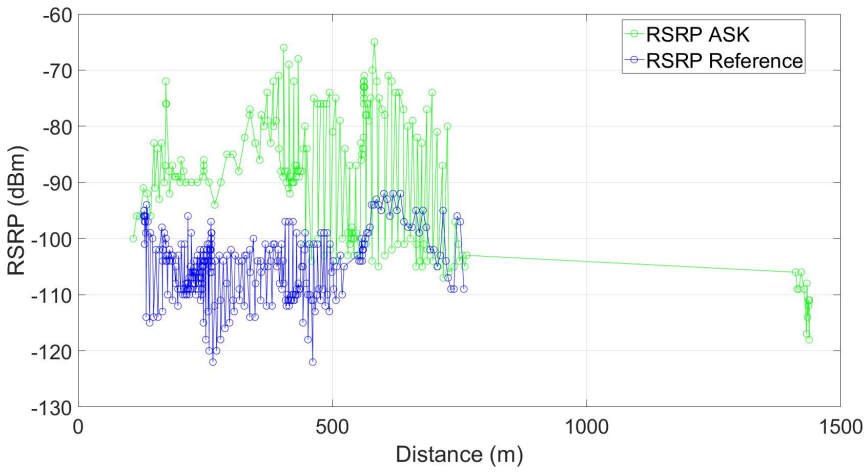

Figure 3.23: RSRP as a Function of the Distance, charted across a test path. The reference antenna serves as a benchmark for the ASK antenna.

3.8.2 RSSI as a function of the Distance

Figure 3.24 contrasts the RSSI values obtained with the reference and ASK antennas. The ASK antenna retains connection down to -90 dBm, whereas the reference antenna does so until -80 dBm. The ASK antenna's peak performance reaches -52 dBm, overshadowing the -62 dBm peak of the reference antenna.

3.8.3 RSRQ as a function of the Distance

Comparing RSRQ values for the reference and ASK antennas, Figure 3.25 reveals that the ASK antenna maintains connectivity down to -19 dB, while the reference antenna does so until -13 dB. Both antennas reach a maximum RSRQ of -10 dB.

3.8.4 Joint RSRP and DL Throughput Analysis

Figure 3.26 provides a joint analysis of RSRP (indicated by color) and DL throughput (represented by the height of the lines), utilizing the ASK antenna over a test path in Reggio Emilia, Italy. Here, a direct correlation between higher RSRQ values and

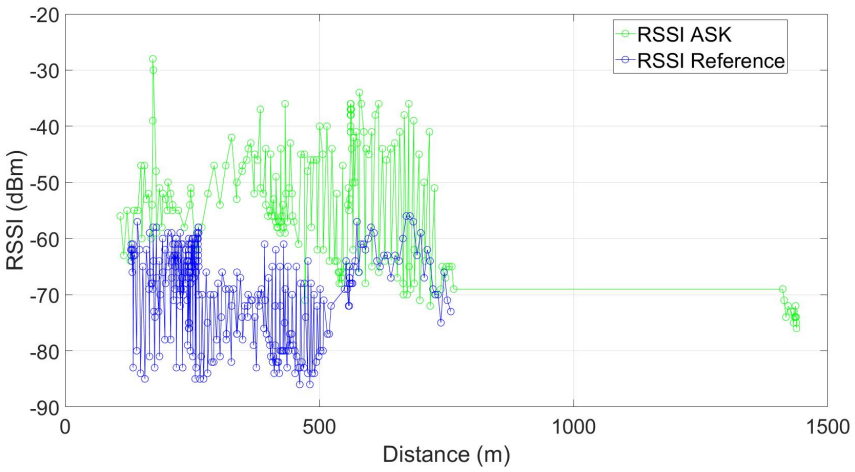

Figure 3.24: RSSI plotted against distance, based on data from a test path with the reference antenna providing a benchmark for the ASK antenna.

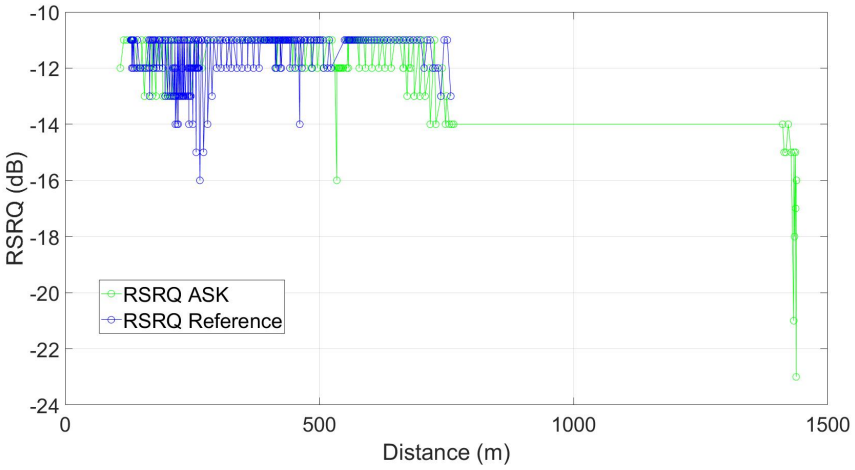

Figure 3.25: RSRQ in relation to distance, presented with data from a test path, using the reference antenna as a benchmark for the ASK antenna.

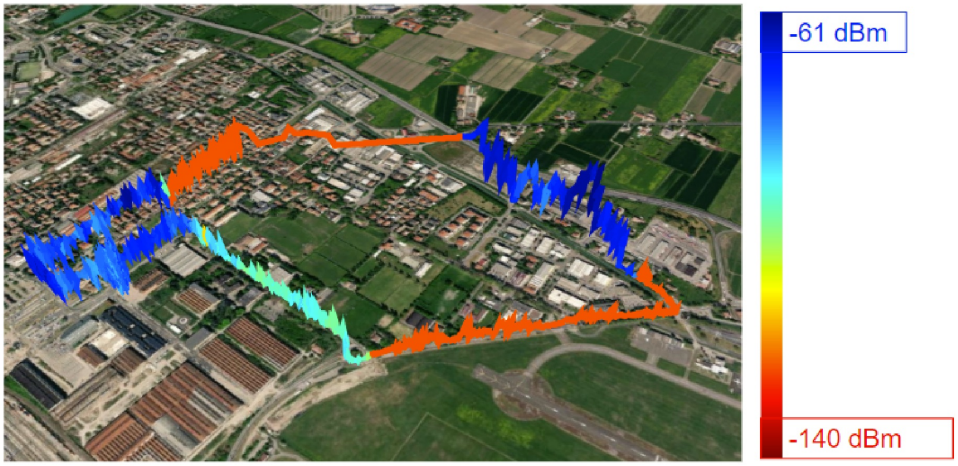

Figure 3.26: A combined presentation of RSRP (color) and DL throughput (line height) across a test path, utilizing the ASK antenna.

increased DL throughput is apparent. The ASK antenna achieves a maximum DL throughput of 218 Mbps and an average of 53.81 Mbps.

Conversely, Figure 3.27 illustrates the performance of the reference antenna in terms of RSRP and DL throughput. Here, the antenna attains a peak throughput of 207 Mbps and averages at 33.53 Mbps. These results unequivocally demonstrate the superior performance of the ASK antenna compared to the reference antenna.

To comprehend the impact of distance on DL throughput, further analysis is required, factoring in additional parameters such as signal quality, which encompasses RSRP, RSSI, and RSRQ.

3.9 Experimental Results: Impact of Velocity

3.9.1 RSRP as a function of Velocity

The impact of vehicle speed on the RSRP is depicted in Figure 3.28, showcasing results for two different speeds: (A) 60 Kmph (represented by green and black lines for

Figure 3.27: A combined presentation of RSRP (color) and DL throughput (line height) using the reference antenna, based on tests conducted across a test path.

ASK and reference antennas, respectively) and (B) 90 Kmph (depicted by blue and red lines for ASK and reference antennas, respectively). The vehicle was travelling in the highways to have constant speed of 60 Kmph and 90 Kmph. The data illustrates that the vehicle's speed has a limited effect on the RSRP, with only minor variations observed across different velocities.

3.9.2 RSSI as a function of Velocity

Figure 3.29 compares the RSSI for ASK and reference antennas under two vehicle speeds: (A) 60 Kmph and (B) 90 Kmph. Similar to the RSRP, the vehicle's speed appears to have a limited impact on the RSSI, with the results showing consistent performance across different speeds.

3.9.3 RSRQ as a function of Velocity

The RSRQ values for ASK and reference antennas at vehicle speeds of (A) 60 Kmph and (B) 90 Kmph are compared in Figure 3.30. Consistent with the previous parameters, the vehicle's speed seems to have a limited effect on RSRQ, showcasing stable performance across different speeds.

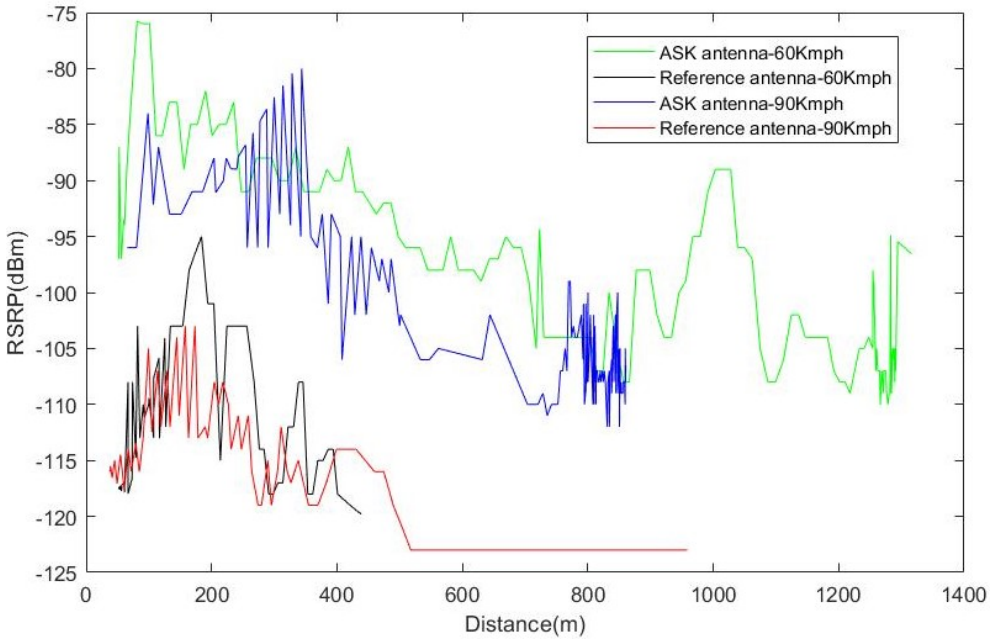

Figure 3.28: Comparison of RSRP as a function of velocity, with results shown for vehicle speeds of (A) 60 Kmph and (B) 90 Kmph. The ASK and reference antennas are represented by green/black and blue/red lines, respectively.

3.9.4 DL Throughput Analysis

The DL throughput performance of ASK and reference antennas at vehicle speeds of (A) 60 Kmph and (B) 90 Kmph is summarized in Table 3.1. While a slight reduction in throughput is observed with the increase in speed, the impact remains limited, with the ASK antenna consistently outperforming the reference antenna across all metrics.

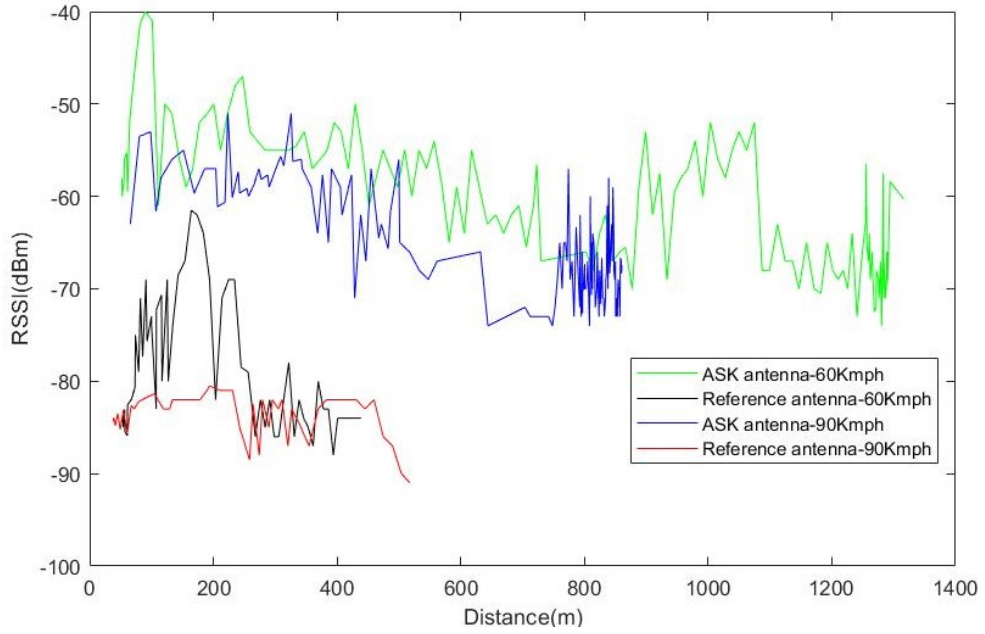

Figure 3.29: Comparison of RSSI as a function of velocity, with results shown for vehicle speeds of (A) 60 Kmph and (B) 90 Kmph. The ASK and reference antennas are represented by green/black and blue/red lines, respectively.

Speed (Kmph)	Antenna	Maximum Throughput (Mbps)	Minimum Throughput (Mbps)	Average Throughput (Mbps)
60	ASK	272	21.9	171.53
60	Reference	245	2.05	106
90	ASK	260	10.6	160
90	Reference	241	4.39	91

Table 3.1: Comparison of DL throughput as a function of vehicle speed, showcasing results for (A) 60 Kmph and (B) 90 Kmph. The ASK and reference antennas are evaluated across maximum, minimum, and average throughput values.

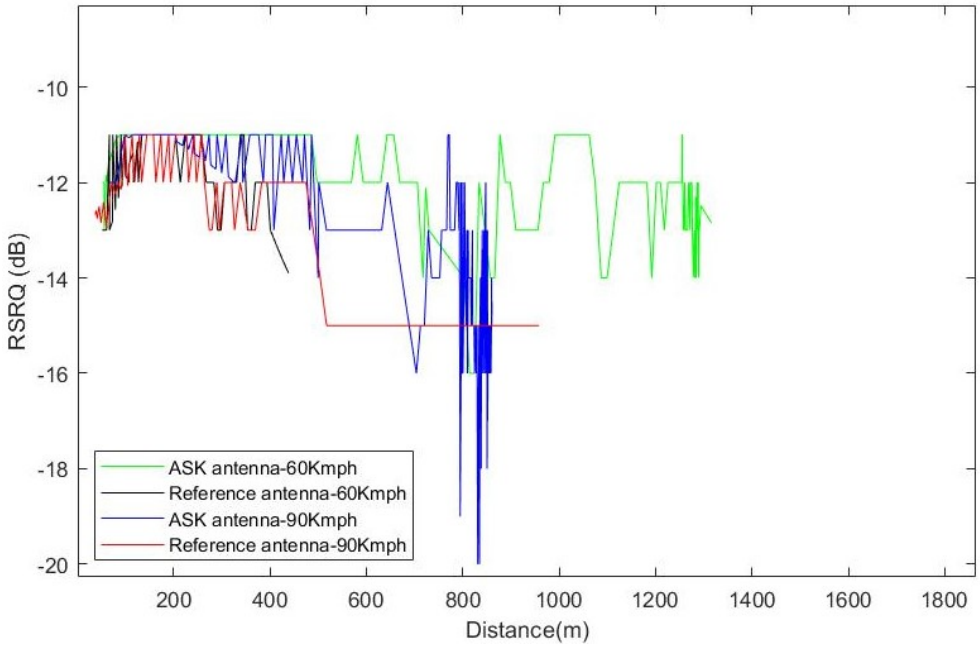

Figure 3.30: Comparison of RSRQ as a function of velocity, with results shown for vehicle speeds of (A) 60 Kmph and (B) 90 Kmph. The ASK and reference antennas are represented by green/black and blue/red lines, respectively.

3.10 Experimental Results: Impact of Environment

3.10.1 RSRP as a function of Distance

Figure 3.31 showcases a comparison of RSRP levels between reference and ASK antennas in both urban and rural environments. The urban scenario is represented by green (ASK) and black (reference) lines, while the rural scenario is depicted by blue (ASK) and red (reference) lines. The results indicate a more pronounced improvement in RSRP when using the ASK antenna in rural areas compared to urban areas. Generally, RSRP levels are higher in rural settings, and the urban environment exhibits significant oscillations.

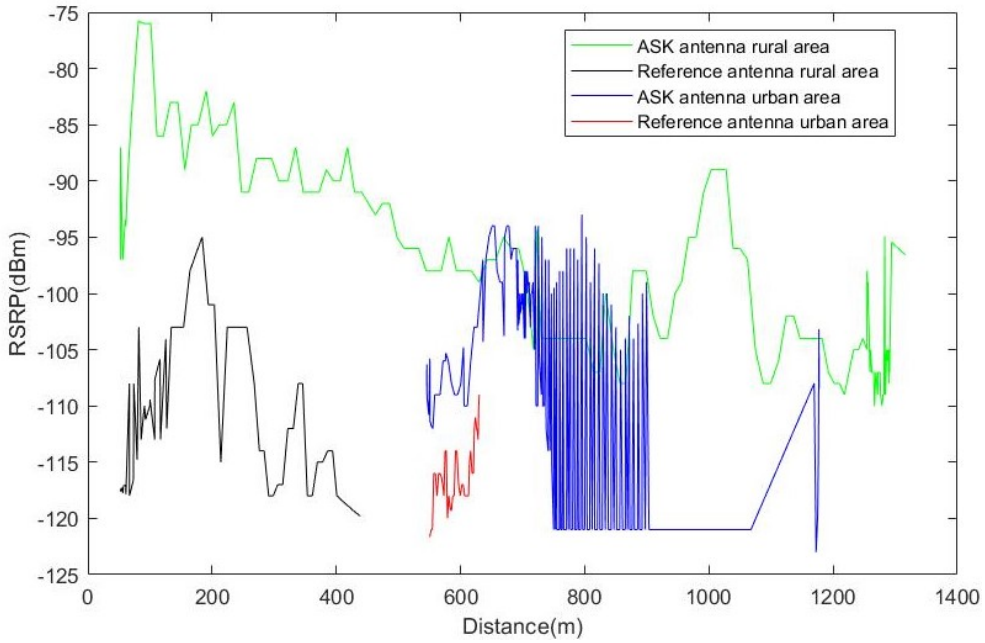

Figure 3.31: RSRP comparison between ASK and reference antennas in (A) urban (green and black lines) and (B) rural (blue and red lines) environments.

3.10.2 RSSI as a function of Distance

Figure 3.32 presents the RSSI results for ASK and reference antennas in urban (green and black lines) and rural (blue and red lines) settings. The ASK antenna demonstrates a notable performance advantage over the reference antenna in rural areas. Additionally, the RSSI stability with the ASK antenna appears improved in urban settings compared to the RSRP stability.

3.10.3 RSRQ as a function of Distance

RSRQ levels for both antenna types in urban and rural scenarios are compared in Figure 3.33, with the urban environment represented by green (ASK) and black (reference) lines, and the rural environment by blue (ASK) and red (reference) lines.

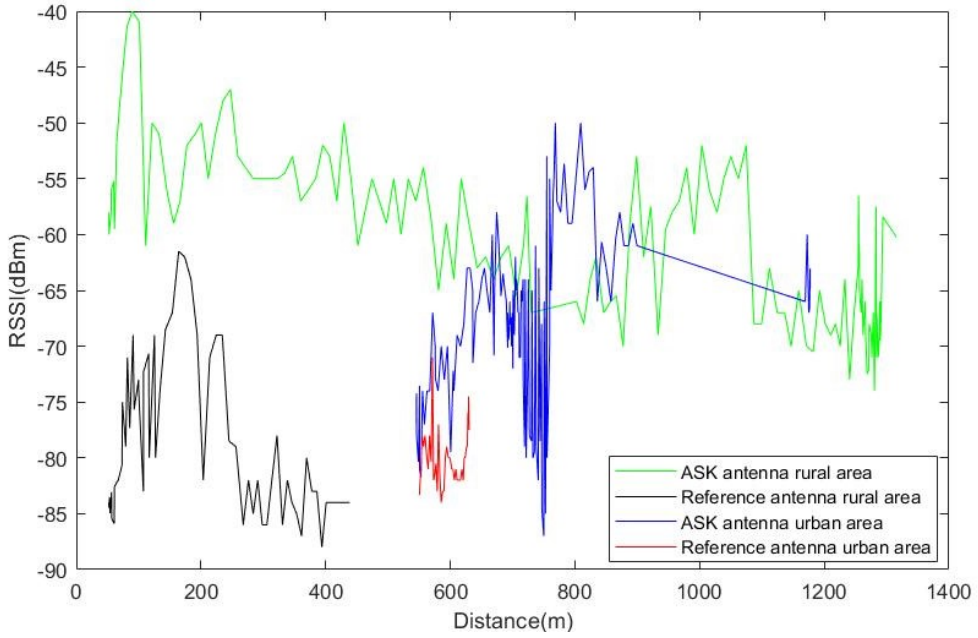

Figure 3.32: RSSI comparison between ASK and reference antennas in (A) urban (green and black lines) and (B) rural (blue and red lines) environments.

3.10.4 DL Throughput Analysis

The DL throughput for both antennas in urban and rural areas is summarized in Table 3.2. The data reveals that average DL throughput is higher in urban environments, possibly due to the higher density of gNBs, facilitating better connectivity on average.

The objective was to establish an experimental test bed for the performance analysis of various antennas in a vehicular communication scenario. Subsequently, a test bed was developed, and various tests were conducted, with the corresponding performances duly noted. In all considered scenarios, the ASK antenna consistently outperforms the reference antenna.

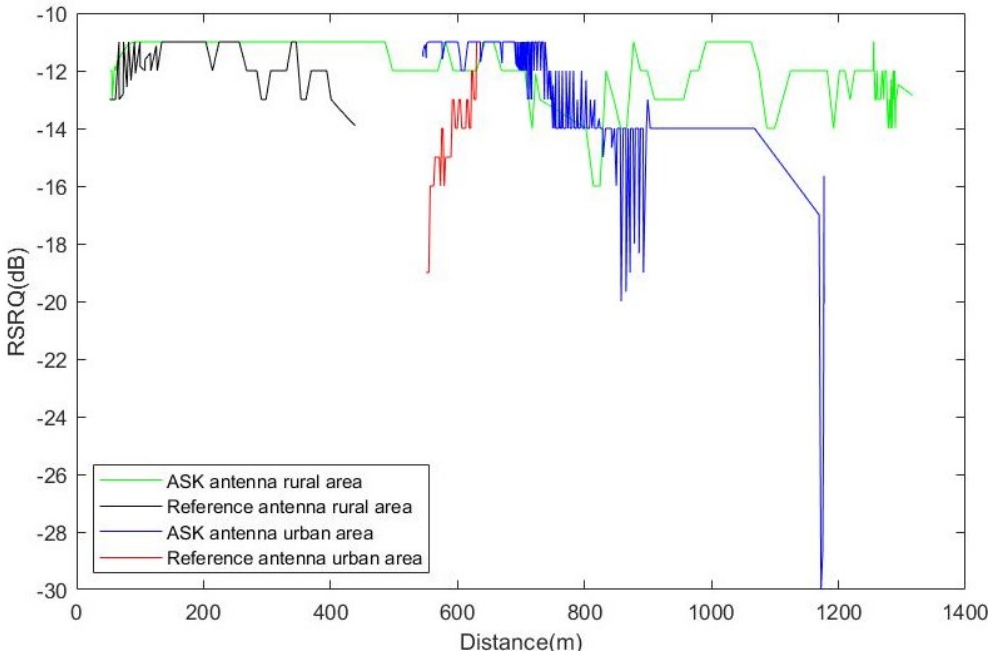

Figure 3.33: RSRQ comparison between ASK and reference antennas in (A) urban (green and black lines) and (B) rural (blue and red lines) environments.

Area	Antenna	Maximum Throughput (Mbps)	Minimum Throughput (Mbps)	Average Throughput (Mbps)
Urban	ASK	305	44.4	201
Urban	Reference	284	187	185
Rural	ASK	272	74.9	167
Rural	Reference	231	33.4	115

Table 3.2: DL throughput comparison between ASK and reference antennas in (A) urban and (B) rural environments.

Chapter 4

Handover Analysis

The transition to 5G networks represents a paramount advancement in the domain of connectivity, driven by unparalleled progress in telecommunications technology. With its strong focus on vital parameters such as latency and throughput, 5G ushers in a new era of remarkable communication improvements.

Despite their extensive reach, traditional 5G gNB towers are not without their challenges. Geo-physical attributes inherent to specific regions can lead to diminished signal strength, creating variances in QoS. Additionally, the geographic positioning of certain locales and the gNBs' locations can cause UEs to momentarily connect to remote gNBs, complicating the HO processes and rendering them less effective. As shown in Figure 4.1, in scenarios where multiple gNBs are situated near an intersection, a UE (in this case, a vehicle) may gather numerous RSRP values (from all visible gNBs) at each point along its path. This scenario can lead to isolated RSRP peaks, resulting in numerous and overly brief HOs, or Unnecessary HandOver (UHO)s. Avoiding UHOs is crucial as frequent HOs can introduce noticeable delays [49], subsequently increasing latency in data transmission and potentially affecting applications that rely on rapid communications. This underscores the necessity of refining HO procedures in 5G networks.

In the pursuit of minimizing UHOs in mobile scenarios, this chapter delves into UHO reduction through the implementation of 5G small cells in smart cities. Specifi-

Figure 4.1: A visual depiction of a vehicle experiencing multiple HOs (during its journey) due to fluctuating signal strengths and coverage areas from various gNBs.

cally, small cells, which are cost-effective mobile devices [50], are strategically positioned in critical locations to not only broaden 5G network coverage but also to bolster connectivity, diminish latency, and enhance UEs' QoS and overall experience. Empirical data obtained from real-world trials on public 5G networks, and simulations to analytically and experimentally validate the enhancement in connectivity and the reduction in UHOs are leveraged.

4.1 Experimental Analysis of 5G Network during HOs

4.1.1 Reference Experimental Path

To gather experimental 5G data in mobile contexts, the detailed experimental setup from Subsection 3.2.3 has been exploited during various experimental campaigns around the Scientific Campus of the University of Parma, Italy. Figure 4.2 illustrates the experimental area, chosen for its known gNBs' location (sourced from open datasets [51]), as well as their orientation, height, cell ID, and from previous

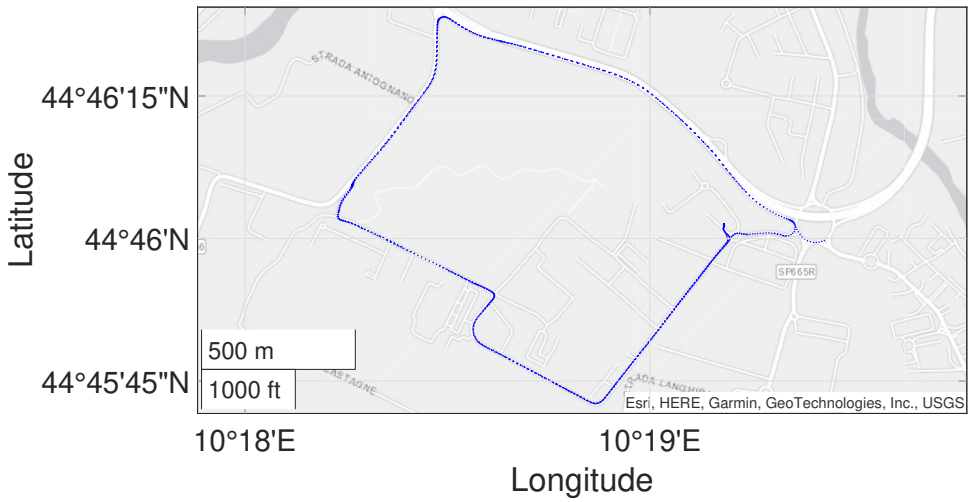

Figure 4.2: Illustration of the selected path for evaluation, highlighted with blue dots.

experimental trials addressing HO management issues [52].

4.1.2 Experimental Evaluation

The aim of this activity described in this doctoral thesis was to investigate the effects of HOs on throughput and latency within 5G networks. To achieve this, a variety of experimental trials were conducted using different DL data traffic loads, across multiple areas to ensure results were not confined to a specific location.

Figure 4.3 showcases the DL throughput at varying data rates—10 Mbps, 100 Mbps, and the maximum allowable data rate (with no restrictions on DL throughput)—as the UE traversed the reference path depicted in Figure 4.2. Accompanying cell IDs connected to the 5G modem are also displayed. As anticipated, a noticeable drop in throughput is visible during HOs, with some being quite close in proximity.

Figure 4.4 shows the latency values corresponding to the DL throughput seen in Figure 4.3. Here, significant latency spikes are evident (up to 3 s at 10 Mbps and 100 Mbps), which are especially detrimental for vehicular communications. These spikes can be attributed to short and unnecessary connections to the gNBs.

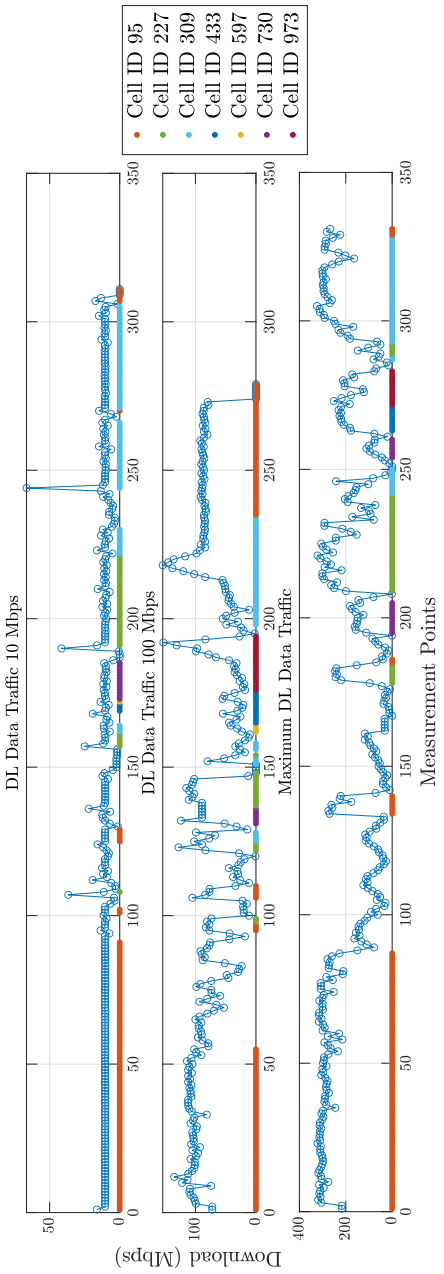

Figure 4.3: Experimental throughput achieved at various data rates by the UE moving along the reference path shown in Fig 4.2. Cell IDs are indicated at the bottom of the plots.

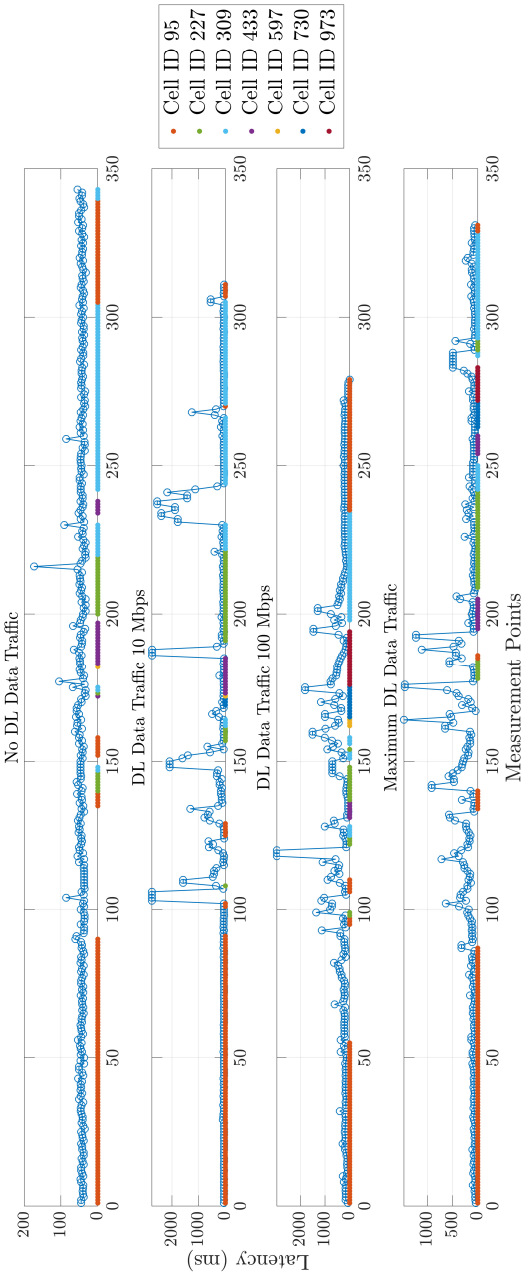

Figure 4.4: Experimental latency achieved at various data rates by the UE moving along the reference path shown in Fig 4.2. Cell IDs are indicated at the bottom of the plots.

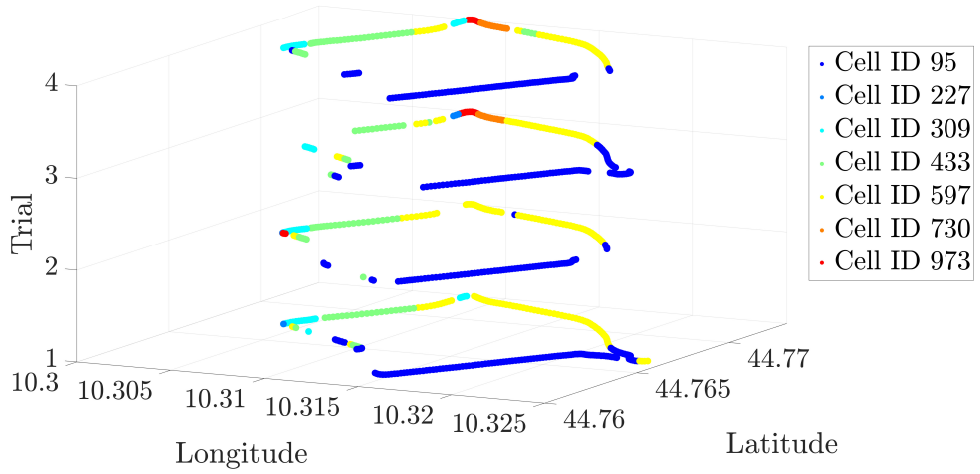

Figure 4.5: Experimental cell IDs recorded during different experimental trials along the reference path shown in Fig 4.2.

Figure 4.5 presents the cell IDs that the 5G modem connected to over four experimental trials, showcased in a three-dimensional manner with the UE's GNSS latitude and longitude values on the x-y plane, and the trial number on the z-axis. The plot reveals multiple cell IDs on its left side, hinting at the occurrence of UHOs.

Finally, Figures 4.6 and 4.7 depict the RSRP and RSRQ values obtained throughout the experimental activities.

4.2 Classic HO procedure

The initiation of the HO procedure is contingent upon satisfying signal quality measurements, a crucial stage in this process. Signal quality in 5G networks can be gauged through either DL or UL measurements [53]. In the NR physical layer's resource grid, standard signals termed reference signals are utilized for this purpose. These include the Downlink Synchronization Signal Block (SSB), the Channel State Information Reference Signal (CSI-RS) block, and the Uplink Sounding Reference Signal (SRS) employed by the gNB. Contrarily, LTE networks predominantly rely on

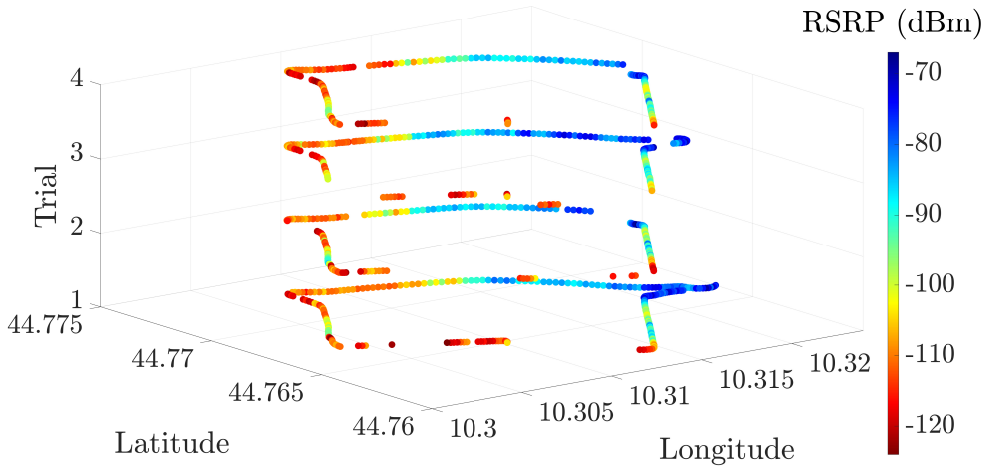

Figure 4.6: Experimental RSRP values recorded during different experimental trials along the reference path shown in Fig 4.2.

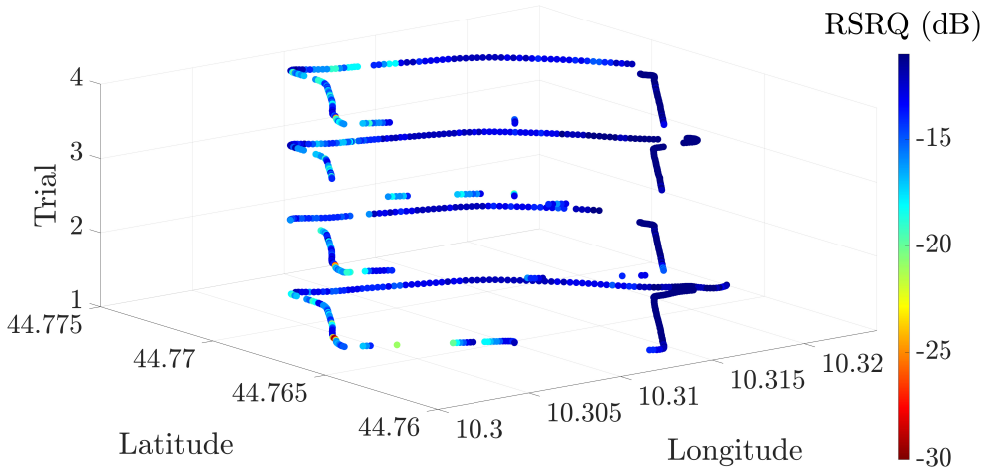

Figure 4.7: Experimental RSRQ values recorded during different experimental trials along the reference path shown in Fig 4.2.

DL measurements through the SSB and cell-specific reference signals [54, 55].

A proper execution of HO management is imperative for enhanced service expe-

rience in the connected mode, needing timely decisions for Base Station (BS) transitions based on channel quality measurements. These measurements can be obtained from the UE in DL (a conventional approach), or from the BS in UL as seen in more recent studies [56].

In DL measurements, UEs convey information and measured values pertaining to the serving and neighboring cells to the serving cell via a control message called the Measurement Report (MR). The MR encompasses data such as received signal quality from both the serving and target BSs, and undergoes a two-phase process. Initially, an RRC message configuring this process is dispatched to the UE by the gNB, followed by the UE measuring signals in the required format and sending them back to the gNB. Subsequent processing and averaging of these measurements occur through the L1 filter in the physical layer and the L3 filter in the RRC layer [57], before being relayed to the serving BS to initiate the HO.

Given the channel fluctuations at high frequencies, a series of signal quality measurements is prepared to aid the decision-making process, as opposed to a single measurement. The three predominant criteria for evaluating channel quality in both 4G and 5G are:

- **Reference Signal Received Power (RSRP):** represents the average received power, exclusive of noise and interference.
- **Received Signal Strength Indicator (RSSI):** denotes the total received power, inclusive of noise and interference.
- **Reference Signal Received Quality (RSRQ):** calculated as the ratio of RSRP to RSSI.

The 3GPP standards provide comprehensive descriptions of these parameters for both LTE and NR [58, 59]. Additionally, the MR can be categorized based on method or transmission time as follows [57]:

- **Event-based MR:** triggered upon occurrence of a specific event, such as a decrease in the power of the serving BS beyond a predefined network threshold.

- **Periodical MR:** sent at predetermined intervals.
- **Requested MR:** dispatched upon request from the serving BS.

Various approaches centered around signal quality measurements in either UL or DL have been proposed, with mathematical models applied to optimize network parameters, enhance successful HOs, and improve overall system performance. Key Performance Indicators (KPIs) crucial for this analysis include:

- **HO Frequency:** the number of HO attempts per second in the serving BS, influenced by the mobile user's speed and the coverage area.
- **HO Success Rate:** the ratio of successful outgoing HO procedures to attempted outgoing HO procedures [60].
- **HO Failure Rate:** the ratio of failed HOs to total HO attempts in the serving BS [61].
- **Ping-pong HO Rate:** the frequency of ping-pong HOs, occurring when a UE swiftly reverts to the serving cell after connecting to a target BS [62].
- **Data Latency:** the average time duration from the last transmitted packet before the HO initiation in the BS to the first received packet in the target BS post-HO [63].

Despite these KPIs highlighting HO performance, it is crucial to note that issues such as premature HO initiation, delayed HO setup, and erroneous target BS selection remain prevalent challenges leading to HO failures.

Main Procedure

Figure 4.8 shows a typical example of a traditional HO process. This process relies on the measurement of received signal power from both the current (serving) and neighboring BS in the DL direction, leading to a successful HO through a series of five distinct stages [64, 54].

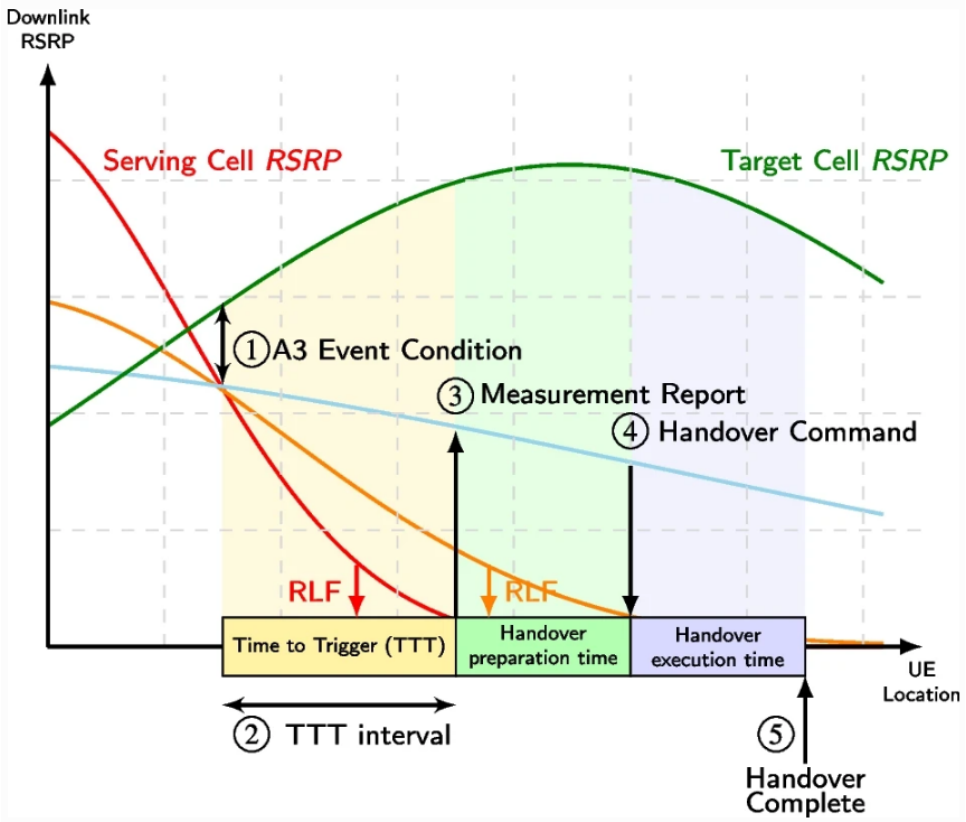

Figure 4.8: Classic HO Procedure.

1. A3 Event Condition

The HO sequence is triggered when specific signal quality conditions are met. As depicted in Figure 4.8, the A3 event kicks off the HO when the signal quality received from the neighboring BS surpasses that of the serving BS, plus a predefined threshold. It is crucial to note that a variety of events are anticipated during the HO preparation phase in 5G networks.

2. Time-to-Trigger (TTT) Interval

This phase represents a critical duration, ensuring the commencement of the HO process. During this interval, the UE pauses, waiting for the Time-to-Trigger (TTT) to elapse before dispatching any measurement reports or HO requests to the serving BS. The TTT is meticulously defined by the network operator to mitigate the risk of ping-pong HOs.

3. Measurement Report

Post TTT, if the conditions for initiating the HO continue to be satisfied, the UE proceeds to send a Measurement Report (MR) or a HO request to the serving BS.

4. HO Command

Upon validation of the HO request and successful negotiations with the target BS, the serving BS issues a HO command. This command facilitates the setup of the HO, alongside the transmission of control messages to the UE.

5. HO Completion

The HO procedure culminates successfully with the UE sending a confirmation message to the newly attached BS.

The optimization of this classical HO process involves determining the optimal Time-to-Trigger, HO entry conditions (such as A3 offset), and coefficients for L1 and L3 filters.

4.3 HO Reduction Strategy

The strategies developed in this section are predominantly based on experimental outcomes, leading to the formulation of a simulator to closely replicate the performance of RSRP. This is further supplemented by the integration of small cells to diminish the occurrence of HO.

Figure 4.9: 5G small cell (provided by Ericsson [1]) installed on a street light.

4.3.1 Small Cells

Small cells are low-powered cellular radio access nodes that operate in licensed and unlicensed spectrum. They have a range from a few meters to a few kilometers and are crucial in providing enhanced coverage and capacity, especially in densely populated urban areas. Figure 4.9 shows a small cell installed on a street light.

- **Network Densification**
  - Small cells play a pivotal role in network densification, a strategy essential for meeting the 5G capacity demands [65]. They help in filling the coverage gaps and ensuring consistent high-speed connectivity.
- **Enhanced Coverage**
  - Small cells are particularly useful in providing service in hard-to-reach areas such as indoor environments or urban canyons, where signals from macro cells might not penetrate effectively [66].
- **Increased Capacity**

  - They provide additional network capacity, helping to alleviate congestion on macro cells and improving overall network performance [67].

- **Reduced Latency**
  - Owing to their proximity to the end-users, small cells can significantly reduce latency, facilitating faster response times for applications and services [68].
- **Energy Efficiency**
  - Small cells consume less power compared to macro cells, contributing to the overall energy efficiency of the network [69].

Challenges and Considerations

- **Interference Management**
  - The dense deployment of small cells can result in interference, necessitating advanced interference management techniques [70].
- **Backhaul**
  - Reliable and high-capacity backhaul connections are crucial for small cells to ensure performance and reliability [71].
- **Site Acquisition and Deployment**
  - Identifying suitable locations for small cell deployment, particularly in urban areas, is a significant challenge [72].
- **Integration with Existing Networks**
  - Ensuring seamless integration of small cells with existing macro cells and network components is crucial for optimal performance [73].

Small cells are an indispensable component of 5G networks, addressing the need for enhanced coverage, increased capacity, and reduced latency. However, addressing the associated challenges is essential for reaping their full benefits.

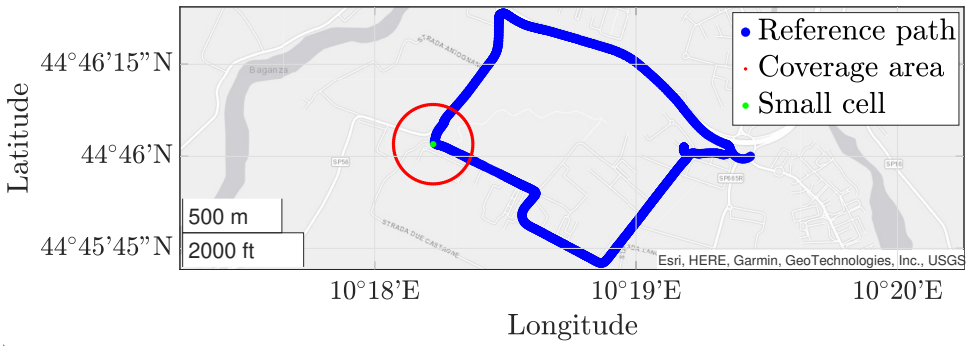

Figure 4.10: Illustration of the selected area, featuring the reference path (as presented in Fig4.2) in a blue hue, a simulated small cell marked by a green indicator, and a 200 m radius coverage area delineated by a red circle.

4.3.2 Small Cell-based UHO Reduction Strategy

Matlab Simulation

Building upon the experimental findings presented in Section 4.1.2, the objective is to enhance network performance by mitigating latency and bolstering throughput. To achieve this, the implementation of small cells as a means to amplify the RSRP and RSRQ of 5G signals, thereby fortifying network strength and reducing UHO, is proposed.

The first phase of the investigation involves utilizing a Matlab-based simulator to generate RSRP values at specific GNSS locations, correlating with where the experimental data was procured. Subsequently, employing Matlab's `los` function [74], the Line-Of-Sight (LOS) conditions across the entire trajectory are ascertened.[1] Furthermore, as depicted in Figure 4.10, the simulation strategically places a small cell at a predetermined location (indicated with a green dot), whereupon it is proceed to assess the RSRP within a 200 m radius of this point.

For the purpose of the simulation, the Tapped Delay Line (TDL) channel model

[1]The assumption of LOS conditions is based on the 200 m effective range of 5G small cells, with the presupposition that the points of interest are situated along roadways, hence in LOS.

is applied to each UE-gNB link, accounting for multi-path propagation and fading phenomena. Specifically, the time domain impulse response is described via a finite number of taps, each characterized by their respective time-varying amplitude and delay:

$$h(t,\tau) = \sum_{i=1}^{N_p} c_i(t) \cdot \delta(\tau - \tau_i) \tag{4.1}$$

where Np denotes the total number of taps/paths, $ci(t)i = 1^{N\mathrm{p}}$ are the time-dependent complex amplitude coefficients, and τ_i signifies the delay associated with the i-th path, for $i \in 1,\ldots,N$p [75]. According to the 3GPP standard [76], there exist five distinct TDL channel models, each defined by specific values of Np and the amplitudes and delays of the taps. Within this context, TDL-A, TDL-B, and TDL-C models depict various channel profiles for Non-Line-of-Sight (NLOS) propagation, while TDL-D and TDL-E models portray LOS propagation scenarios. Given the detection of LOS conditions along the path, this work opts for the TDL-D channel model.

As for the Path Loss (PL), the Urban Macrocell (UMa) PL scenario is adopted [76].

The PL-UMa in LOS conditions is calculated, as follows:

$$\mathrm{PL}_{\mathrm{UMa-LOS}}(d_{3\mathrm{D}}) = \begin{cases} \mathrm{PL}_{1,\mathrm{UMa}}(d_{3\mathrm{D}}), \\ \qquad \text{for } 10 \text{ m} \leq d_{2\mathrm{D}} \leq d'_{\mathrm{BP}} \\ \mathrm{PL}_{2,\mathrm{UMa}}(d_{3\mathrm{D}}), \\ \qquad \text{for } d'_{\mathrm{BP}} \leq d_{2\mathrm{D}} \leq 5 \text{ km} \end{cases} \tag{4.2}$$

where d'_{BP} is a break point distance, defined as

$$d'_{\mathrm{BP}} = 4\, h'_{\mathrm{gNB}}\, h'_{\mathrm{UT}}\, \frac{f_{\mathrm{c}} \times 10^9}{c} \tag{4.3}$$

being $c \simeq 3 \cdot 10^8$ m/s the speed of light. The parameters h'_{gNB} and h'_{UT} are referred to as effective antenna heights and can be computed as $h'_{\mathrm{gNB}} = h_{\mathrm{gNB}} - h_{\mathrm{E}}$ and $h'_{\mathrm{UT}} = h_{\mathrm{UT}} - h_{\mathrm{E}}$, respectively. The parameter h_{E} is referred to as effective environment height, whose exact value form depends from $d_{2\mathrm{D}}$ and h_{UT} [77, p. 27].[2] In (4.2), $\mathrm{PL}_{1,\mathrm{UMa}}$ and $\mathrm{PL}_{2,\mathrm{UMa}}$ can be expressed as follows:

[2] In the remainder of this paper, $h_{\mathrm{E}} = 1$ m for the considered parameters.

Table 4.1: Simulation parameters for 5G NR DL.

Parameter	**Value**
$N_{\text{cell}}^{\text{ID}}$	1
N_{FFT}	2048
Δf	15 kHz
f_c	3.5 GHz
SS Burst Power	17.2 dBm
P_{TX}	24 dBm
H_{TX}	5 m
H_{RX}	1.5 m
v	60 km/h
T_{RX}	290 K
F_{RX}	6 dB

$$\begin{aligned}&\text{PL}_{1,\text{UMa}}(d_{\text{3D}})\\&\quad = 28.0 + 22\log_{10}(d_{\text{3D}}) + 20\log_{10}(f_{\text{c}})\end{aligned} \tag{4.4}$$

$$\begin{aligned}&\text{PL}_{2,\text{UMa}}(d_{\text{3D}})\\&\quad = 28.0 + 40\log_{10}(d_{\text{3D}}) + 20\log_{10}(f_{\text{c}})\\&\qquad - 9\log_{10}\left(\left(d'_{\text{BP}}\right)^2 + \left(h'_{\text{gNB}} - h'_{\text{UT}}\right)^2\right).\end{aligned} \tag{4.5}$$

The values of the main simulator parameters are shown in Table 4.1. In particular, the transmitted power P_{TX} is set to 24 dBm (corresponding to the transmission power of a small cell [78]) and the height of the transmitter H_{TX} is set to 5 m (corresponding to the height of a lamp post, which could represent a viable installation infrastructure [79]).

In Figure 4.11, the simulation-based CSI-RSRP $\rho^{(\text{sim})}$ is shown, as a function of the distance between the gNB and the UE, together with the experimental values. It can be observed that, despite some acceptable differences due to external factors that

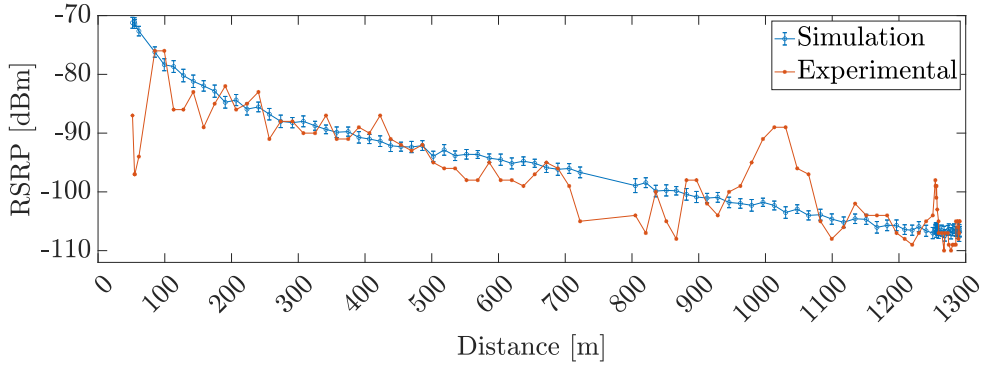

Figure 4.11: RSRP as a function of the distance between UE and gNB: average simulated (blue line with 95% confidence interval bars) and experimental (orange line with asterisks) values are directly compared.

cannot be perfectly replicated in the simulator, simulated and experimental values are consistent. The experiments were conducted to verify the simulator performance.

Simulation Results

The results, in terms of RSRP, obtained from the simulations conducted as discussed in Subsection 4.3.2, are shown in Figure 4.12. The simulation was carried out only close and under the coverage area of the small cell. Looking at these results, a significant improvement, with respect to the results shown in Figure 4.6, can be observed in the area where the small cells have been deployed. Moreover, a comparative analysis on the RSRP values in the reference area is shown in Figure 4.13, where the experimental data are indicated in red and the simulated RSRP values associated with the deployment of the small cell are represented in green. From this comparison, one can observe a significant increase of RSRP near the small cell.

Finally, in Figure 4.14 the simulated cell IDs determined by evaluating the signal strengths of neighbouring cells are shown. Looking at these results, it can be concluded that the introduction of small cells leads to a reduction of UHOs.

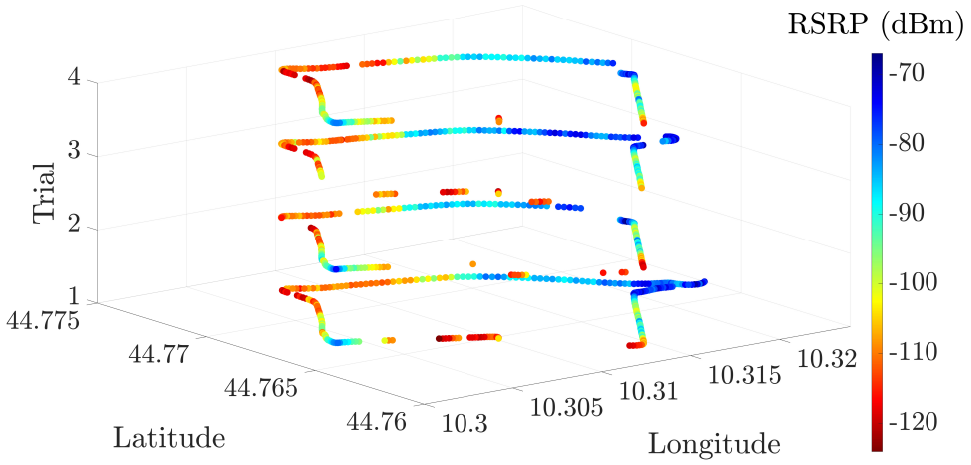

Figure 4.12: RSRP values obtained by means of different simulation trials with a 5G small cell along the reference path shown in Fig 4.10.

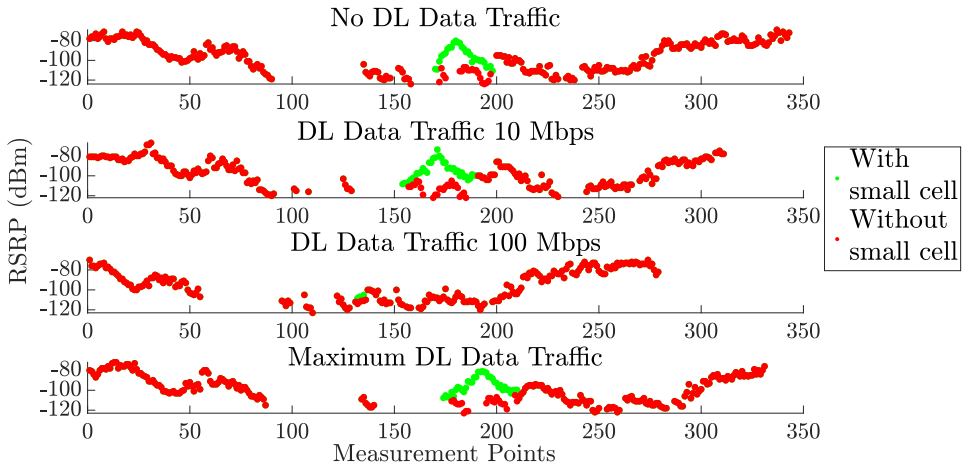

Figure 4.13: Comparison between experimental (in red color) and simulated (in green color) RSRP values retrieved and obtained (after the installation of a 5G small cell) along the reference path (shown in Fig 4.10) at various points during multiple trials.

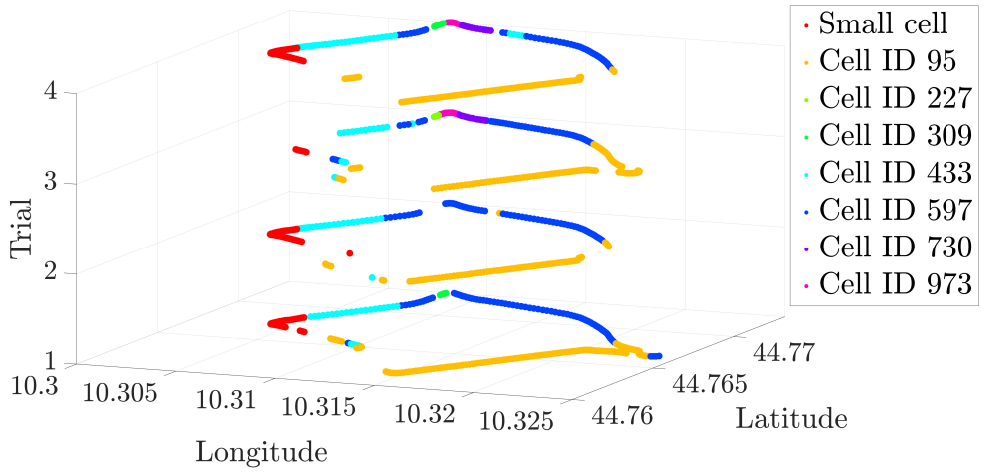

Figure 4.14: Simulated cell IDs obtained by means of different trials in the presence of a 5G small cell along the reference path shown in Fig 4.10.

4.3.3 Unnecessary HO Mitigation through Linear Regression

This section of the doctoral thesis discusses the development of a method aimed at minimizing UHOs in mobile networks, where a mobile UE may switch from one gNB (next generation NodeB) to another for very short time periods. To address this issue, a linear regression approach is utilized to analyze the Channel State Information - Reference Signal Received Power (CSI-RSRP) values. The RSRP values are obtained through simulations, as mentioned in a Section 4.3.2.

In the linear regression, the concept of polynomial regression is introduced, and for the purpose of this study, a linear regression (i.e., a first-degree polynomial) is chosen. The approach is based on a sliding window mechanism, where the polynomial coefficients for the linear regression are periodically updated based on a set number of observed RSRP values from six different gNBs. The RSRP values are predicted for future points, and the most frequently connected cell in this predicted interval is chosen as the candidate gNB for the UE to connect to. This approach aims to avoid short and unnecessary hand-overs, enhancing the stability and efficiency of the network connection.

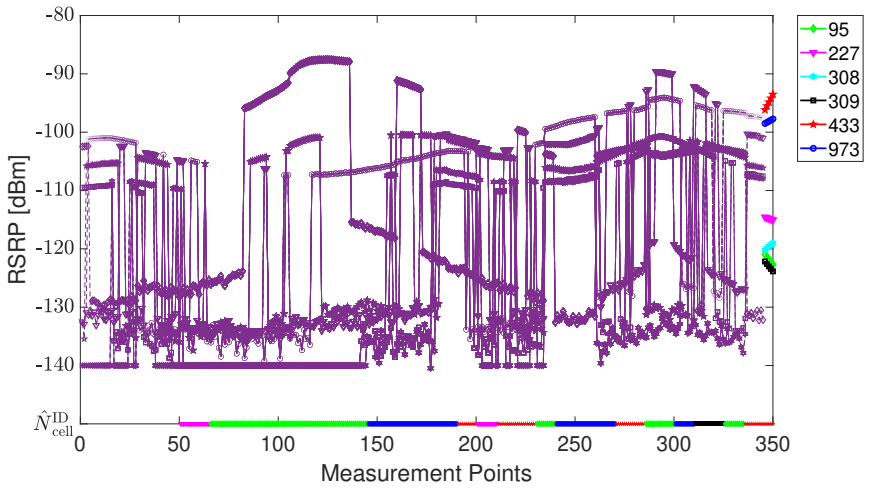

Figure 4.15: RSRP values linear regression-based identification of cell ID $\hat{N}_{\text{cell}}^{\text{ID}}$ along the considered path.

The results, in terms of selected values of the cell ID obtained using the approach along the considered path, are shown in Figure 4.15: only 13 HOs are performed, which is smaller than the 19 HOs experimentally observed.

The potential reduction of UHOs in 5G networks is significantly enhanced through the strategic deployment of small cells, which serve as a cost-effective and efficient solution to improve network performance. This doctoral thesis provides comprehensive evidence, derived from both experimental observations and simulation results, highlighting the advantages of utilizing small cells in critical areas. By leveraging existing infrastructure, such as lamp posts, these small, mobile devices can be strategically positioned to optimize network coverage and signal strength.

Furthermore, the integration of a linear regression approach, plays a crucial role in minimizing UHOs. This approach involves analyzing CSI-RSRP values to predict the most stable and reliable gNB for the UE to connect to. By employing a sliding window mechanism, the polynomial coefficients for the linear regression are periodically updated, ensuring that the predictions are based on the most recent and relevant

data. This method enhances the ability of the network to make informed decisions about hand-overs, thereby reducing the frequency of UHOs.

Conclusion

This doctoral thesis has focused on the development of experimental 5G testbeds and on the (experimental and simulative) performance analysis of 5G networks for vehicular communications (both at physical and application layers) by investigating performance metrics of interest, such as throughput, latency, RSRP, RSSI, and RSRQ.

As a *first* activity, a literature analysis has been performed, looking at the characteristics of the 5G protocol stack, together with the signals and the channels of interest for this doctoral thesis. Then, key differences between 4G and 5G, in terms of critical parameters in vehicular communications, as well as different use cases, together with the need of low latency in vehicular communications, have been discussed.

Then, given the evidences highlighted in the literature, the idea has been to develop a gNB and a UE for 5G-based vehicular communications to be used as a testbed to test antennas and to analyse the performance capabilities of 5G connections. For this purpose, a Matlab toolbox (namely: 5G Toolbox) has been identified as a viable tool, together with other well-known toolboxes useful to define a software-oriented 5G modem (designing both gNB and UE). With regard to available 5G networks, no public 5G networks were available (during the first times of the development) in the immediate and surrounding neighbourhoods of the areas of interest.

Furthermore, a closer look on the hardware software co-design approach was carried out by utilising a Zynq UltraScale+ MPSoC ZCU102 Evaluation Kit, consisting of a FPGA and an ARM processor, and an Analog Devices AD-FMCOMMS3-EBZ which performed as a radio FE to be connected to different antennas. Hence, start-

ing from simulations by transmission over a channel in Matlab, the tests have shifted towards successful real-world experiments. Due to the time frame and the launch of different public networks combined with multiple factors, as explained in Chapter 2, the development in this direction was frozen.

In the *next stage*, due to the availability of public 5G networks in the vicinity, the development of experimental testbeds for road tests using different COTS modems, and testing different external antennas, has started. For the real-time data collection and post processing, a GUI has been created in order to be able to set different test configurations, thus acting as a simple post-processing tool. In order to deepen the analysis, a Matlab-based post processing tool has also been designed, in order to evaluate the impact of distance, velocity and environment for different antennas.

During the post processing of the data recorded during the road tests, we have observed throughput drops and latency peaks, which can be considered as an undesired phenomenon in vehicular communications. Further analyses in this direction led to the identification of handovers (HOs) as the cause of this performance degradation, with 5G claiming to be able to reach 1 ms HO latency, but with current networks offering latencies far higher than this desired limit. Given these observed behaviours, further experiments have been conducted in this doctoral thesis at different geographical locations, in order to verify that these HOs are not unique to a particular test site. Then, efforts have been devoted in order to try to avoid some of these HOs, in particular referring (in this doctoral thesis) to this phenomena as unnecessary handovers (UHOs).

On the basis of this need, different road tests with various DL throughput loads have been carried out to understand the severity of this behaviour, leading to some instances resulting in a latency equal to 3 s that can be considered as being extremely undesirable in this era of wireless communications. Two main solutions for reducing these UHOs have been proposed in this doctoral thesis: (i) the use of 5G small cells and (ii) a linear regression-based approach, both exploiting a properly designed (on the basis of experimental data) Matlab-based simulator. From the obtained results, the simulator allowed to observe how using 5G small cells could lead to a coverage area increment (around 200 m) and signal strength improvement in the immediate vicinity

of a small cell, while the use of a linear regression has been shown to be handy in wide areas, whereas the signal strength remains the same. Furthermore, even if 5G small cells are low cost and easy to install, it can be argued that the use of linear regression-based approach will be better. However, the installation of 5G small cells not only allows to at reduce the number of HOs, but also opens further options.

Finally, future improvements in this research direction can lead to the installation of 5G small cells to increase the network coverage and to remove pockets with low signal strength. In vehicular communications, the limited user capacity of 5G small cells could be a disadvantage, but by using cell presence to issue warnings to other users it can be negated, this approach exploits the capability of a UE to receive signals from multiple gNBs simultaneously. Additionally, 5G small cells could lead to synergies with traffic signals and other technologies to enhance road safety and efficiency. Although solutions to UHOs may evolve, the current deployment of 5G small cells could offer multifaceted benefits in the near future.

This doctoral thesis embarks on a journey commencing with an exploration of 5G technology. It then progresses to the simulation of 5G gNB and UE using Matlab, followed by a focused effort on developing an experimental testbed utilizing the Matlab hardware-software co-design approach. However, this approach revealed limitations in the development process. Additionally, the thesis presents the creation of an experimental testbed employing a COTS modem and a software tool for evaluating the performance of various antennas. The analysis of these antennas exposes drawbacks in existing public 5G networks, such as UHOs, leading to latency and throughput degradation. Consequently, the findings suggest the incorporation of 5G small cells in UHO-prone areas to enhance QoS.

List of Publications

- Eleonora Oliosi, Sunil Mathew, Luca Davoli, Nicolò Strozzi, Filippo Manghi, Fabio Casoli, Andrea Notari, Gianluigi Ferrari: Simulation-based Analysis of Experimental 5G NR Downlink CSI-RSRP-based Handover Performance. In *2023, 28th European Wireless, Rome, Italy.*

- Sunil Mathew, Eleonora Oliosi, Luca Davoli, Nicolò Strozzi, Andrea Notari, Gianluigi Ferrari: On the Reduction of Unnecessary Handovers Using 5G Small Cells in a 5G NR Environment. In *2023, IEEE International Conference on The Confluence of Advancements in Robotics, Vision, and Interdisciplinary Technology Management IC RVITM'23, Bengaluru, India.*

Bibliography

[1] Ericsson. Street Radio 4402 Small Cell, 2021. https://tinyurl.com/ericssonsc21. Accessed on October 13, 2023.

[2] 5G Network. https://www.livescience.com/65959-5g-network.html. Accessed on 29 October 2023.

[3] A. Gupta and R. K. Jha. A survey of 5g network: Architecture and emerging technologies. *IEEE Access*, 3:1206–1232, 2015.

[4] 3GPP. 5g system overview. https://www.3gpp.org/technologies/5g-system-overview. Accessed on 29 October 2023., 2023.

[5] S. Sun, G. R. MacCartney, and T. S. Rappaport. Millimeter-wave distance-dependent large-scale propagation measurements and path loss models for outdoor and indoor 5G systems. In *European Conf. Antennas and Propagation (EuCAP)*, pages 1–5, Davos, Switzerland, 2016.

[6] 5G mmWave. http://www.techplayon.com/what-is-sub-6-ghz-mmwave-in-5g-and-why-mmwave-bands-are-required/. Accessed on 29 October 2023.

[7] M. Hyder and K. Mahata. Zadoff–chu sequence design for random access initial uplink synchronization in lte-like systems. *IEEE Transactions on Wireless Communications*, 16(1):503–511, 2017.

[8] European Telecommunications Standards Institute (ETSI). 3GPP TS 38.211, V15.2.0 (2018-07): 5G-NR: Physical channels and modulation . Technical report, European Telecommunications Standards Institute (ETSI), Sophia Antipolis Cedex, FRANCE, July 2018.

[9] European Telecommunications Standards Institute (ETSI). 3GPP TS 38.213, V15.6.0 (2019-07): 5G-NR: Physical layer procedures for control . Technical report, European Telecommunications Standards Institute (ETSI), Sophia Antipolis Cedex, FRANCE, July 2018.

[10] 5G V2X Communication. https://5gaa.org/wp-content/uploads/2019/07/5GAA_191906_WP_CV2X_UCs_v1-3-1.pdf. Accessed on 29 October 2023.

[11] European Telecommunications Standards Institute (ETSI). 3GPP TS 22.186, V16.2.0 (2019-06): Service Requirements for enhanced V2X Scenarios. Technical report, European Telecommunications Standards Institute (ETSI), Sophia Antipolis Cedex, FRANCE, June 2019.

[12] MathWorks. Nr pdsch throughput. https://it.mathworks.com/help/5g/ug/nr-pdsch-throughput.html. Accessed on 29 October 2023., 2023.

[13] MathWorks. Nr pusch throughput. https://it.mathworks.com/help/5g/ug/nr-pusch-throughput.html. Accessed on 29 October 2023., 2023.

[14] Zynq UltraScale+ MPSoC ZCU102. https://www.xilinx.com/products/boards-and-kits/ek-u1-zcu102-g.html. Accessed on 29 October 2023.

[15] Wireless Communications. https://in.mathworks.com/solutions/wireless-communications.html. Accessed on 29 October 2023.

[16] Frequency Offset Calibration. https://in.mathworks.com/help/supportpkg/xilinxzynqbasedradio/ug/frequency-offset-calibration-transmitter-using-analog-devices-ad9361-ad9364.html. Accessed on 29 October 2023.

[17] Transmit and Receive LTE MIMO Using Analog Devices AD9361/AD9364. https://in.mathworks.com/help/supportpkg/xilinxzynqbasedradio/examples/transmit-and-receive-lte-mimo-using-a-single-analog-devices-ad9361-ad9364.html.

[18] LTE MIB Recovery and Cell Scanner Using Analog Devices AD9361/AD9364. https://in.mathworks.com/help/supportpkg/xilinxzynqbasedradio/examples/LTE-MIB-Recovery-Using-Analog-Devices-AD9361-AD9364.html. Accessed on 29 October 2023.

[19] NR Synchronization Procedures. https://in.mathworks.com/help/5g/examples/NR-Synchronization-Procedures.html. Accessed on 29 October 2023.

[20] NR PDSCH Throughput. https://it.mathworks.com/help/5g/examples/nr-pdsch-throughput.html. Accessed on 29 October 2023.

[21] NR PDSCH Throughput. https://in.mathworks.com/help/5g/ug/nr-pdsch-throughput.html. Accessed on 29 October 2023.

[22] NR PUSCH Throughput. https://in.mathworks.com/help/5g/ug/nr-pusch-throughput.html. Accessed on 29 October 2023.

[23] NR UL-SCH Encode. https://in.mathworks.com/help/5g/ref/nrulsch-system-object.html. Accessed on 29 October 2023.

[24] NR PUSCH Encode. https://in.mathworks.com/help/5g/ref/nrpusch.html. Accessed on 29 October 2023.

[25] NR SRS. https://in.mathworks.com/help/5g/ref/nrsrs.html. Accessed on 29 October 2023.

[26] NR PUSCH Decode. https://in.mathworks.com/help/5g/ref/nrpuschdecode.html. Accessed on 29 October 2023.

[27] NR UL-SCH Decode. https://in.mathworks.com/help/5g/ref/nrulschdecoder-system-object.html. Accessed on 29 October 2023.

[28] European Telecommunications Standards Institute (ETSI). Physical layer measurements (version 16.2.0, Release 16). Technical Report TS 38.215, 3rd Generation Partnership Project (3GPP), Jul. 2020. https://www.etsi.org/deliver/etsi_ts/138200_138299/138215/16.02.00_60/ts_138215v160200p.pdf.

[29] Zexian Li et al. 5G URLLC: Design Challenges and System Concepts. In *2018 15th International Symposium on Wireless Communication Systems (ISWCS)*, pages 1–6, Lisbon, Portugal, 2018. doi:10.1109/ISWCS.2018.8491078. doi:10.1109/ISWCS.2018.8491078.

[30] 5G Technology: 5G mobile communications. https://www.electronics-notes.com/articles/connectivity/5g-mobile-wireless-cellular/technology-basics.php. Accessed on 29 October 2023.

[31] European Telecommunications Standards Institute (ETSI). Physical channels and modulation (version 16.2.0, Release 16). Technical Report TS 38.211, 3rd Generation Partnership Project (3GPP), Jul. 2020. https://www.etsi.org/deliver/etsi_ts/138200_138299/138211/16.02.00_60/ts_138211v160200p.pdf.

[32] Wind Tre S.p.A. Wind tre, 2023. Accessed on October 27, 2023. URL: https://www.windtre.it/.

[33] 5G & C-V2X AG55xQ Series. https://www.quectel.com/product/5g-c-v2x-ag55xq-series/. Accessed on 29 October 2023.

[34] Arch Linux Wiki. Working with the serial console, 2023. Accessed on October 27, 2023. URL: https://wiki.archlinux.org/title/working_with_the_serial_console.

[35] 5G-Tools. 5g nr frequency band, 2023. Accessed on October 27, 2023. URL: https://5g-tools.com/5g-nr-frequency-band/.

[36] Sierra Wireless. EM9191 5G NR Sub-6 GHz Module. https://www.sierrawireless.com/iot-modules/5g-modules/em9191/. Accessed on April 3, 2023.

[37] ASK Industries S.p.A. Home Page. https://www.askgroup.global/. Accessed on October 14, 2023.

[38] D-flife vk-162 g-mouse usb gps dongle navigation module. https://web.archive.org/web/20231026/https://manualzz.com/doc/52938665/d-flife-vk-162-g-mouse-usb-gps-dongle-navigation-module-e... Accessed: 2023-10-26.

[39] iPerf3. https://iperf.fr/. Accessed on 29 October 2023.

[40] Speedtest CLI. https://www.speedtest.net/apps/cli. Accessed on 29 October 2023.

[41] ICMP Protocol. https://www.ionos.com/digitalguide/server/know-how/what-is-icmp-protocol-and-how-does-it-work/. Accessed on 29 October 2023.

[42] MathWorks. geoplot3, 2023. MATLAB function. URL: https://it.mathworks.com/help/map/ref/geoplot3.html.

[43] 5G Coverage, Prediction, and Trial Measurements. https://arxiv.org/pdf/2003.09574.pdf. Accessed on 29 October 2023.

[44] RSRP. https://telecompedia.net/rsrp/. Accessed on 18 May 2022.

[45] RSSI (Received Signal Strength Indicator). https://www.techplayon.com/rssi/. Accessed on 18 May 2022.

[46] RSRQ (Reference Signal Received Quality). https://www.techplayon.com/rsrq-received-signal-received-quality/. Accessed on 18 May 2022.

[47] Path Loss Analysis Considering Doppler Shift Effect on Cellular Communication for Connected Car Application at Rural Area. https://iopscience.iop.org/article/10.1088/1757-899X/557/1/012042/pdf. Accessed on 18 May 2022.

[48] ETSI (European Telecommunications Standards Institute). Technical report tr 138 900: Study on scenarios and requirements for next generation access technologies, 2017. URL: https://www.etsi.org/deliver/etsi_tr/138900_138999/138900/14.02.00_60/tr_138900v140200p.pdf.

[49] European Telecommunications Standards Institute (ETSI). Handover Delay. Technical Report TS 38.133, Section 6.1.1.2.1, 3rd Generation Partnership Project (3GPP), Jul. 2019. https://www.etsi.org/deliver/etsi_ts/138100_138199/138133/15.06.00_60/ts_138133v150600p.pdf.

[50] Marcus De Ree et al. Key Management for Beyond 5G Mobile Small Cells: A Survey. *IEEE Access*, 7:59200–59236, 2019. doi:10.1109/ACCESS.2019.2914359. doi:10.1109/ACCESS.2019.2914359.

[51] Cell Mapper. Home page. https://www.cellmapper.net/. Accessed on October 14, 2023.

[52] Eleonora Oliosi et al. Simulation-based Analysis of Experimental 5G NR Downlink CSI-RSRP-based Handover Performance. In *2023 European Wireless Conference (EW 2023)*, Rome, Italy, October 2023.

[53] Amiraslan Haghrah, Mehran Pourmohammad Abdollahi, Hosein Azarhava, and Javad Musevi Niya. A survey on the handover management in 5g-nr cellular networks: aspects, approaches and challenges. *EURASIP Journal on Wireless Communications and Networking*, 2023(52), 2023.

[54] 3rd Generation Partnership Project (3GPP). Nr; nr and ng-ran overall description; stage 2. Technical Specification TS 38.300, European Telecommunications Standards Institute (ETSI), April 2023. URL: https://www.etsi.org/deliver/etsi_ts/138300_138399/138300/16.04.00_60/ts_138300v160400p.pdf.

[55] 3rd Generation Partnership Project (3GPP). Nr; physical channels and modulation (release 16). Technical Specification TS 138.211, European Telecommunications Standards Institute (ETSI), April 2023. URL: https://www.etsi.org/deliver/etsi_ts/138200_138299/138211/16.02.00_60/ts_138211v160200p.pdf.

[56] Michele Polese, Marco Giordani, Marco Mezzavilla, Sundeep Rangan, and Michele Zorzi. Improved handover through dual connectivity in 5g mmwave mobile networks. *IEEE J.Sel. A. Commun.*, 35(9):2069–2084, sep 2017. doi:10.1109/JSAC.2017.2720338.

[57] European Telecommunications Standards Institute (ETSI). 5g; nr; radio resource control (rrc); protocol specification. Technical Report TS 138 331, European Telecommunications Standards Institute, 12 2016. URL: https://www.etsi.org/deliver/etsi_ts/138300_138399/138331/16.01.00_60/ts_138331v160100p.pdf.

[58] European Telecommunications Standards Institute (ETSI). Lte; evolved universal terrestrial radio access (e-utra); physical layer; general description. Techni-

cal Report TS 136 214, European Telecommunications Standards Institute, 12 2016. URL: https://www.etsi.org/deliver/etsi_ts/136200_136299/136214/16.01.00_60/ts_136214v160100p.pdf.

[59] European Telecommunications Standards Institute (ETSI). Nr; nr; physical layer procedures for control. Technical Report TS 138 214, European Telecommunications Standards Institute, 6 2020. URL: https://www.etsi.org/deliver/etsi_ts/138200_138299/138214/16.02.00_60/ts_138214v160200p.pdf.

[60] European Telecommunications Standards Institute (ETSI). Digital cellular telecommunications system (phase 2+); universal mobile telecommunications system (umts); lte; mme and sgsn related interfaces based on diameter protocol. Technical Report TS 132 455, European Telecommunications Standards Institute, 6 2020. URL: https://www.etsi.org/deliver/etsi_ts/132400_132499/132455/16.00.00_60/ts_132455v160000p.pdf.

[61] Xavier Gelabert, Guohua Zhou, and Peter Legg. Mobility performance and suitability of macro cell power-off in lte dense small cell hetnets. In *2013 IEEE 18th International Workshop on Computer Aided Modeling and Design of Communication Links and Networks (CAMAD)*, pages 99–103, Berlin, Germany, 09 2013. doi:10.1109/CAMAD.2013.6708097.

[62] Muhammad Tayyab, George Koudouridis, and Xavier Gelabert. *A Simulation Study on LTE Handover and the Impact of Cell Size: 9th International EAI Conference, Broadnets 2018, Faro, Portugal, September 19–20, 2018, Proceedings*, pages 398–408. Springer, Cham, 01 2019. doi:10.1007/978-3-030-05195-2_39.

[63] Ardian Ulvan, Robert Bestak, and Melvi Ulvan. The study of handover procedure in lte-based femtocell network. In *Joint IFIP Wireless and Mobile Networking Conference (WMNC)*, pages 1 – 6, Budapest, Hungary, 11 2010. doi:10.1109/WMNC.2010.5678766.

[64] European Telecommunications Standards Institute. Lte; evolved universal terrestrial radio access (e-utra); physical channels and modulation. Technical Report TS 136 300, European Telecommunications Standards Institute, 12 2012. URL: https://www.etsi.org/deliver/etsi_ts/136300_136399/136300/11.06.00_60/ts_136300v110600p.pdf.

[65] Marko Höyhtyä, Olli Mämmelä, and Markus Eskola. Spectrum sharing for small cell networks: A survey. *Journal of Electrical and Computer Engineering*, 2017, 2017.

[66] Hong Zhang, Lingyang Song, and Zhu Han. Small cell networks: Deployment, management, and optimization. *IEEE Transactions on Wireless Communications*, 18(3):1413–1423, 2019.

[67] Jeffrey G Andrews, Stefano Buzzi, Wan Choi, Stephen V Hanly, Angel Lozano, Anthony CK Soong, and Jianzhong Charlie Zhang. What will 5g be? *IEEE Journal on selected areas in communications*, 34(3):1065–1082, 2016.

[68] Mehdi Bennis, Merouane Debbah, and H Vincent Poor. Ultrareliable and low-latency wireless communication: Tail, risk, and scale. *Proceedings of the IEEE*, 106(10):1834–1853, 2018.

[69] Zhisheng Niu, Yiqun Wu, Jun Gong, and Zexi Yang. Cell zooming for cost-efficient green cellular networks. *IEEE Communications Magazine*, 49(11):74–79, 2011.

[70] David Lopez-Perez, Alvaro Valcarce, Guillaume de la Roche, and Jie Zhang. Enhanced inter-cell interference coordination challenges in heterogeneous networks. *IEEE Wireless Communications*, 18(3):22–30, 2011.

[71] Umair Siddique, Mubashir Husain Rehmani, and Mischa Dohler. Wireless backhaul network solutions for heterogeneous small cell networks: A survey. *IEEE Access*, 3:2122–2138, 2015.

[72] Jacek Kibilda, Marco Di Renzo, and Luiz A DaSilva. Backhaul for low-density deployments. *IEEE Transactions on Wireless Communications*, 15(12):8385–8399, 2016.

[73] Vikram Chandrasekhar, Jeffrey G Andrews, and Alan Gatherer. Femtocell networks: a survey. *IEEE Communications Magazine*, 46(9):59–67, 2008.

[74] The MathWorks, Inc. Display or compute line-of-sight (LOS) visibility status - los(), 2023. `https://www.mathworks.com/help/antenna/ref/txsite.los.html`. Accessed on October 13, 2023.

[75] Marion Berbineau, Romain Behaegel, Juan Moreno Garcia-Loygorri, Raul Torrego, Raffaele D'Errico, Ali Sabra, Ying Yan, and José Soler. Channel Models for Performance Evaluation of Wireless Systems in Railway Environments. *IEEE Access*, 9:45903–45918, 2021. doi:10.1109/ACCESS.2021.3066112.

[76] European Telecommunications Standards Institute (ETSI). Study on channel model for frequencies from 0.5 to 100 GHz. Technical Report TR 38.901, 3rd Generation Partnership Project (3GPP), Jul. 2018. `https://www.etsi.org/deliver/etsi_tr/138900_138999/138901/15.00.00_60/tr_138901v150000p.pdf`.

[77] European Telecommunications Standards Institute (ETSI). Study on channel model for frequencies from 0.5 to 100 GHz. Technical report, 3rd Generation Partnership Project (3GPP), Sophia Antipolis Cedex, FRANCE, July 2018. 3GPP TR 38.901 version 15.0.0 Release 15.

[78] European Telecommunications Standards Institute (ETSI). UMTS; Base Station (BS) classification (FDD) (3GPP TR 25.951 version 6.3.0 Release 6). Technical Report TR 125.951, 3rd Generation Partnership Project (3GPP), Oct 2006. `https://www.etsi.org/deliver/etsi_tr/125900_125999/125951/06.03.00_60/tr_125951v060300p.pdf`.

[79] Ericsson. Outdoor Coverage - Small Cells. https://www.ericsson.com/en/small-cells/outdoor-coverage. Accessed on October 13, 2023.

Thanks

Completing my PhD was a lengthy journey that significantly expanded my knowledge, and I want to express my gratitude to all those who supported me throughout this process. I extend my sincere thanks to everyone who played a role in my doctoral years.

First and foremost, I want to acknowledge and thank my supervisor, Prof. Gianluigi Ferrari, for providing me with this opportunity and for his continuous guidance and motivation. Prof. Luca Davoli also deserves my gratitude for his support and guidance throughout the journey.

I would like to express my appreciation to Antonio Cilfone for his assistance at the outset of this research direction. Special thanks to all the members of the IoT Lab, and a heartfelt note of thanks to Eleonora for her valuable help.

I extend my thanks to my family and friends who stood by me during this challenging journey. Your support was my pillar of strength. I also want to express my gratitude to ASK Industries for funding this research, and a special thank you to Nicolo for hosting me during my visits to the company.

I want to convey my deep appreciation to everyone who contributed to my PhD journey. Your support, guidance, and encouragement were vital in making this academic endeavor a reality.